Physiological Chemistry and Physics and Medical NMR Volume 35, Number 1, 2003

Addresses of Chief Editor and Editorial College

George M. Mrevlishvili
Department of Physics
Tbilisi State University
380028 Tbilisi
Republic of Georgia

Toshihiko Ubuka
Department of Clinical Nutrition
Kawasaki University of Medical Welfare
Kurashiki, Okayama, 701-0193, Japan

Vasile Vasilescu
Department of Biophysics
Faculty of Medicine
Bucharest 76241, Romania

Denys Wheatley
Department of Pathology
University of Aberdeen
Aberdeen AB9 2ZD, Scotland

EDITORIAL AND BUSINESS OFFICE

Physiological Chemistry and Physics
and Medical NMR
P.O. Box 1452
Melville, New York 11747

Editor In Chief, Dr. Gilbert N. Ling
Managing Editor, Margaret M. Ochsenfeld

SCOPE: PCP provides a forum for the review and publication of reports of original research in a broad range of subjects in biophysics, biochemistry and cellular physiology. Reports of direct applications of basic knowledge to human studies are invited; examples would include the measurements of relaxation times as part of NMR imaging. Single experiments, conclusions based on inadequate statistics, purely speculative papers, and clinical case reports are not accepted.

POLICY: The pages of PCP are accessible to competing viewpoints, interpretations, theories and opinions. Debate is invited via Editorial Comments and Letters to the Editor. Criteria for evaluating submissions include soundness of the study and clarity of presentation, and papers are not rejected on the basis of interpretation or theory, however controversial. PCP believes that scientific issues should be settled by investigation and open debate, not by an appeal to anonymous authority.

PCP attempts to achieve a balance between freedom of expression and constructive peer review. All papers are refereed by reviewers who may remain anonymous, but the Chief Editors make all final decisions, and will handle appeals from authors who feel their papers are unfairly reviewed.

The Editors endeavor to make decisions regarding acceptance or rejection of manuscripts quickly, and have set self-imposed deadlines for doing so. Referees also are given deadlines.

TYPES OF PAPERS: *Regular papers* may be experimental or theoretical. *Short notes, Priority notes* and *Letters* in response to published papers are invited. *Reviews* are desired, but authors are urged to contact an Editor before sending a finished review manuscript. *Symposia* may be published as regular or supplemental issues.

SUBSCRIPTIONS: Price is US$80.00 per volume in the United States and US$87.00 outside the United States. *Physiological Chemistry and Physics and Medical NMR* is published biannually, 2 issues per year, the volume numbered yearly. New subscriptions will start with the first issue of the volume in progress, unless the subscriber directs otherwise. Most back issues are available

Instructions to Authors

SUBMISSIONS: An original and two copies of all material are requested. The original must be typewritten on one side only, but the copies may be double-sided to reduce cost of mailing. Papers should be sent to Dr. Gilbert N. Ling, Editor, P.O. Box 1452, Melville, New York 11747 U.S.A. Authors, especially those outside of North America, may send their papers to a member of the Editorial College in the same or a nearby country; the member of the college may elect to review the manuscript and/or obtain a second review before forwarding it to the Chief Editors. Manuscripts should be submitted only to this journal and not have been published in part or whole in another publication, except as short preliminary notes, abstracts, or as unpublished work in reviews or symposia. Be sure to keep a copy of your manuscript.

NOTE: Referees will be instructed to destroy their copies of the manuscript after reviewing them. We will return only the original manuscript to you for revision or if rejected.

MANUSCRIPTS: All material should be typed double-spaced with margins at least one inch wide and pages numbered beginning with the title page. In addition to a paper copy, you may send an IBM-compatible file on a floppy disk in Word, Wordperfect, ASCII or text. *Title Page* should include title (of at most 100 characters and spaces), full names of authors as you wish them to be published, names and cities of institutional affiliation(s) of authors and of institution(s) where the studies were performed, and name, full address and telephone number of the person to whom correspondence, proofs, and reprint requests are to be sent. Three or four *key words* should be listed on the title page.

Abstract should be concise and no longer than 225 words. *Body* may or may not be divided into Introduction, Materials and Methods, Results and Discussion, depending on the length and nature of the paper. Introductory remarks should indicate clearly the significance of the work presented. *References* may be indicated in the text and listed in the reference list in whatever style the author prefers, but we prefer that titles of articles be omitted.

TABLES: Tables should be typewritten on separate sheets and identified by roman numerals (eg. Table 111) and titles. Table notes should be keyed by superscript italic lower-case letters (eg. ^{a}Control). The approximate locations of *tables* and *figures* should be indicated in the margins of the manuscript.

EQUATIONS should be broken in a manner estimated to fit into a column 5 inches wide when published. Solidus fraction (a/c) should be used instead of built-up ones ($\frac{a}{c}$) wherever possible.

ILLUSTRATIONS: Original artwork or glossy photostatic prints, together with two photocopies (like Xerox copies) should be provided. Each illustration should be numbered on the back in pencil, along with the authors' names. It is preferred that line drawings be made on paper that is not larger than $8^1/_2$ by 13 inches, and that the drawing be its intended size in the printed paper. Most figures will occupy $^1/_2$ to full column, that is 5 inches wide. Lines and lettering should be thick enough to allow reduction. A drawing of overall dimension of 8 by 10 inches that will be reduced to $^1/_4$ of its original size should be lettered with 18-point (capitals 6 mm high, lower-case 4 mm high) or larger lettering. Graphs and line drawings must be drawn and labeled in black India ink. Glossy photostatic prints are acceptable, and should be attached firmly to a sheet of paper the same size as the manuscript.

PHOTOGRAPHS: High-quality black and white glossy prints should be provided in triplicate, and may be provided as one print plus two photocopies if the photocopies are sufficiently clear to portray the original to referees. Photographs should be attached firmly to a sheet of paper the same size as the manuscript.

REFEREES: Two anonymous referees will be sought for each paper. Authors are encouraged to suggest names and addresses of suitable referees. Referees will be given deadlines for mailing manuscripts back or phoning reviews in, and will be invited to provide editorial statements or Letters that deal with issues raised by submitted papers.

REPRINTS: An order form is enclosed with proofs sent to authors.

PAGE CHARGES: Page charge is $20.00 per published page. It may be waived in the case of severe international exchange difficulties. An additional charge of $10.00 will be levied for photographs that require screening (eg., E.M's, chromatograms, scans).

Physiol. Chem. Phys. & Med. NMR (2003) *35*: 1–11

Effect of Endogenously Generated Nitric Oxide on the Energy Metabolism of Peritoneal Macrophages

Masafumi Miyamoto[1], Eisuke F. Sato[1*], Manabu Nishikawa[1], Yoshiki Nishizawa[2], Hirotoshi Morii[2], and Masayasu Inoue[1]

Departments of Biochemistry & Molecular Pathology[1] and Internal Medicine[2]
Osaka City University Medical School
1-4-3 Asahimachi, Abeno, Osaka 545-8585, Japan
**Author for correspondence*

Abstract: To understand the role of nitric oxide (NO) in the regulation of cellular metabolism in peritoneal macrophages under physiological low oxygen tension, its effect on the respiration and energy metabolism was examined with casein-induced peritoneal macrophages from the rat. Intraperitoneal injection of casein transiently induced peritoneal infiltration of neutrophils (peaked on day 1) followed by the migration of macrophages that peaked on day 2. Western blotting analysis using antibodies against inducible type of NO synthase (iNOS) revealed that macrophages appeared in the peritoneal cavity during an early stage (~day 2) but not during the late stage (day 3~) of inflammation expressed iNOS and generated substantial amounts of NO by a mechanism that was inhibited by N-iminoethyl-L-ornithine (NIO), a specific inhibitor of iNOS. Although NO reversibly but strongly inhibited the respiration of macrophages from both stages particularly under physiologically low oxygen tension, NIO markedly enhanced the respiration of macrophages obtained from the early period but not from the late period of inflammation. The ATP level in the macrophages from the late period but not from the early period was markedly decreased by NO. Biochemical analysis revealed that the glycolytic activity in the macrophages obtained from the early period was significantly higher than that from the late period of inflammation. These results indicate that significant fractions of cellular ATP in iNOS-positive peritoneal macrophages are synthesized by the increased activity of glycolysis particularly under physiological low oxygen tensions where the mitochondrial respiration is strongly inhibited by endogenously generated NO by macrophages and neutrophils.

NITRIC OXIDE (NO) is synthesized in various types of cells, such as endothelial cells, nerve cells and macrophages (1–3). It has been well known that various stimuli induce iNOS in macrophages (4, 5). Because NO rapidly reacts with oxygen ($K = 6 \times 10^6\ M^{-2}S^{-1}$), its lifetime and biological functions increase under physiologically low oxygen tensions

(6). It should be noted that the oxygen tension in the peritoneal cavity is fairly low and, hence, the lifetime and biological functions of NO would be significantly longer and greater in this component than those expected from *in vitro* experiments performed under air atmospheric conditions in which the oxygen tension is unphysiologically high. Although roles of NO derived from activated macrophages have been studied extensively, only limited information is available for the effect of this gaseous radical on the energy metabolism of NO-generating cells under physiologically low oxygen tensions.

Because the number and properties of macrophages infiltrated in a site of inflammation differ depending on tissues and phases of inflammation, effects of NO on inflammatory tissues and cells might change significantly *in vivo*. The present work describes the effect of endogenously generated NO on the energy metabolism of peritoneal macrophages obtained at different phases of inflammation. Kinetic analysis revealed that endogenously generated NO significantly suppressed the mitochondrial respiration but enhanced the glycolytic activity of iNOS-positive macrophages that appeared in the peritoneal cavity during an early phase of inflammation.

Materials and Methods

Materials. Argon, N_2 and NO gases were obtained from Kinkisanki Co. (Osaka, Japan). ATP bioluminescence assay kit CLS II was purchased from Roche Diagnostics Co. (Mannheim, Germany). All other regents used were of the highest grade commercially available and obtained from Wako Pure Chemical Co. (Osaka, Japan).

Preparation of NO solution. Saturated NO solution was prepared at 25°C after bubbling NO gas through 50 mM HEPES-NaOH buffer (pH 7.4) as described previously (7). Briefly, two small tubes were fitted with an airtight septum with tubes inserted for delivery and escape of gases with the first tube containing 5 M KOH and a second tube containing 20 mM HEPES-NaOH buffer. Argon was delivered into two tubes at a flow rate of 100 ml/min. After 15 min, argon was replaced with NO at a flow rate of 100 ml/min. After 30 min, NO saturated solution (1.9 mM) was kept on ice and freshly used for experiments. The concentration of NO in the stock solution remained unchanged during the storage (~6 hr).

Preparation of peritoneal macrophages. Male Wistar rats weighing 230–250 g were obtained from SLC Japan (Shizuoka, Japan) and used for the preparation of macrophages. Peritoneal macrophages were obtained from rats after intraperitoneal injection of 2% casein in 10 mM Tris buffered saline (pH 7.4, 100 ml/kg of body weight). At the indicated times after intraperitoneal injection of casein, peritoneal cells were isolated from peritoneal ravage fluid by washing with 50 ml of Ca^{++}-free Krebs-Ringer phosphate buffer (KRP: 0.9% NaCl, 6 mM KCl, 1 mM $MgCl_2$, 10 mM phosphate buffer, pH 7.4). Peritoneal cells suspended in 5 ml of KRP were layered on 3 ml of Ficoll Paque. After centrifugation at 280 g for 20 min, macrophage-enriched fractions were collected from the interface. Neutrophils were isolated from the precipitated fractions. Contaminated erythrocytes were removed by treating cells with 0.2% NaCl solution for 10 sec. An equal volume of 1.6% NaCl was rapidly added to the mixture. After washing cells by centrifugation, the precipitated cells were used for experiments. Macrophages and neutrophils were examined under light microscopy (90% <) for purity.

Western blotting analysis of iNOS. Cellular levels of iNOS were determined by Western blotting using specific monoclonal antibodies (TL, Lexington, NY) against mouse iNOS (8). Briefly, 0.1 ml of 45% trichloroacetic acid solution was added to 1 ml of cell suspension (1×10^7 cells/ml). After incubating at 4°C for 15 min, the mixture was centrifuged at 12,000 *g* for 5 min. The precipitated fractions were sonicated in 80 µl of 2% Triton X-100 solution containing 9 M urea and 5% 2-mercaptoethanol. After adding 20 µl of 10% lithium dodecylsulfate, pH was neutralized by adding 1 M Tris. The samples thus treated were sonicated and centrifuged at 15,000 *g* for 5 min. The supernatant fractions were used for Western blotting analysis. After electrophoresis on a 7.5% SDS-polyacrylamide gel electrophoresis (2×10^6 cells/lane), proteins were transferred to a PVDF membrane by a semi-dry blotting system. The membranes were incubated at 4°C in Tris-buffered saline solution (pH 7.5) containing 5% skim milk and 0.05% Tween-20 (TBS-T) for 16 h. The membrane was further incubated with anti-iNOS antibody (1:1000 dilution) for 60 min and subsequently with horseradish peroxidase-linked rabbit anti-mouse IgG antibodies. After incubation for 30 min, the membranes were washed three times with TBS-T. Immunoreactive bands were detected with an ECL detection system on autoradiography films (Hyper film-ECL, Pharmacia Biotech).

Generation of NO by peritoneal macrophages. Generation of NO by peritoneal macrophages was determined by measuring nitrite in the medium using a Griess reagent. Briefly, peritoneal macrophages (1×10^7 cells/ml, 1 ml each well) were incubated in KRP containing 1 mM $CaCl_2$, 5 mM glucose and 1 mM L-arginine in a 24-well culture plate at 37°C for 30 min. Experiments were performed in the presence or absence of 100 µM NIO.

Analysis of cell respiration and ATP levels. Oxygen consumption by macrophages was determined polarographically at 37°C using a Clark-type oxygen electrode with a 2-ml waterjacketed closed chamber. Reaction mixtures contained KRP, 1 mM $CaCl_2$, 5 mM glucose and other additions in a final volume of 1 ml. The reaction was started by adding 10^7 or 2×10^7 cells. During the experiments, aliquots of NO-saturated solution were added to the mixtures.

Levels of ATP in macrophages were determined according to the luciferin-luciferase method (8) using an ATP bioluminescence assay kit CLS II. Cells were incubated under the same conditions used for the analysis of respiration. During the incubation, aliquots of 50 µl were removed, mixed with 150 µl of 100 mM Tris-HCl buffer (pH 7.8) containing 4 mM EDTA, and incubated at 95°C for 2 min. After centrifugation at 12,000 *g* for 5 min, ATP was determined in the supernatant fractions.

Under oxygen concentration of approximately 25 µM, macrophages (1×10^7 cells/ml) were incubated at 37°C for 30 min. Aliquots of 200 µl were removed and immediately incubated at 100°C for 5 min. After centrifugation at 12,000 *g* for 5 min, the supernatant fractions were used for the analysis of glucose and lactate. Glucose concentration was determined using a glucose assay kit (Glucose CII-Test Wako, Osaka). Lactate concentration was determined according to the method of Gutmann (9).

Statistics. Student's *t*-test for unpaired data was used for statistical analysis, and $P<0.05$ was considered significant.

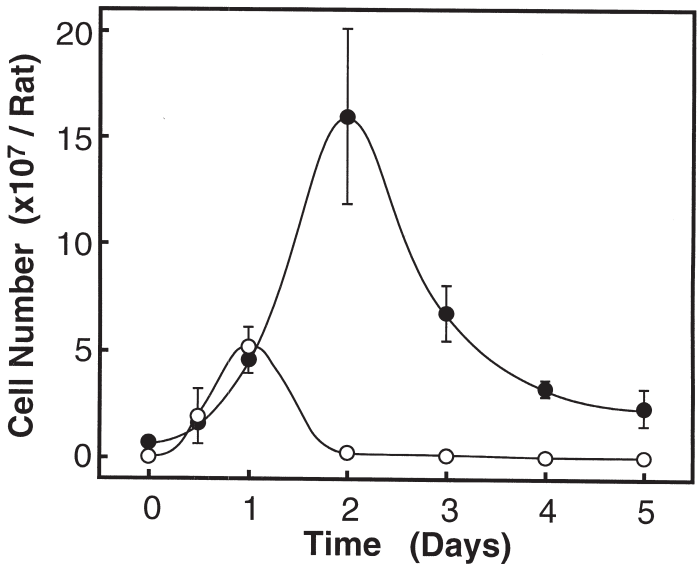

FIGURE 1. *Profiles of peritoneal leukocytes induced by casein.* Peritoneal cells were obtained from rats after intraperitoneal injection of casein (2 g/kg body weight). At the indicated times after injection of casein, peritoneal cells were isolated and counted as described in the text. Open circles, neutrophils; closed circles, macrophages. Data shows mean ± SEM derived from 6 animals.

Results

Property of peritoneal cells after administration of casein. At the indicated times after injection of casein, peritoneal cells were obtained and analyzed under a light microscopy. As shown in Figure 1, the number of neutrophils rapidly increased, peaked at day 1, and rapidly decreased thereafter. The number of macrophages also increased rapidly, peaked on day 2, and slowly decreased thereafter.

Expression of iNOS in peritoneal cells. The time-dependent changes in the expression of iNOS in macrophages and neutrophils as determined by Western blotting analysis is shown in Figure 2. Macrophages obtained from the rat at an early stage of inflammation expressed substantial amounts of iNOS. The expression of iNOS rapidly decreased on day 2 and became negligible on day 4. Neutrophils that appeared at an early stage of inflammation (~day 1) also expressed iNOS.

Generation of NO by peritoneal cells. To determine the cellular activity of iNOS, concentrations of nitrite, a major metabolite of NO, in the culture medium were measured after 30 min of incubation. Macrophages isolated 1 and 4 days after the administration of casein generated NO at a rate of 104.5 ± 4.7 and 8.2 ± 3.1 pmol/10^7 cells/min, respectively, as determined from nitrite levels (Figure 3). Generation of NO was completely inhibited by the presence of 100 μM NIO, a potent inhibitor of iNOS. Thus, peritoneal macrophages with high iNOS activity isolated on day 1 and those with low iNOS activity prepared on day 4 were used for the following experiments.

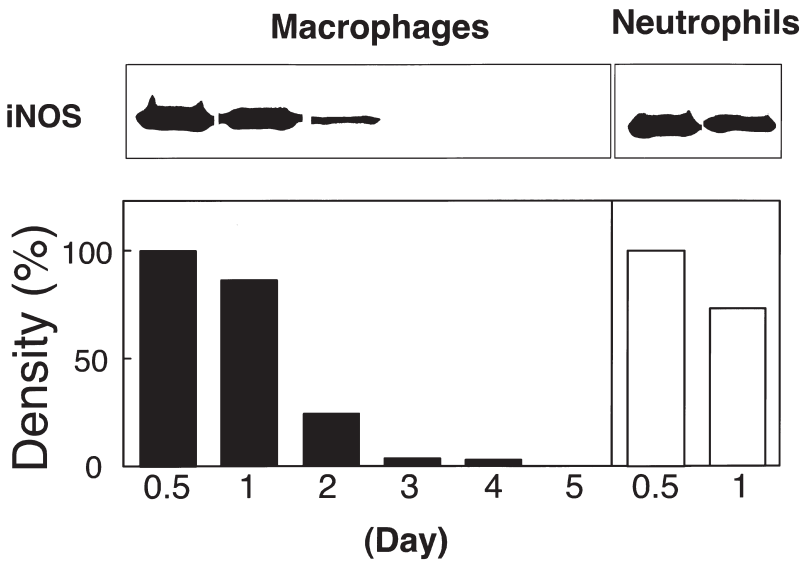

FIGURE 2. *Western blotting analysis of iNOS.* Cellular levels of iNOS were determined by Western blotting using specific monoclonal antibody against rat iNOS. Detailed conditions were as described in the text.

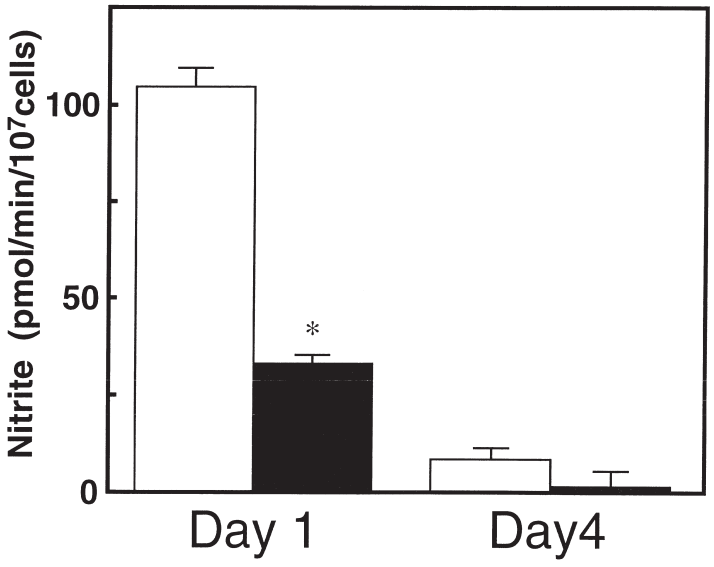

FIGURE 3. *Generation of NO by macrophages.* Macrophages obtained from day 1 and 4 were incubated in a RPMI medium at 37°C (1×10^7 cells/ml) in a 5% CO_2 incubator for 30 min. Concentrations of nitrite in the culture medium were measured by Griess reagent. Experiments were performed in the presence (closed columns) or absence (open columns) of 100 μM NIO. Results are mean ± SEM of triplicate experiments. *P <0.05 compared with control.

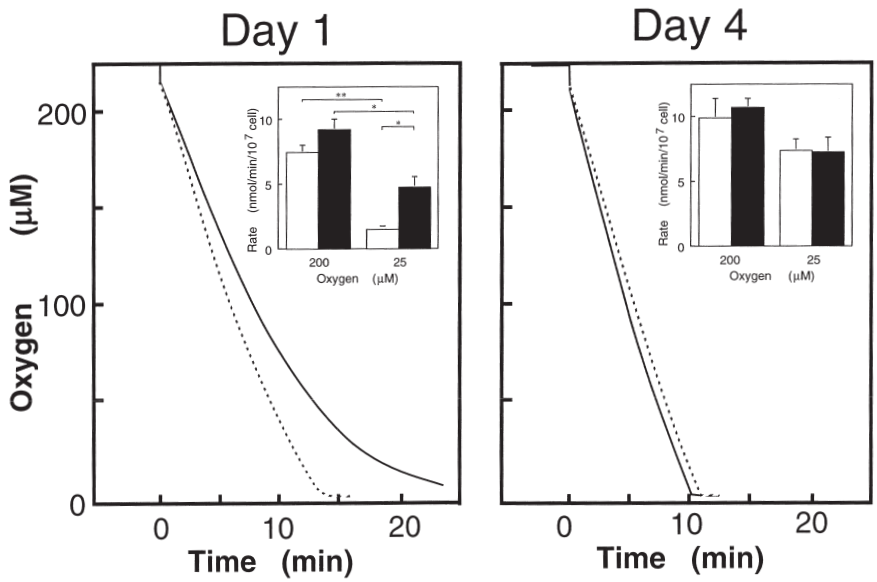

FIGURE 4. *Effect of NIO on the respiration of macrophages.* Peritoneal macrophages (2×10^7 cells/ml) were incubated in a closed chamber containing 1 ml of KRP at 37°C. During the incubation, the oxygen concentration in the medium was monitored as described in the text. Respiration of macrophages was monitored in the presence (dotted lines) or absence (solid lines) of 100 μM of NIO. These data shows typical trace. Insertion: Rate of oxygen consumption at 200 μM and 25 μM oxygen tension. Open column: control, closed column: with 100 μM NIO. Results are mean ± SE of triplicated experiments. *P< 0.05 (unpaired T test).

Analysis of cellular respiration. Macrophages, isolated on day 1 after the administration of casein rapidly consumed oxygen (Figure 4). However, the rate of oxygen consumption decreased time-dependently with concomitant decrease in oxygen tension. To study the effect of endogenously generated NO on the oxygen consumption in macrophages, their respiration was determined in the presence or absence of NIO. The rate of oxygen consumption was higher in the presence of NIO than in the absence of the inhibitor. Although macrophages prepared on day 4 also consumed oxygen as rapidly as those prepared on day 1, NIO had no appreciable effect on their respiration. In the presence of erythrocytes (0.1% hematocrit), the respiration of macrophages obtained on day 1 but not on day 4 under low oxygen tension was reversed (data not shown).

Effect of NO on cellular respiration and ATP levels. To elucidate the mechanism underlying the marked difference in the sensitivity of macrophages to NIO, effects of exogenously added NO on the respiration of cells obtained on day 1 and 4 were studied. When NO was added to the buffer, the respiration of macrophages was transiently but strongly inhibited particularly under physiologically low oxygen tension (Figure 5). No significant difference in the inhibitory effect of NO was found between the two cell types. Under high oxygen tensions such as room air (220 μM), no appreciable inhibition was observed with the same concentration of NO (data not shown).

Because NO equally inhibited the respiration of both types of macrophages, ATP levels in these cells might also be affected soon after the inhibition. To test this possibility, the

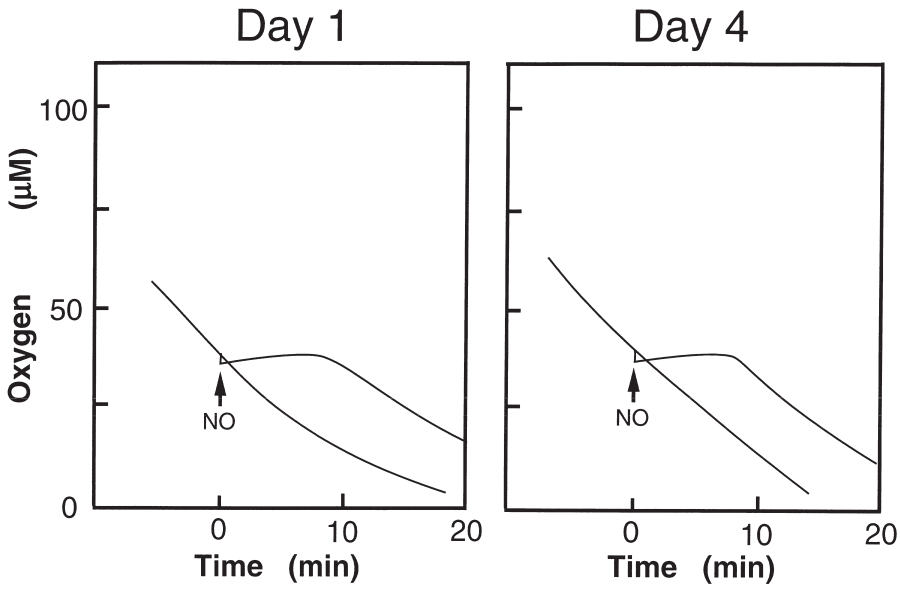

FIGURE 5. *Effect of NO on the respiration of macrophages.* In the presence of 100 μM of NIO, effect of NO on the respiration of macrophages was observed at oxygen concentration of 35 μM. At the indicated points (arrows), 10 μM of NO was added to the cell suspension. Other conditions were the same as in Figure 4.

effect of NO on cellular ATP levels was determined with the two cell types in the presence and absence of NIO (Figure 6). Although ATP levels in macrophages obtained on day 1 remained unaffected by the presence of NO, those in cells obtained on day 4 markedly decreased during the incubation.

Effect of NIO on the glycolytic activity of macrophages. To elucidate the mechanism by which NO decreased ATP levels in macrophages obtained from day 4 but not from day 1 after the administration of casein, its effect on the cellular activity of glycolysis was compared with the two cell types. As seen in Figure 7, rates of glucose consumption and lactate generation were 4~5-fold greater with macrophages obtained from day 1 than those from day 4. However, the presence of NIO had no appreciable effect on the rates of glucose consumption and lactate production by the two types of macrophages.

Discussion

The present work shows that biochemical properties of macrophages infiltrated in the peritoneal cavity of casein-treated rats change markedly during the time of inflammation. The macrophages appearing in the peritoneal cavity during an early stage (~day 2), but not a late stage (day 3~4), of inflammation strongly expressed iNOS and generated substantial amounts of NO. Reichner *et al.* (10) reported that macrophages in healing wounds express iNOS temporally only during the initial 48 to 72 hours. This process is similar to our model. It has been shown that NO reversibly interacts with cytochrome c oxidase, complex I and

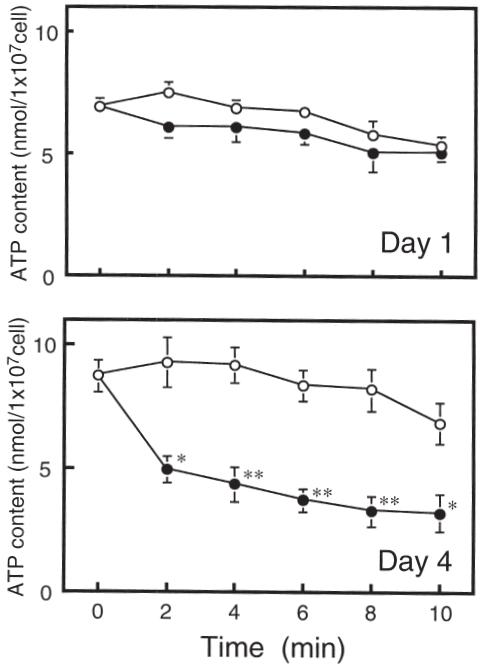

FIGURE 6. *Effect of NO on ATP levels in macrophages.* Peritoneal macrophages (1×10^7/ml) were incubated in 1 ml of KRP containing 100 μM of NIO at 37°C. NO was added to the mixture to give a final concentration of 10 μM. At the indicated time, levels of cellular ATP were measured as described in the text. Open circles: control; closed circles: experiments in the presence 10 μM of NO. *P <0.05 compared with control.

II in mitochondria (11–13), thereby inhibiting their respiration particularly under low oxygen tensions (14, 15). Thus, the NIO-enhanced respiration of macrophages obtained from an early period of inflammation might reflect the inhibition of mitochondrial respiration by endogenously generated NO.

It should be noted that, in the absence of NIO, the respiration of macrophages obtained from day 1, but not day 4, decreased markedly with the decrease in oxygen tensions in the medium. Because biological activities of NO are enhanced under low oxygen tensions, such as those in the peritoneal cavity (approx. ~10 μM) (16), the respiration and ATP synthesis in iNOS-enriched macrophages might be inhibited significantly *in situ*. Exogenously added NO equally suppressed the respiration of macrophages irrespective of their expression of iNOS; biochemical properties of mitochondria and their sensitivity to NO might be similar with the two cell types.

The present work also shows that the macrophages enriched with iNOS have higher activity of glycolysis than those lacking the enzyme. Although the respiration of macrophages was strongly suppressed by NO irrespective of the expression of iNOS, their ATP levels decreased only with cells lacking the enzyme. These observations suggest that the ATP synthesis of macrophages expressing iNOS might preferentially depend on the increased activity of glycolysis presumably due to inhibition of mitochondrial respiration by endogenously generated NO.

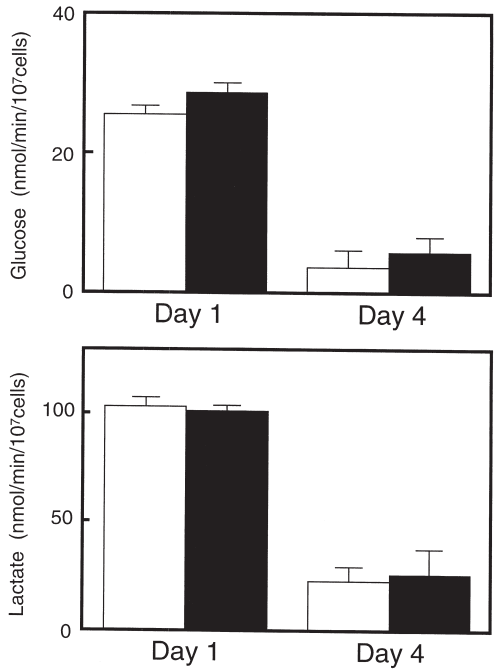

FIGURE 7. *Effect of NIO on the glycolytic activity of macrophages.* Peritoneal macrophages (1×10^7 cells/ml) were incubated in KRP containing 5 mM glucose at 37°C for 30 min at oxygen concentration of about 25 μM. The rates of glucose consumption and lactate production were determined as described in the text. Experiments were performed in the presence (closed columns) or absence (open columns) of 100 μM NIO. Results are mean ± SEM of triplicate experiments.

Previous reports also demonstrated that NO producing cells exhibited increased activities of glycolysis and lactate production (17–20). Paradoxically, some of the glycolytic enzymes are inhibited by NO. Glyceraldehyde-3-phosphate-dehydrogenase (GAPDH), a key enzyme in the glycolytic pathway, is inhibited in its enzyme activity by S-nitrosylation following S-ribosylation of NO and related metabolites. (21–24). Although this enzyme can be inhibited by NO *in vitro*, concentrations of NO required for the sufficient inhibition are unphysiologically high. Hence, a low level of endogenously generated NO might seem not to inhibit the cellular activity of glycolysis.

Albina *et al.* reported that NO inhibited GAPDH dehydrogenase activity and induced its acylphosphatase activity. Uncoupling of glycolytic flux by the acylphosphatase activity of NO-modified GAPDH causes reduced GAPDH activity increased glycolysis and decreased ATP content in the NO-producing cell (25). This might play a part in the mechanism of the dissociation with increased glycolysis and inhibition of gyloclytic enzymes in the NO producing cell.

It should be noted that the presence of NIO had no appreciable effect on the glycolytic activity of both types of macrophages but NO decreased ATP levels only with cells lacking iNOS obtained from day 4. Thus, the increase in the activity of glycolysis in macrophages obtained from day 1 and the decrease in ATP levels by NO in cells obtained from day 4 could be explained on the basis of selective inhibition of mitochondrial respiration by NO

without affecting cellular activity of glyceraldehyde-3-phosphate-dehydrogenase under the present experimental conditions.

It should be noted that the inflammatory responses of peritoneal macrophages and neutrophils are higher during an early period (day 1 and 2) after the administration of various stimuli than those in a healing stage (day 3~). In fact, neutrophils appeared in the peritoneal cavity during the early phase also expressed iNOS and generated substantial amounts of NO and reactive oxygen species. Furthermore, the properties of macrophages obtained 4 days after the administration of casein were similar to those of resident macrophages as measured by cellular activity to generate reactive oxygen species and NO.

Thus, although endogenously generated NO of iNOS-positive macrophages and neutrophils might inhibit mitochondrial respiration in macrophages particularly under low oxygen tensions in the peritoneal cavity, the steady-state level of cellular ATP would be maintained around its control levels by the increased activity of glycolysis. Because NO has a potent activity to kill bacteria [26, 27], this gaseous radical derived from activated macrophages and neutrophils in and around inflammatory tissues might play a critical role in the early events required for the defense mechanism against pathogens without perturbing energy metabolism in activated leukocytes. Thus, enhanced expression of iNOS and glycolysis in activated macrophages during the early period of inflammation would be of pathophysiological importance in the defense mechanism against pathogens particularly under low oxygen tensions where the bactericidal action of NO is significantly increased.

References

1. Bredt, D.S., Hwang, P.M., Glatt, C.E., Lowenstein, C., Reed, R.R. and Snyder, S.H. (1991) *Nature 351:* 714–8.
2. Lamas, S., Marsden, P.A., Li, G.K., Tempst, P. and Michel, T. (1992) *Proc. Natl. Acad. Sci. USA 89:* 6348–52.
3. Xie, Q.W., Cho, H.J., Calaycay, J., Mumford, R.A., Swiderek, K.M., Lee, T., Ding, A., Troso, T. and Nathan, C. (1992) *Science 256:* 225–8.
4. Ding, A.H., Nathan, C.F. and Stuehr, D.J. (1988) *J. Immunol. 141:* 2407–12.
5. Lorsbach, R.B., Murphy, W.J., Lowenstein, C.J., Snyder, S.H. and Russell, S.W. (1993) *J. Biol. Chem. 268:* 1908–13.
6. Nishikawa, M., Sato, E.F., Utsumi, K. and Inoue, M. (1996) *Cancer Res. 56:* 4535–40.
7. Clancy, R.M., Miyazaki, Y. and Cannon, P.J. (1990) *Anal. Biochem. 191:* 138–43.
8. Nishikawa, M., Sato, E.F., Kuroki, T., Utsumi, K. and Inoue, M. (1998) *Hepalology 28:* 1474–80.
9. Gutmann, I. and Wahlefeld, A.W. (1974) *Methods of Enzymatic Analysis 3:* 1464–1468.
10. Reichner, J.S., Meszaros, A.J., Louis, C.A., Henry, W.L., Jr., Mastrofrancesco, B., Martin, B.A. and Albina, J.E. (1999) *Am. J. Pathol. 154:* 1097–104.
11. Cleeter, M.W., Cooper, J.M., Darley-Usmar, V.M., Moncada. S. and Schapira, A.H. (1994) *FEBS Lett 345:* 50–4.
12. Drapier, J.C. and Hibbs. J.B., Jr. (1988) *J. Immunol. 140:* 2829–38.
13. Granger, D.L. and Lehninger, A.L. (1982) *J. Cell Biol. 95:* 527–35.
14. Takehara, Y., Kanno, T., Yoshioka, T., Inoue, M. and Utsumi, K. (1995) *Arch. Biochem. Biophys. 323:* 27–32.
15. Schweizer, M. and Richter, C. (1994) *Biochem. Biophys. Res. Commun. 204:* 169–75.
16. Bornside, G.H., Donovan, W.E. and Myers, M.B. (1976) *Proc. Soc. Exp. Biol. Med. 151:* 437–41.
17. Albina, J.E. and Mastrofrncesco, B. (1993) *Am. J. Phvsiol. 264:* CI594–9.

18. Bereta, J. and Bereta, M. (1995) *Biochem. Biophys. Res. Commun. 217:* 363–9.
19. Erecinnska, M., Nelson, D. and Vanderkooi, J.M. (1995) *J. Neurochem. 65:* 2699–705.
20. Stefanovic-Racic, M., Stadler, J., Georgescu, H.I. and Evans, C.H. (1994) *J. Cell. Physiol. 159:* 274–80.
21. Dimmeler, S., Ankarcrona, M., Nicotera, P. and Brune, B. (1993) *J. Immunol. 150:* 2964–71.
22. Mohr, S., Stamler, J.S. and Brune, B. (1994) *FEBS Lett. 348:* 223–7.
23. Molina y Vedia, L., McDonald, B., Reep, B., Brune, B., Di Silvio, M., Billiar, T.R. and Lapetina, E.G. (1992) *J. Biol. Chem. 267:* 24929–32.
24. Mohr, S., Stamler, J.S. and Brune, B. (1996) *J. Biol. Chem. 271:* 4209–14.
25. Albina, J.E., Mastrofrancesco, B. and Reichner, J.S. (1999) *Biochem. J. 341:* (Pt 1), 5–9.
26. Nagata, K., Yu, H., Nishikawa, M., Kashiba, M., Nakamura, A., Sato, E.F., Tamura, T. and Inoue, M. (1998) *J. Biol. Chem. 273:* 14071–3.
27. Yu, H., Sato, E.F., Nagata, K., Nishikawa, M., Kashiba, M., Arakawa, T., Kobayashi, K., Tamura, T. and Inoue, M. (1997) *FEBS Lett. 409:* 161–5.

Received November 12, 2002;
accepted May 19, 2003.

Physiol. Chem. Phys. & Med. NMR (2003) *35*: 13–25

Spectral Properties of Adrenaline in Micellar Environment

Krzysztof Polewski

Department of Physics, August Cieszkowski Agricultural University, 60-637 Poznan, Poland

Abstract: An absorption and fluorescence spectral and temporal studies on the solubilzation properties of adrenaline in micellar environment in sodium dodecyl sulfate (SDS) and in tetradodecyltrimethyl ammonium bromide (TTABr) has been carried out. Observed Stokes shifts have been correlated with polarity parameters which allowed an estimate of the dielectric constant of the adrenaline environment in SDS and TTABr micelles at 44 and 58, respectively. Experiments with methanol-water mixtures indicate that the hydrogen bonding formation with solvent and the hydrophilic nature of adrenaline influence its solubilization in micelles. Fluorescence and anisotropy decay analysis has shown that neutral adrenaline in SDS micelle is partitioned between aqueous phase (70%) and less polar, micellar phase (30%) and the interactions are limited to the Guy-Chapman layer without deeper penetration into micellar hydrophobic core.

THE CONFORMATION of pharmacologically active small molecules is relevant to any consideration of their interaction with a receptor. Many such molecules are potentially flexible and thus may exist in solution in a number of conformations. Assuming that the small molecule has only a single conformation in its complex with a receptor, the formation of the complex must involve a process of conformational selection, which will influence the kinetics and energetics of complex formation. Thus there is considerable interest in characterizing the conformational distribution of molecules such as catecholamines or the other neurotransmitters in order to know the conformation of these molecules when bound to the receptor. However, it must be clearly understood that information on the preferred conformation in crystal, solution or micelle may not necessarily be that one found during biological activity of the neurotransmitter.

One can expect that in an heterogeneous environment the mechanism of transformation and the kinetic of the process may occur in a different way compared to homogeneous solutions (17). The differences may arise from local concentration effects, electrostatic charges of molecule or/and medium or from cage effects, which protect some molecules from the interaction by placing them inside micelles or membranes.

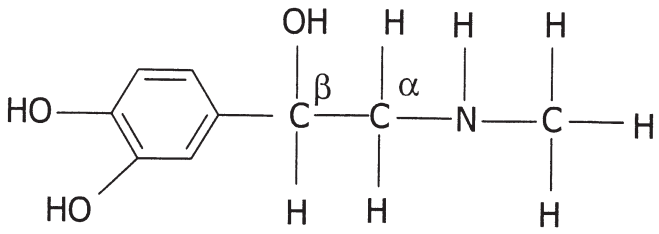

FIGURE 1. Scheme of adrenaline molecule.

Fluorescence spectroscopy provides a variety of ways to obtain information about the properties of the molecules. The changes in fluorescence intensity, shift of the peak maximum or changes in polarization can be used to follow the chemical reaction or determine the microenvironment of the excited molecule. More detailed information about adrenaline conformation and dynamic properties of the fluorophore in local microenvironment can be evaluated through time-resolved fluorescence intensity and anisotropy decays on the subnano- and nanosecond scale (12).

Adrenaline, (Figure 1) with a pKa equal to 8.59 where deprotonation at hydroxyl group occurs (6), belongs to biogenic catecholamines which play important functions in the brain and in the nervous system (11, 20). Adrenaline is found mainly in the adrenal medulla and it is readily released by physiological stimulation and is known as the "emergency hormone". There exists also the minor pathway, which transforms adrenaline into adreno-melanine, an important component of *substatnia nigra* in brain (2, 5). The other catecholamines, like dopa which is an important intermediate in melanine formation (16, 23) or dopamine and nor-adrenaline which play an important role in such diseases as schizophrenia (7, 21) and Parkinson's disease (1, 15, 18) are widely distributed in the body. Most of the catecholamines are intrinsically fluorescent and this technique was used to study their occurrence and distribution in cells; however, very little is known about the fluorescence or absorbance characteristic of adrenaline itself. Such information about molecules is a necessary step during new drug design or drug encapsulation in microstructures. In view of the multiple roles played by adrenaline in the nervous system, adrenaline fluorescence could prove to be a convenient tool for physiological and biochemical studies involving that hormone. The first step to approaching the problem of receptor binding was a thorough examination of fluorescence characteristics of the potential receptor in a nonpolar environment so that one would be able to mimic the changes that could take place during binding. Luckily a number of compounds like catecholamines, serotonin or propranolol are intrinsically fluorescent which allows their use as 'endogenic reporters' of local environment.

In this work the detailed spectroscopic studies in homogeneous solvents and in micellar environment were carried out in order to study structural and dynamic properties of adrenaline in organized media.

Materials and Methods

Adrenaline, cyclohexane, (α,β,γ — cyclodextrins, all alcohols, sodium dodecyl sulphate, SDS, (anionic) and tetrado-decyltrimethyl-ammonium bromide, TDABr, (cationic) deter-

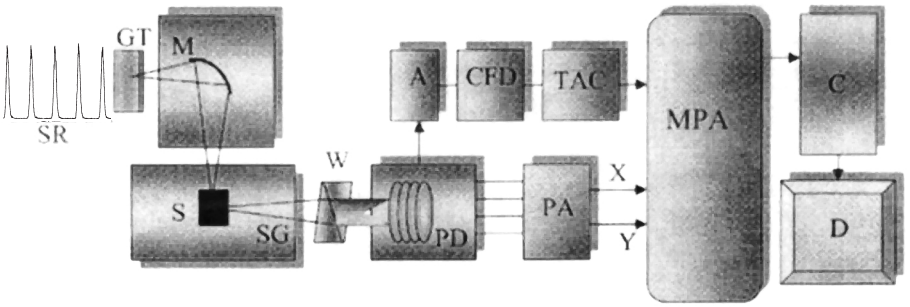

FIGURE 2. Scheme of the apparatus used for the fluorescence lifetimes and anisotropy measurements at port U9B at NSLS at BNL; SR—synchrotron radiation, GT—Glan Thompson polarizer, M—Spex 1680 monochromator, S—sample, SG—imaging spectrograph (Chromex), W—Wollaston polarizer, PD—position sensitive detector ITT F4164M, PA—position analyzer, A—fast amplifier model 1762 (PRA), CFD—constant fraction discriminator 583 (EG&G Ortec), TAC—time to amplitude converter 467 (Ortec), MPA—multiparametric analyzer CISE 904 (Canberra), C—PC computer, D—display.

gents and membrane lipid dioctadecyl dimethyl ammonium bromide (DODAB) were purchased from Sigma Chemical Co. (St. Louis, MO). Membranes were prepared from DODAB using the typical procedure. First, lipid and adrenaline were dissolved in chloroform:ethanol 2:1 mixture. Then the sample was evaporated and the film obtained was incubated with appropriate buffer solution. Next the sample was sonicated from 5 to 10 min with 50 W power. After cooling to room temperature the sample solution was centrifuged at 3000 rev/min. Obtained membranes were used for further measurements. The choice of DODAB micelle comes from the fact that this membrane does not show any fluorescence. Red blood cell membranes (RBC) were prepared by a standard method and were a generous gift from Dr. Dwight Norman from Stony Brook University, NY. Solvents used were of analytical or spectroscopic grade. All reagents were used without further purification and studied at 20°C. Water in aqueous solutions was purified through a millipore filter from Milli-Q system (Bedford, MA). Buffers used: 50 mM sodium acetate (pH 2–5) and 50 mM sodium phosphate (pH 5–9). Micelles concentrations were 10 fold of their cmc values. In order to avoid autooxidation of adrenaline most of the measurements were done in the range of physiological pH, about 6. In the case of higher pH the sample was first purged with nitrogen and then filled with argon. In such conditions the reaction of the adrenaline deprotonation was reversible which clearly indicates that the peak with maximum at 294 nm is connected with the ionized form of adrenaline.

Absorption spectra were measured on a PhotoDiode spectrophotometer HP 3287. As a fluorescence quantum yield standard tryptophan with $\Phi = 0.13$ was used (4). Steady-state fluorescence was measured using a Shimadzu 5001 PC fluorimeter using 3 mm quartz cuvettes. Fluorescence lifetime and anisotropy measurements were taken at beamline U9B at the National Synchrotron Light Source at Brookhaven National Laboratory, Upton, NY, USA with an Omnilyzer. Omnilyzer is the 1997 *Research & Development Journal 100* prizewinner. The details of the apparatus and the method of calculation have been previously described (10) and the scheme of the system is given in Figure 2. Briefly, excitation light (SR) from the U9B, quartz-windowed, bending magnet port at the National Synchro-

tron Light Source was focused into a Spex Model 1680 0.227 m double monochromator (Spex Industries, Edison, NJ) fitted with a 1200 g/mm grating. The sample was contained in a 1 cm x 1 cm standard quartz fluorescence cuvette placed in a Model 1692 "T Box" (Spex Industries) sample chamber which allowed fluorescence detection in both right-angle and front-face geometries. The fluorescence was focused into a Model 250 Imaging Spectrograph (Chromex, Inc., Albuquerque, NM) and the spectrum dispersed across the 2.5 cm diameter bialkali (BA-1) photocathode of an ITT F4146M position sensitive detector (PD).

For the polarization measurements the Wollaston polarizer (W) separates the spectra of the two polarizations in opposite directions from the center of the photocathode perpendicular to the direction of spectral dispersion. Charge amplification is achieved by the five microchannel plate detectors. The imaging spectrograph (SG) was fitted with two selectable 150 g/mm gratings, blazed at 300 and 500 nm, allowing a spectral range of ca. 500 nm to be dispersed across the horizontal face. The charge pulse resulting from the photon-induced electron cascade is split proportionally among the four output corners of the detector's resistive anode, amplified, and routed to the position analyzer for coordinate analysis. The analog signal corresponding to the horizontal coordinate of the measured charge was digitized in a Model 8075M 100 MHz ADC (Canberra Industries, Meriden, CT) in SVA mode. In all of the experiments the detector was cooled to −25 °C to reduce dark counts. Reported spectra were not corrected for the detector's wavelength dependent quantum efficiency

Photon timing information was obtained by monitoring the current-induced voltage change after the last microchannel plate, at the "Z-Out" high-voltage BNC on the base of the detector. A RC circuit consisting of a 10 nF capacitor and 50 resistor were placed near the detector base. The signal from the RC circuit provided the "start" for a time-correlated single-photon counting experiment after amplification (×100) and discrimination in a Model 1762 Fast Amplifier/Discriminator (PRA, Ontario, Canada) (A) and Model 583 Constant Fraction Discriminator (EG&G Ortec, Oak Ridge, TN) (CFD). Typically, count rates of 500–5000 cps were obtained after proper discrimination. The "stop" signal was provided by a square wave signal with a frequency equal to 1/9 of the rf cavity frequency (53 MHz) and synchronized with the group of nine bunches in the ring. Thus, one "stop" is obtained for up to nine starts (typically 1 or 7), depending upon the number of electron bunches in the storage ring. A fast timing signal was derived with a Model 821 (LeCroy, Chestnut Ridge, NY) Quad Discriminator. This implementation of the "inverted" configuration has been previously described (22). The 2–3 ms duration analog signal from the Ortec Model 467 TAC is internally strobed to a Canberra 8075M 100 MHz Wilkinson ADC (PHA mode) (TAC) approximately 6 ms after a "stop" was received. In a given excitation cycle, both the digitized wavelength and timing information of the fluorescence photon are stored in the histogramming memory of a Canberra CISE 904 Multiparameter Analyzer operating in a multidependent mode (MPA). Typically 512×512 channels are used to store the wavelength and timing information. All data were collected with the synchrotron operating with a powered fourth-harmonic cavity. The measured full width at half-maximum (FWHM) of the instrument response was about 1 ns.

The obtained image is a representation of the histogramming memory in which the photon counts as a function of time and wavelength are stored. To obtain fluorescence decay all the traces from the histograms are integrated over the wavelength whereas the summation over the times gives the actual spectrum. The example of fluorescence decay,

excitation pulse and calculated fit to obtain fluorescence lifetime is given in Figure 3a. The deconvolution method with the non-linear least square Marquardt-Leveberg method fitting procedure was applied to calculate fluorescence lifetime parameters. Reduced chi-square value, residuals and autocorrelation of residuals were used to estimate the goodness of the fit. Rotational correlation times were obtained directly from the fit as shown in Figure 3b. The obtained results are given in Table II.

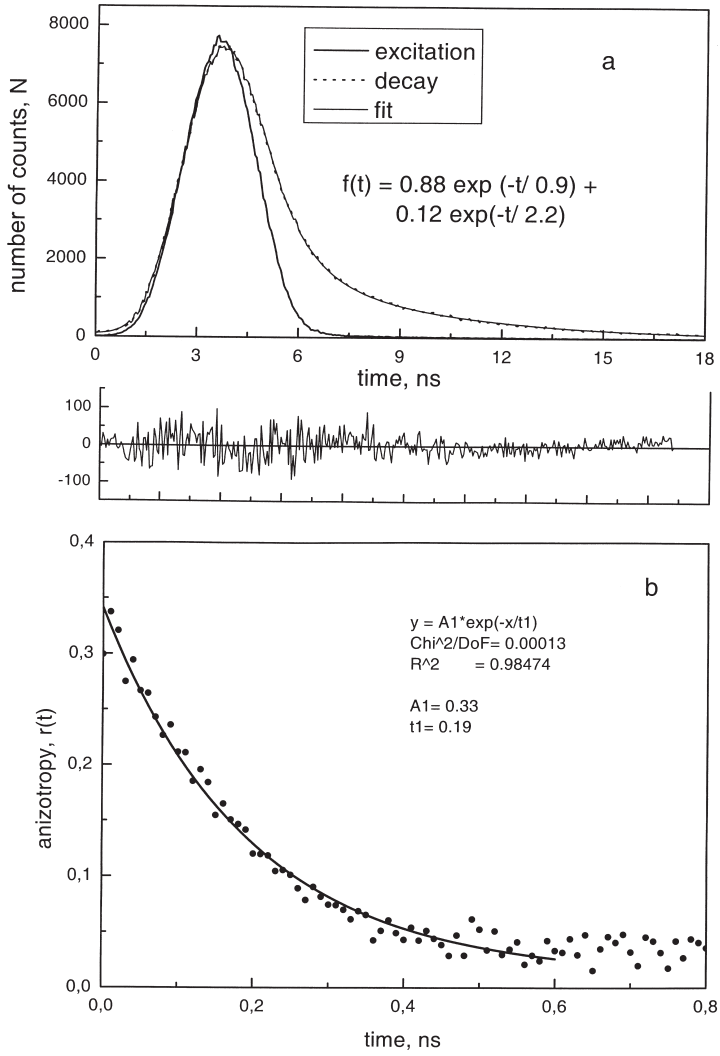

FIGURE 3. a) Fluorescence decay of $5x10^{-4}$ M adrenaline in β-cyclodextrine excited at 280 nm. Upper figure shows excitation profile, decay and fit to biexponential decay, 51 ps/channel, reduced chi square 1.28. Other parameters are given in on graph. Lower panel displays residuals of the fit.

b) Anisotropy decay of adrenaline in ethanol, solid line is fit to monoexponential decay with correlation rotational time τ_r = 0.19 ns. Other parameters are given on graph.

Results

Absorption and fluorescence measurements

Absorption and fluorescence properties of adrenaline in different solvents and micells are collected in Table I. From that Table it is seen that decreasing dielectric constant of the solvent results in batochromic shift of absorbance maximum, from 279 nm in water to 284 nm in dioxane ($\varepsilon = 2.2$). In heterogeneous environment the biggest absorbance maximum shift with $\lambda_{max} = 281$ nm is observed for adrenaline in anionic micelle, SDS. In the buffered aqueous solvents from pH 2 to 8 the absorption spectrum does not change. At higher pH the lowest absorption maximum is shifted from 279 nm to 294 nm. The positions of fluorescence maxima and fluorescence quantum yield also depend on the protic and dielectric properties of the solvent. The position of maximum emission changes from 316 nm in water and alcohols to 306 nm in cyclo-hexane. The fact that the position of the maximum fluorescence in water and in aqueous micelles does coincide with those observed in alcohols, regardless of their lower dielectric constant, indicates that some other interaction occurs in the micellar systems. The problem will be discussed in more detail in the next section *Dielectric environment study.* It is also seen that the position of the absorbance and fluorescence peaks depends on the ionization state of the adrenaline molecule. Above pH 8.5, where the deprotonation of the phenolic hydrogen occurs, the formation of anionic form of adrenaline is observed. Those changes in the electron charge distribution cause the absorption maximum shift to 294 nm and the molecule becomes nonfluorescent. Neutral adrenaline interacts with both micelles with negatively charged SDS and positively charged TTABr demonstrated by the shift in absorbance position and the changes in fluorescence quantum yield compared to homogeneous aqueous solutions. However, the observed changes are more pronounced for adrenaline in SDS micelle than in TTABr micelle.

It is worth noticing that increasing concentration, up to 10^{-3} M, of adrenaline does not change the position of absorption and emission maxima indicating that adrenaline in aqueous solvents exists as a monomer. Ison (8) who investigated adrenaline in aqueous solutions using NMR methods gave a similar conclusion. This finding is important from a physiological point of view because dimerization leaves adrenaline devoid of hormonal properties.

Dielectric environment study

In order to estimate the nature of the binding site of adrenaline in different environment the Lippert equation has been used to correlate the Stokes shift with polarity of the homogeneous solvents. Such correlation has been found for the alcohols and aqueous solutions. The Lippert plot based on the data from Table I is presented in Figure 4. The plotted data are split into two regions, one with a negative slope which represents alcohols only and the other with a positive slope which represents methanol-water mixtures and micelles. The observed difference between those regions is connected mainly with the presence of water. In methanol-water mixtures, the water molecule is acting as an hydrogen bond donor to the lone pair of the terminal amino group in adrenaline. This leads in aqueous solutions to the formation of ground electronic state hydrogen bonding complexes.

In alcohols the spectroscopic properties of adrenaline respond to changing dielectric environment. However, the negative slope indicates that some other interactions must

TABLE I. Spectral properties of adrenaline in different polar environment ε, positions of absorbance maxima A, emission maxima F and calculated Stokes shift ΔI.

Environment	ε	A [nm] /[cm^{-1}]		F [nm]/ [cm^{-1}]		ΔI[cm^{-1}]
Buffer pH 6	80	279	35842	316	31645	4195
Buffer pH 9.5	80	294	34015	non-fluorescent		—
TTABr, pH 6	56	280.5	35650	315.5	31695	3985
SDS, pH 6	40	281	35587	315	31746	3840
Methanol	32	282	35570	315	31746	3840
Ethanol	24	281.5	35520	315	31746	3805
Propanol	20	282	35590	316.3	31620	3840
Dioxane	2.2	284	35210	308	32258	2740
Cyclohexane	2.2	284	35200	306	32679	2530
β-cyclo-dextrin	46	281	35590	315	31746	3820

TABLE II. Photophysical parameters of adrenaline in various media; fluorescence lifetime τ[ns] (in case of biexponential decay preexponential factors in parenthesis are given), quantum yield Φ; radiative rate constant $k_{fl} * 10^8$ [s^{-1}], non-radiative rate constant $k_{nr} * 10^9$ [s^{-1}]; rotational correlation time τ_r[ns].

Environment	τ 0.05 [ns] (α_1/α_2)	Φ	k_{fl} [s^{-1}]	k_{nr} [s^{-1}]	τ_r [ns] + FWHM
Buffer pH 6	0.87	0.051	0.58	10.9	0.11±0.06
TTABr	0.9/1.96 (0.96/0.05)	0.07	0.4	4.7	0.12±0.08
SDS	0.9/1.67 (0.67/0.33)	0.09	0.54	5.4	0.12±0.07 β_1=0.25 0.54±0.11 β_2=0.3
Methanol	1.95	0.055	0.28	4.12	0.19±0.06
Ethanol	2.11	0.072	0.34	4.35	0.18±0.06
Propanol	2.2	0.12	0.5	4.0	0.11±0.06
Dioxane	2.1/4.1 (0.78/0.22)	0.2	0.5	2.1	0.1±0.05
Cyclohexane	1.9/3.45 (0.81/0.19	0.19	0.55	2.3	0.1±0.05
β-cyclo-dextrin	0.9/2.2 (0.88/0.12)	0.09	0.4	4.1	0.14±0.08

Note: in case of rotational correlation times τ_r preexponential factors in the fitting two exponential curve were denoted as β_1 and β_2 not to be mistaken for preexponential factors calculated for biexponential fluorescence decays and given in Table II as α_1 and α_2.

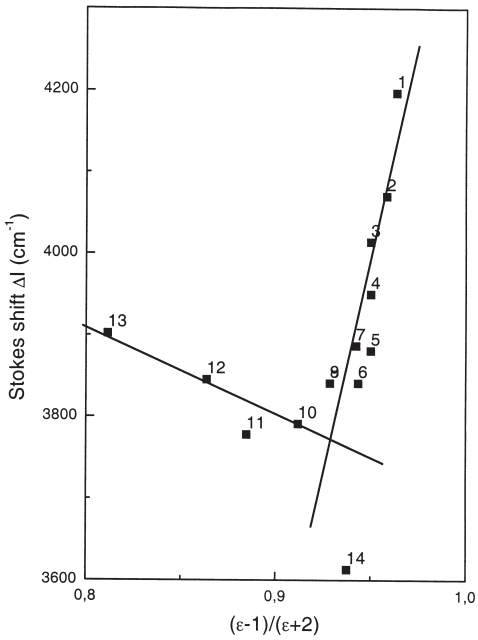

FIGURE 4. Stokes shifts of adrenaline *versus* Lippert function: (2ε–l)/2(ε+1) in: **1**-water, **2**-1Me:4W, **3**-TTABr, **4**-2Me:3W, **5**-membrane, **6**-RBC, **7**-3Me:2W, **8**-SDS, **9**-4Me:1W, **10**-methanol, **11**-ethanol, **12**-propanol, **13**-pentanol, **14**-β-cyclodextrin; where Me-methanol, W-water.

TABLE III. Parameters to calculate rotational correlation time of SDS and TTABr micelles

Medium	Viscosity Ns/m2 10^{-3}	Radius m 10^{-9}	Volume m^3 10^{-26}	Rotational correlation time 10^{-9}
Water	0.98	0.33	0.046	0.1
SDS	2.7	1.8	2.4	15.9
TTABr	5.01	1.9	2.9	35

occur in alcohols, very probably hydrogen bonding of the solvent with adrenaline. As may be seen from Table I in dioxane or in cyclohexane, both nonprotic solvents, the Stokes shift is much lower than that observed for the alcohols and does not show any correlation to the alcohols.

Using the existing linear dependence between Stokes shift of adrenaline and dielectric constant of water-methanol mixtures it was possible to estimate dielectric environment of adrenaline in micelles. The line describing Stokes shift data in the aqueous environment gives a linear equation expressed as $\nu_a - \nu_f = 3380 + 6.9*D$. This equation allowed us to calculate the dielectric constant of micellar environment where adrenaline is present in SDS

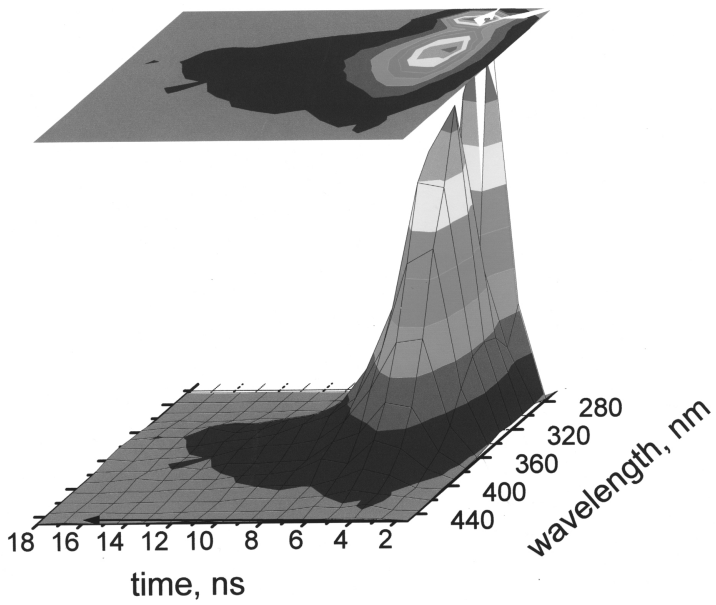

FIGURE 5. 3D and contour presentation of fluorescence decay and fluorescence spectra of 0.4 mM adrenaline in 50 mM SDS micelle, excitation wavelength λ_{ex} = 280 nm.

or TTABr. The constants are 40 and 56, respectively. Considering the dielectric constant of the micellar core is about 2 and that of water is 80 our calculated dielectric constant values for micelles indicate that adrenaline seems to be located in the interface region of those media. From Figure 4 we are able to determine the extent of polar environment and hydrogen bonding interaction. We can then estimate the properties of the binding site in micelles. The data given in Table I indicate that apart from the solvent polarity the binding of adrenaline in both micelles is connected with the formation of hydrogen bonding involving water molecules. Compared to previously obtained polarity values for polar and hydrophobic probes in SDS and TTABr given in literature (3, 9, 13, 14, 19) our values are in better agreement with those for SDS. In the case of TTABr, electrostatic repulsion between positively charged micellar surface and positively charged amino nitrogen displace adrenaline molecules into the Gouy-Chapman layer where interactions with counterions may occur. However, the obtained results reflect the fact that neutral adrenaline molecule in micelle resides in a more polar and protic environment and the interactions are limited to the Guy-Chapman layer without deeper penetration into the micellar hydrophobic core.

Fluorescence and anisotropy decay.

In order to probe the dynamics of adrenaline in microenvironment in different media the fluorescence lifetimes and fluorescence rotational correlation times were calculated. The obtained results are presented in Table II whereas the example of 3 dimensional presentation of simultaneous fluorescence spectrum and fluorescence decay taken with the Omnilyzer is given in Figure 5. The details of the calculations are given in Materials and Methods.

In all homogeneous solvents the fluorescence decay of adrenaline is singly exponential. In aqueous solutions the fluorescence lifetime is 0.87 ns. The rotational correlation time of the molecule was found to be near 120 ps, which reflects the free rotation of a small molecular entity with solvated water molecules. In alcohols, the longer fluorescence lifetime describes adrenaline in lower polarity environment. Single rotational correlation time with maximum at 190 ps indicates that adrenaline rotates solvated by layer of solvent molecules. In aprotic solvents and micelles the fluorescence decay is biexponential. In dioxane or cyclohexane the main component of the fluorescence decay with lifetime of 1.9 ns results from the weaker interaction of the transition moment with aprotic solvent dipole compared to water. Calculated rotational correlation time at 100 ps describes free rotation of the emitting molecule in low polar, aprotic environment and indicates on the lower hindrance exerted by the solvent molecules on the rotating fluorescent molecule. This suggests that the minor component of fluorescence decay arise rather from the association of adrenaline molecules than from the other fluorescent site in the molecule. In anionic micelle, SDS, the shorter component with a lifetime of 0.87 ns is characteristic for the aqueous phase whereas the longer one 1.67 ns, describes the molecules located in the micellar environment. Two fluorescence lifetimes in both micelles indicate the partition of adrenaline between two phases, aqueous and micellar. The polarity studies located adrenaline in SDS close to 80:20 methanol-water mixture. In TTABr, the second component of the double exponential function is weak. On the polarity graph adrenaline in TTABr micelle is located close to 20:80 methanol-water mixture which indicates that very probably hydrated adrenaline is prevented from entering the micelle and is located rather in the Guy-Chapman layer which is more aqueous then the interior of the micelle. In cationic micelle, TTABr, at pH 6 only 2% of emitting molecules exhibit longer lifetime, 1.9 ns. The molecules with 0.87 ns lifetime fluoresce from aqueous environment.

Two rotational correlation times observed in SDS micelle are indications of two dynamical processes occurring in the system. Longer rotational correlation time, 0.54 ns, is connected with the reduced rotational freedom of adrenaline, probably due to the higher viscosity and confined space in micelle. The shorter rotational correlation time, 0.12 ns, describes free rotation of hydrated adrenaline in aqueous phase. To estimate the interaction of adrenaline with micelle the calculation of rotational correlation time of both micelles have been carried out. Data on viscosity and radius of the micelles used in the calculation are given in Table III. With spherical approximation for the both micelles using Debye-Stokes-Einstein equation the calculated rotational correlation times are 15.9 ns for SDS and 35 ns for TTABr. Unfortunately, our rotational correlation time analysis is limited to a few nanoseconds and we cannot see such long rotational correlation times of adrenaline. The calculations also have shown that relatively slow rotation of the micelles makes a negligible contribution to the adrenaline decays observed in the nanosecond range. Additionally, steady-state anisotropy values for micelles are 0.08 and 0.05 for SDS and TTABr, respectively. This indicates that there are no other depolarization processes occurring.

An increase in fluorescence quantum efficiency and lifetimes is observed in micelles. This is in agreement with our results from dielectric studies, which show the adrenaline in micelles is located in lower polarity environment and still is influenced by hydrogen bonding from water. Higher values ϕ (quantum yield), τ (fluorescence lifetime) and lower values of k_{nr} (non-radioactive rate constant) in micelles compared to water suggests that adrenaline occupies more viscous but rather polar and protic environment in those media.

Discussion

The measured and calculated photophysical parameters of adrenaline in different media are summarized in Table II. All data given in the Table II are sensitive to polarity and viscosity of the environment. However, one can expect that changes in quantum yield or fluorescence lifetime should be larger when adrenaline is in low polarity or heterogeneous environment. The presence in adrenaline structure of the ethylamino tail should be considered as a main pathway of the radiationless processes; k_{nr} changes in all media is within 10% except for water. Lower than expected values of fluorescence quantum yield and fluorescence lifetimes are probably connected with the fact that the amino tail has less torsional freedom mainly because of the interaction between the benzoic ring and the nitrogen lone pair from its own amino group. In aqueous solutions the hydration through the formation of hydrogen bonds with hydroxyl groups and ethylamino tail gain more torsional freedom because the interaction between nitrogen and the aromatic ring is screened by the water molecules which increases radiationless process. The support for such a picture is given by NMR study of catecholamines in aqueous solutions (8) showing that in the adrenaline amino group is in *trans* position to the aromatic ring and *gauche* to the β-hydroxyl group which stabilizes the whole molecule. The main interaction is shown to be electrostatic with hydrogen bonding between the amino and β-hydroxyl group.

The neutral adrenaline, which is less hydrophobic than ionic forms, is barely solubilized in TIFABr coming from the fact that the quaternary nitrogen group is more hydrophobic then the sulfate group in SDS. Moreover, a longer alkyl chain, which offers polarity equivalent to cyclohexane, and a positively charged surface, which should destabilize any cationic species, are very probably main factors that adrenaline is less solubilized in TTABr compared to SDS.

Spectral correlation of adrenaline with the polarity parameters in alcohols and methanol-water mixtures allowed us to determine the polarity and the nature of the binding sites in micelles. Additionally, the dielectric constant value at the adrenaline location was estimated. It has also been shown that hydrogen bonding plays a role during solubilization of the molecule in the micellar environment. Fluorescence and anisotropy decay measurements and the other photophysical parameters given in Table II have shown that in aqueous micellar environment adrenaline fluoresces from two sites. In principle, the anisotropy decay should be given by the sum of five exponentials. The fact that anisotropies in homogeneous solvents are well fitted by single exponential decay function suggests that these molecules can be modeled ellipsoids or spheres. Based on the Debye-Stokes-Einstein equation the calculated hydrodynamic radius is between 3 to 4 Å. This is the case with adrenaline where in all homogenous solutions one rotational correlation time was found. The observation of two distinct correlation times in the anisotropy decays in micelle implies the existence of two dynamic processes that occur with different mechanisms. One obvious explanation is that the short component arises from the rotational diffusion of the free dye in solution and longer time arises from micelle-bound dye. We should remember that micelle-bound adrenaline resides in the Gouy-Chapman layer and its binding to micellar core is weak. Such behavior seems to reflect biological situation where adrenaline despite many possible targets effectively binds only to a specific receptor. If the partitioning between water and micelle were correct then the ratio of preexponential factors would then give the ratio of free to micelle-bound dye. This has been

confirmed by the fluorescence lifetime measurements where the obtained ratio in SDS is similar to that calculated from dielectric studies.

These studies have shown that the applied model describing the process of the adrenaline partition between aqueous and heterogeneous phase gives structural and dynamical parameters that are physically reasonable and will be exploited during our further studies of adrenaline in heterogeneous systems.

Special thanks to Dr. J.C. Sutherland from Biology Dept. at Brookhaven National Laboratory for his support and assistance of his Lab staff during measurements at U9B port at National Synchrotron Light Source. Brookhaven National Laboratory is supported by the US Department of Energy, Office of Materials Sciences and Office of Chemical Sciences; the spectrometer at U9B is supported by the Office of Health and Environmental Research, US Department of Energy. This work was supported by grant DS 508/82-2 from the Agricultural University of Poznan, Poland.

References

1. Adams, J.D.J. and Odunze, I.N. (1991) Oxygen free radicals and Parkinson's disease., *Free Rad. Biol. Med. 10:* 161–169.
2. d'Ischia, M., Palumbo, A. and Prota, G. (1988) Adrenaline oxidation revisited. New products beyond the adrenochrome stage. *Tetrahedron 44*: 6441–6446.
3. Drummond, C.J., Grieser, F. and Healy, T.W. (1986) Faraday Discuss. *Chem. Soc. 81:* 95.
4. Eftink, M.R. (1991) Fluorescence techniques for studying protein structures. In: *Methods in Biochemical Analysis*, Suelter, C.H., Editor, John Wiley & Sons, New York pp. 127–205.
5. Graham, D.G. (1979) On the origin and significance of neuromelanin. *Arch. Pathol. Lab. Med. 103:* 359–362.
6. Hansch, C. and Leo, A. (1985) Medchem. Project Issue 26, Pomona College, Clermont, CA.
7. Hegedus, Z.L. and Altschule, M.D. (1970) Studies on aminochromes. IV. Hemolysis associated with the transformation of l-epinephrine, adrenochrome and adrenolutin into rheomelanins in human whole blood. *Arch. Int. Pharmacodyn. Ther. 186(1):* 39–47.
8. Ison, R.R., Partington, P., Roberts, G.C. (1973) The conformation of catecholamines and related compounds in solution. *Mol. Pharmacol. 6(9):* 756–765.
9. Kalyanasundaram, K. and Thomas, J.K. (1977) Solvent-dependent fluorescence of pyrene-3-carboxyaldehyde and its application in the estimation of polarity at micelle-water interface. *J. Phys. Chem. 81:* 2176.
10. Kelly, L.A., Trunk, J.G., Polewski, K., Sutherland, J.C. (1995) Simultaneous resolution of spectral and temporal properties of UV and visible fluorescence using single-photon counting with a position-sensitive detector. *Rev. Sci. Instrum. 66(2):* 1496–1498.
11. Kopin, I.J. (1985) Catecholamine metabolism: Basic aspects and clinical significance. *Pharm. Rev. 3:* 333–386.
12. Lakowicz, J.R. (1983) *Principles of Fluorescence Spectroscopy*. New York and London: Plenum Press.
13. Law, K.Y. (1981) Fluorescence prob from microenvironments. A new probe for micelle solvent parameters and premicellar aggregates. *Photochem. Photobiol. 33:* 799.
14. Mukherjee, P. and Cardinal, J. (1978) Benzene derivatives and naphthalene solubilized in micells. Polarity of microenvironment, location and distribution in micells and correlation with surface activity in hydrocarbon-water system. *J. Phys. Chem. 82:* 1676.
15. Palumbo, A., d'Ischia, M., Misuraca, G. and Prota, G. (1989) A new look at the rearrangement of adrenochrome under biomimetic conditions. *Biochim. Biophys. Acta. 990(3):* 297–302.

16. Pileblad, E., Slivka, A., Bratvold, D. and Cohen, G. (1988) Studies on the autooxidation of dopamine: Interaction with ascorbate. *Arch. Biochem. Biophys. 263:* 447–452.
17. Polewski, K. (2000) Spectroscopic detection of adrenaline-quinone formation in micelles., *Biophys. Biochem. Acta. 1519(1):* 56–64.
18. Prota, G. (1989) Melanin and pigmentation. In: Glutathione, Chemical, Biochemical and Medical Aspects Part B. Dolphin, D., Avramovich, O., Paulson, R., Editors. John Wiley & Sons, New York, pp. 441–466.
19. Schanze, K.S., Shin, D.M. and Whitten, D.G. (1985) Micelle and vesicle stabilization sites. Determination of micropolarity and microviscosity using photophysics of dipolar olefin. *J. Am. Chem. Soc. 107:* 507.
20. Smythies, J. and Galzinga, L. (1998) The oxidative metabolism of catecholamines in the brain: a review. *Biochim. Biophys. Acta. 1380(2):* 159–162.
21. Smythies, J.R. (1997) Oxidative, reactions and schizophrenia: a review-discussion. *Schizophr. Res. 24(3):* 357–364.
22. Sutherland, J.C., Desmond, E.J. and Takacs, P.Z. (1980) Versatile spectrometer for experiments using synchrotron radiation at wavelengths greater than 100 nm. *Nuclear Instrumentation and Methods 172:* 194–199.
23. Van der Wende, C. and Spoerlein, M.T. (1963) Oxidation of dopamine to melanin by an enzyme of rat brain. *Life Sci. 2:* 386–392.

Received September 2, 2002;
accepted March 11, 2003.

Physiol. Chem. Phys. & Med. NMR (2003) *35*: 27–42

Melanocytes: Morphological Basis for an Exteroceptive Sensory System for Monitoring Ultraviolet Radiation

Arthur Dale Ericsson, MD[*], Jonathan Dora, MD, Shinian Cao, MD[**]

Institute of Biologic Research, 6560 Fannin, Suite 720, Houston, Texas 77030
**Director of the Institute of Biologic Research*
***Fellow in Pathology, University of Texas School of Medicine, Houston, Texas*

Abstract: From the conventional medical perspective, melanocytes have been traditionally viewed as epidermal responders/reactors to ultraviolet radiation. In this paper we have begun an analysis of the functional significance of melanocytes as monitors for ultraviolet radiation with their neuronal, endocrinological and immunological intercalations. This preliminary study was performed using as a human model unilateral sural nerve sensory blockade before and after ultraviolet exposure to both feet while the unblocked foot acted as the control. Full thickness surgical skin biopsies were taken of (*I*), normal pre-exposure skin, in the center of the two centimeter exposure area of both the sural nerve blocked area (*II–III*) and control (*IV–V*) one centimeter outside the exposed area in both the sural nerve blocked foot and the control or non-blocked foot. The objective clinical, blinded morphological and immuno-histochemical data from this experiment support the initial conclusion that neuronal connection is necessary for the normal ultraviolet exposure dermal reaction. Based upon this study, we further propose the existence of an exteroceptive sensory system in which melanocytes, with direct nervous system connection initiate an ultraviolet radiation reactive response that mobilizes both conventional endocrine and immune pathways.

MELANOCYTES THAT are found throughout the skin differentiate from neural crest cells, detach from the neural tube in the sixth week and migrate to the developing dermis of the embryo. (1, 2, 3) Although morphological and histological studies have not detected melanocytes in the human epidermis until the 10th or the 11th week, (4, 5) studies using monoclonal antibodies directed against antigens characteristic of melanocyte precursors have been identified in cells in the epidermis as early as the 6th or 7th week. (6) Thus it may take neural crest cells only a few days to a week to migrate to the epidermis. Melanocytes are also found in the dermis during fetal life, but the vast majority of these

are in transit to the epidermis. (7, 8) The density of melanocytes increases during fetal life, reaching a peak of 2,300 cells/mm^3 at the end of the third month, after which they decrease to a final value of about 2,000 cells/mm^3, representing between 5 and 10 percent of the cells of the basal layer of the epidermis in the adult. (9) In the 10th week many melanocytes become associated with the developing hair follicles where they function to donate pigment to the hair. (10) In the adult, melanocytes take a shape of a cell body deeper in the epidermis with dendrites extending more superficially in the layer, interdigitalizing with peripheral nerve fibers. (11) Due to the aforesaid, it has been traditionally thought that melanocytes function only as a sun-screen, thus protecting the deeper layers of the skin from solar radiation, however, our evidence will demonstrate melanocytes play an important additional role as neuronal sensors located in the skin. In addition to their role as sensors, melanocytes appear to control keratinocytic skin regeneration.

Melanocyte Study: Assertions

1. Melanocytes and Langerhan's cells in the skin are derived from embryonic neural crest tissue and migrate rather early in development to the skin: thus they are nerve cells. (3, 6)
2. Melanocytes have an unusual morphological appearance in which the cell body lies deepest in the epidermis and arms (podia or dendrites) extend more superficially: resembling Purkinje cells in the cerebellum. (12, 13, 14)
3. Extensive nerve fibers tranverse these podia. (15, 16, 17)
4. Melanocytes, using tyrosine as an amino acid precursor, manufacture melanin that is secreted and endocytosed by melanophores: a process which is not unlike the production of norepinephrine or dopamine. (18, 19)
5. After exposure to ultraviolet light there is a marked increase, locally restricted to the area of exposure of Langerhan's cells, antigen presenting cells (APC's) and lymphocytes. (21–23)
6. Langerhan's cells, when thus activated, become antigen presenting cells (APC'S). (24)
7. After exposure, these APC's migrate to regional nodes and/or to the thymus gland for presentation to naïve T lymphocytes. (25–27)

Hypothesis for this study

There is a melanocyte-nervous system connection that represents the exteroceptive sensory system in which ultraviolet and/or not to exclude other radiation energy is monitored and a reaction is orchestrated by these cells in concert with the central nervous system.

Corollary: It is this exteroceptive sensory system when activated by ultraviolet radiation that coordinates the nervous and immune/endrocrine system activity for protection of the organism.

Basic Energy from Sunlight and Ultraviolet Source

1. *Energy from sunlight has wavelengths from 300–700 nm and a mean of 550 nm.* (20)
2. *Energy derived from sunlight may be calculated as* ***51,881 calories/mol or 52 Kcal/mol*** (17)

$$\text{Energy} = \frac{\textit{Avogadro's Number} \times \textit{Plank's Constant} \times \textit{Velocity of Light}}{\text{Wavelength of Sunlight}}$$

3. Ultraviolet source of 800 watts 375 nm UV 93 that is produced by the Sperti Sunlamp used in this study.

Methods

Melanocyte Study Design: The skin supplied by the Sural Nerve bilaterally on the dorsum of both feet was selected:

1. Surgical biopsy of the dorso-lateral portion of the left foot taken as a baseline control.
2. Right Sural nerve block using plain 1% xylocaine producing an area of anesthesia over the dorsal lateral portion of the right foot.
3. Circular area of 2 cm exposure on the exact same dorso — lateral surface of both feet — the left without a nerve block and the right with a nerve block.
4. Irradiation of a circular area of 2 cm on both feet with UV radiation (15 cm from the surface) at 375 nm for 10 minutes.
5. Repeat surgical biopsy (immediately following irradiation) of the dorsum of both feet as follows:
    A. Control biopsy of left foot (slides Ia–Ie)
    B. Biopsy of right (Sural Nerve blocked) foot center of UV lesion (slides IIa–IId)
    C. Biopsy of left (control) foot center of UV lesion (slides IIIa–IIIe)
    D. Biopsy of right (Sural Nerve blocked) foot 1 cm outside of UV lesion (slides IVa–IVe)
    E. Punch biopsy of left (control) foot 1 cm outside of UV lesion (slides Va–Ve)
    F. Present each biopsy specimen for coded/blinded for processing

Morphological Observations and Study Measurements

Histological Studies

All histological studies were performed by an independent observer and special stains were used to define the histological characteristics as summarized in the table.

a. Structure: Cell definition of epidermis and dermis and cyto-architecture.
b. Migrating cells: APC's, Langerhan's and melanocyte cells, macrophages, plasma cells, eosinophils, and lymphocytes.
c. Comparison of the migrating cells by maximal specific immuno-histochemical stain positive cells at 40X field under strict double blind observation.

Results

A. Clinical Observations

1. The immediate area of inflammation (redness) and slight swelling was measured at 1.5 cm over the left (non-blocked) foot.
    a. Control before ultraviolet radiation: slides Ia–Ie.
    b. Center of ultraviolet radiation: slides IIIa–IIIe.
    c. 1 cm outside of the area of ultraviolet radiation: slides Va–Ve.
2. The area of inflammation (redness) and moderate swelling was measured as 4 x 6 cm over the right (Sural Nerve blocked) foot.
    a. Center of ultraviolet irradiation: slides IIa–IIe.
    b. 1 cm, outside of area of ultraviolet radiation: slides IVa–IVe.
3. These areas remained inflamed and swollen for 3 days then gradually receded.

B. Histological Studies

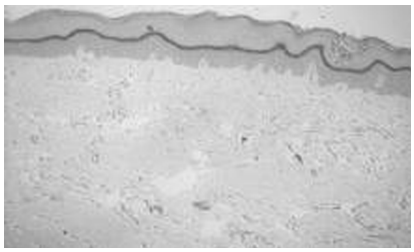

Ia. Baseline normal control Hematoxylin and Eosin (H&E) Stain: Pre-exposure-left foot

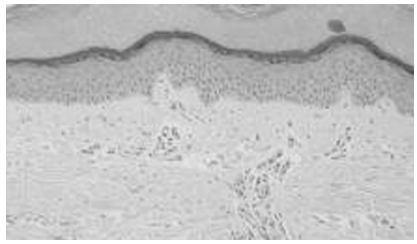

Ib. H&E Stain: Enlarged section

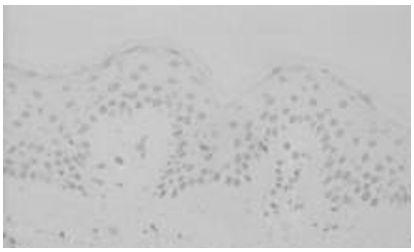

Ic. CD1a cell stain: Langerhan's cells

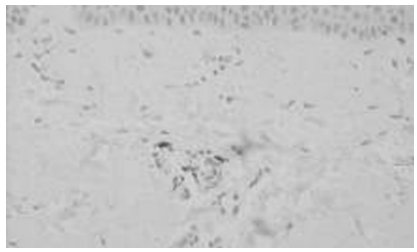

Id. CD3 T cell stain: Antigen Presenting Cells (APC Cells)

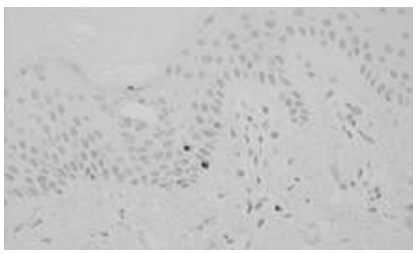

Ie. S-100 Stain: Melanocytes and Langerhan's Cells

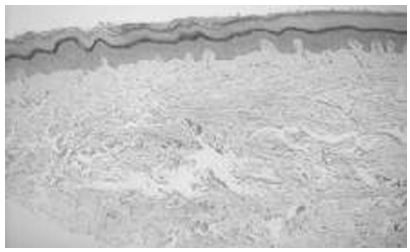

IIa. H&E stain: Center of 2 cm exposure on dorsum of the Sural Nerve blocked foot: note marked edema

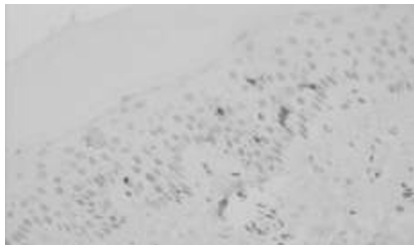

IIb. CD 1a Stain: Langerhan's Cells-note marked increase in number of Langerhan's cells

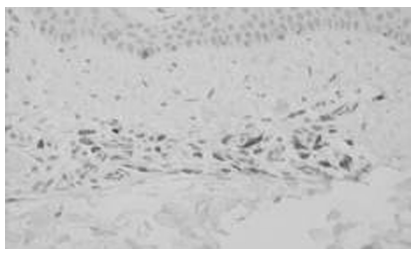

IIc. CD-3 Stain: APC Cells-note the marked increase in number of APC's and melanin

IId. S-100 Stain: Melanocytes and Langerhan's Cells

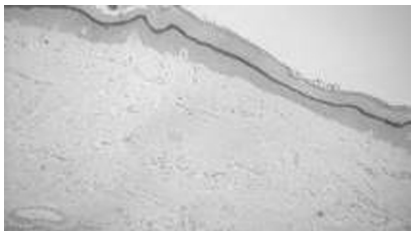

IIIa. H&E Stain: Center of 2 cm exposure in dorsum control foot

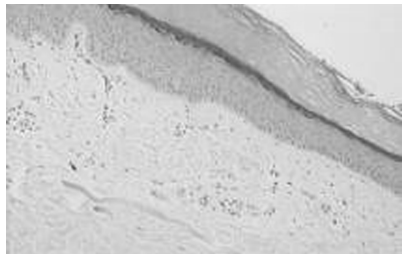

IIIb. H&E Stain: Enlarged Section-note only slight edema

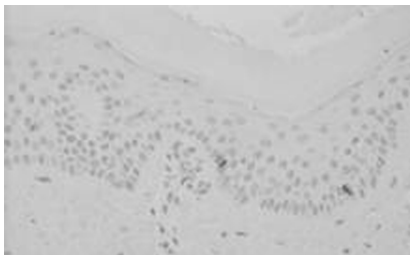

IIIc. CD 1a Stain: Langerhan's Cells-note only slight increase in the number of Langerhan's cells

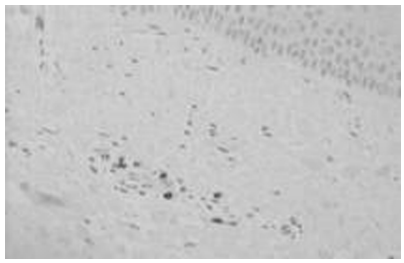

IIId. CD-3 Stain: APC Cells-note only slight increase in the number of APC's and melanin

IIIe. S-100 Stain: Melanocytes and Langerhan's Cells

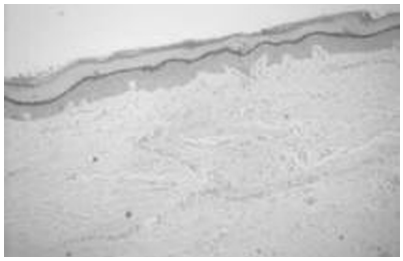

IVa. H&E stain: 1 cm dorsal to area of exposure on Sural Nerve blocked foot

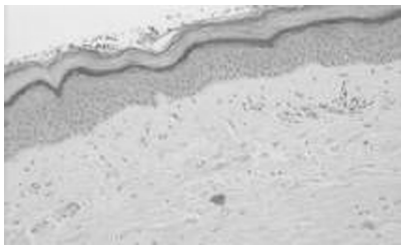

IVb. Enlarged Section H&E Stain-note increased amount of edema

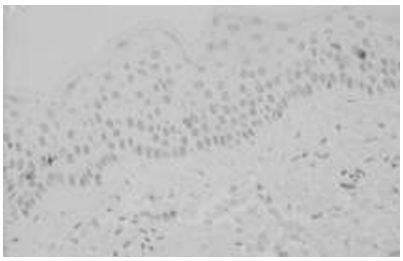

IVc. CD 1a Stain: Langerhan's Cells-note marked increase in the number of Langerhan's cells

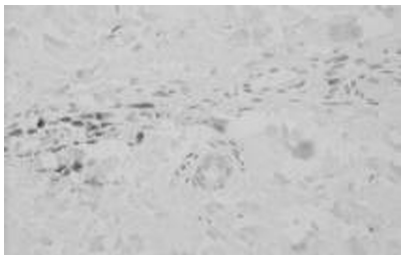

IVd. CD3 Stain: APC's Cells-note marked increase in number of APC's and increased melanin

IVe. S-100 Stain: Melanocytes and Langerhan's Cells

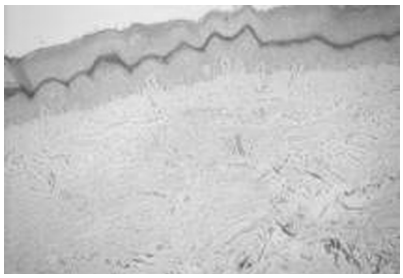

Va. H&E Stain: 1 cm dorsal to area of exposure on control foot

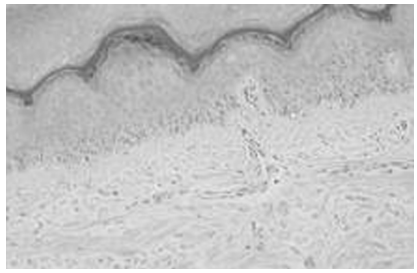

Vb. H&E Stain: Enlarged Section-note almost no edema

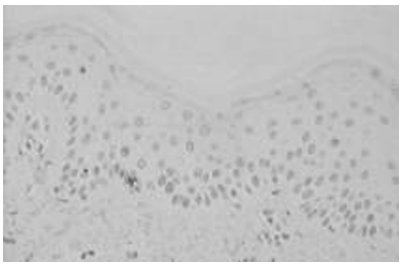

Vc. CD 1a Stain: Langerhan's Cells-note only slight increase in the number of Langerhan's cells

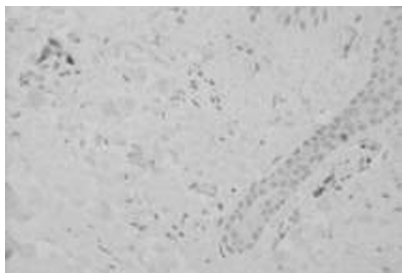

Vd. CD 3 Stain: APC Cells-note normal appearance or slight increase in the number of APC's

Ve. S-100 Stain: Melanocytes and Langerhan's Cells

Discussion

Biosynthesis of melanin

Synthesized from the essential amino acid phenylalanine, tyrosine serves as the precursor to many compounds which include hormones (thyroxine and melanin), neurotransmitters (norepinephrine, dopamine and epinephrine) and, more importantly, as cellular signal transduction catalytic receptors (tyrosine kinase). (28) The basic amino acid precursor of all of these reactions is phenylalanine, which is readily absorbed in the gastrointestinal tract. Following absorption, the first chemical biosynthesis in the body is that of hydroxylation in which l-tyrosine is formed. Phenylalanine hydroxylase is the enzyme responsible for the reaction. (29) The second chemical reaction is catalyzed by tyrosine hydroxylase and the product of this reaction is 3, 4-dihydrozxyphenylalanine (L-DOPA). Dopa decarboxylase is utilized as the catalyst by which DOPA is transformed into dopamine and hydroxylated into norepinephrine and finally, transmethylated into epinephrine. Another enzyme, tyrosine aminotransferase (tyrosine transaminase) mediates the deamination of tyrosine and, as with many other aminotransferases; alpha ketoglutarate is the amino acceptor. This intracellular process may be induced by the administration of steroid hormones, which leads to an increase in messenger ribonucleic acid (mRNA) for the enzyme. Melanocytes are not attached to keratinocytes by desmosomes, but they are attached to the basal lamina by hemidesmosomes. (30) They produce melanin, a pigment, which protects the nuclei of the dividing cell from the mutating effects of ionizing or electromagnetic radiation. The melanin is transferred *via* dendritic processes to basal keratinocytes and accumulates above the nucleus and shields the dividing nuclei from the harmful effects of ultraviolet radiation. (31)

The melanins form free radicals and this may be significant in the cellular protection from radiation. The enzyme tyrosinase produces an aerobic oxidation to 3, 4 dihydroxyphenlalanine (DOPA) and tyrosinase continues to act on DOPA to produce dopaquinone, which is converted to melanin (eu or pheo). Melanin pigment is formed by additional reaction with tyrosinase in the dendritic processes of the melanocytes. Within keratinocyte cells the melanin tends to be distributed, initially, in perinuclear caps. Melanocytes, as compared with other skin cells, have a limited capacity to proliferate and it is rare to find these cells dividing.

Melanosomes are membrane bound granules in the cytoplasm of melanocytes. Tyrosinase vesicles fuse with premelanosomes to form melanosomes. Tyrosinase is synthesized in the rough endoplasmic reticulum (rER) and moves to the Golgi region. It forms tyrosinase vesicles, which then fuse with premelanosomes. (28) The enzyme action matures the content to melanosomes, or melanin containing granules. The tips of the dendritic processes of melanocytes containing the membrane bound melanosomes are broken off and phagocytosed (clatherin endocytosis) by keratinocytes. (29) This mechanism, whereby the melanosomes are secreted, similar to neurotransmitter emission, is called *cytocrine secretion.* Melanin production can be stimulated by the hormone MSH (melanocyte stimulating hormone), by estrogen and progesterone in pregnancy, and by chronic exposure to sunlight. (32) Human melanocytes from individuals with different skin types, as well as from the skin of the same individual, are heterogeneous in their melanin content. This heterogeneity may be attributed to differences in the activity and expression of the three-melanogenic proteins: tyrosinase and tyrosinase-related proteins 1

and 2 (gp75 and DOPA chrome tautomerase, respectively) (33), which in turn are affected by certain regulatory factors. There is a direct correlation between melanin content, tyrosinase activity and the expression of the three-melanogenic proteins in melanocyte strains established from different skin types. Addition of the two epidermal cytokines, tumor necrosis factor-alpha or interleukin-1alpha, to cultures of human melanocytes from different skin types causes decreased proliferation, tyrosinase activity and expression of tyrosinase, tyrosinase-related protein-1 and DOPA chrome tautomerase. Similar results may be obtained when Percoll-derived melanocyte subpopulations are treated with tumor necrosis factor-alpha and interleukin-alpha. These results indicate that the variation in melanin content in human melanocytes is due to the differences in the activity and expression of the melanogenic proteins, which are, in turn, influenced by autocrine and paracrine factors (chemokines or other cytokine receptor activators such as MSH). The local release of growth factors including epidermal growth factor, transforming growth factor and keratinogenic growth factor are all important for the process of continued regeneration of cells of the skin. Repair is dependent upon the local production and release of transforming growth factors B (1, 2, 3), transforming growth factor A, fibroblast growth factor, vascular endothelial growth factors, platelet derived growth factors, insulin like growth factors, keratinocytes growth factors and many other growth and differentiation co-factors. Substantiated animal studies have confirmed the role of cytokines and growth factors produced by cellular elements in the epidermis and dermis in the process of and enhancement of skin healing and wound remodeling. (33)

Melanocyte Stimulating Hormone (MSH)

Melanocyte stimulating hormone is synthesized by the intermediate lobe of the pituitary gland and is developed for a precursor called propiomelanocortin. (34) One form, alpha-MSH is identical to the first 13 amino acids of the amino terminal of Adreno-Cortical-Trophic-Hormone (ACTH). MSH is named for its direct effect on melanocytes of the epidermis. Animals (fish, amphibians, reptiles and humans) injected with alpha-MSH show a dramatic immediate darkening of the skin. Microscopically, melanocytes demonstrate melanin dispersed throughout the dendrites of these cells and into melanophores. (31) Granules of melanin may be seen traversing outward using kinesin as a carrier along the microtubules. They assemble in the actin-rich periphery of the cell and enter the melanophores along the microtubules using dynein as a carrier. (35, 36) During this latter event, the skin color appears to lighten. Moreover, alpha MSH is found in the brain where it also acts to suppress appetite and in clinical studies appears to increase penile erections. Control of the development of melanocyte stimulating hormone appears to be the T-pit/Tbx19 gene. (34) These data support the conception that there is a direct neuronal-melanocyte neuro-endocrine connection.

Melanin: Endocytosis by Keratinocytes

In stark contrast to phagocytosis of macromolecules, receptor mediated endocytosis provides the mechanism for selective uptake of small molecules. The receptors are specialized regions on the plasma membrane called clathrin-coated pits. These pits bud from the membrane to form small clathrin-coated vesicles. These clathrin-coated vesicles then fuse with endosomes and their contents are sorted. A specialized kind of recycling from endosomes plays an important role in the transmission of nerve impulses across synaptic junc-

tions. Melanocytes are displaced nerve cells. The arrival of the stimulus at the terminal dendritic arm of the melanocyte triggers the fusion of the synaptic vesicles containing melanin with the plasma membrane, thus releasing melanin. The keratinocyte then acts to phagocytize the melanin by receptor mediated endocytosis. (37) The synaptic vesicles are retrieved by endocytosis from the clathrin-coated pits and the endocytic vesicles fuse with the early endosomes of the melanocyte. The synaptic vesicles are then regenerated by budding from the endosome and refilled by the uptake of melanin from the cytosol of the melanocyte. A protein destined for the apical domain of the plasma membrane is first transported from the Golgi apparatus to the basolateral domain. It is the endocytosed and selectively transported to the apical domain from early endosomes.

Function of Melanin and Ultraviolet Light Exposure

As noted, the melanocytes differentiate from neural crest cells that detach from the neural tube and then migrate to the developing epidermis. A diverse number of structures are similarly derived from neural crest cells that migrate from the central nervous system. These include odontoblasts, connective tissue surrounding the eye, including the papillary and ciliary muscles, truncoconal septum of the heart and aorta, arteries of the head and neck, pharyngeal arch cartilages, adrenal medulla, autonomic chain ganglia, glial cells, Schwann cells, enteric ganglia, dorsal root ganglia, arachnoid and pia matter, neurosecretory cells of the heart and lungs, C cells of the thyroid gland and Hassell's corpuscles of the thymus gland. In each case the sensory, integrative and regulatory functions of these adult cells are similar. The fact that ultraviolet radiation stimulates melanocytes is hardly debatable; however, the fact that there is a radical change in localized migrating Langerhan's cells suggests that the melanocyte has both a primary sensory in addition to regulatory function. (38) The melanocyte, therefore, may be considered as a primary sensor of ionizing and/or ultraviolet radiation effects and regulates the response system, while the photoprotective effect is secondary.

The evidence that melanin provides effective photoprotection is suggested by the fact that poorly melanized skin is far more vulnerable than melanized skin to acute and chronic injury caused by ultraviolet radiation (sunburn and photoaging or photocarcinogenesis). (39) The photoprotective role of melanin is evident in the phenomenon of tanning or darkening of the skin that occurs within several days after exposure to ultraviolet radiation. The duration of tanning exposure depends on the total dose of ultraviolet radiation, its spectral characteristics, and the overall pattern of exposure and the genetic predisposition of the person. A single exposure to solar-stimulating light which may induce slight sunburn at 24 hours causes, within three or four days, a moderate tan that persists unchanged for at least 3 weeks. After sun-exposure, keratinocytes, which are driven to undergo apoptosis, called dyskeratotic "sunburn cells", may be easily identified. On the other hand, during this process, neighboring melanocytes are unaffected. While there is a marked increase in Langerhan's cells initially it is followed by, in a few hours, of a striking reduction of these immune cells. (38) Keratinocytic stem cells, which reside in the basal layer of the epidermis or in hair follicles, give rise to cells in the basal layer that divide several times before entering the supra-basilar layers. There they no longer proliferate, but rather differentiate, move upward, and are eventually shed from the skin surface. After exposure to high dose ultraviolet radiation, the most severely damaged keratocytes undergo apoptosis, leaving the less damaged keratocytes to up-regulate their DNA repair

capacity and to undergo repair. With each subsequent ultraviolet exposure, the most severely damaged cells will be removed, so that cells with minimal incremental damage gradually accumulate in the skin. In contrast, the first dose of ultraviolet radiation will cause substantial damage to melanocytes but not apoptosis. Therefore, these melanocytes will survive, mutate and divide. The appearance of freckles after high-dose sun exposure represent clones of mutated melanocytes. Moreover, there is a correlation between sun exposure and the development of melanocytic nevi in the exposed areas. (23) Low dose exposure of ultraviolet radiation that is accumulated over a lifetime is associated, epidemiologically, with the development of basal cell and squamous cell carcinomas. The relative contribution of ultraviolet A (320–400 nm) or B (290–320 nm) to carcinogenesis had been exhaustively studied. (24) Ultraviolet A radiation is far more abundant in native sunlight than is ultraviolet B radiation and it causes oxidative DNA damage that is potentially mutagenic. Ultraviolet B radiation is overwhelmingly responsible for the formation of the principal DNA lesions, cyclobutane pyrimidine dimmers and pyrimidine-pyrimidone photoproducts, whose incorrect repair may lead to cell mutations. (33) Experimentally, UV-B radiation has been associated with the development of squamous cell carcinoma, while UV-A is capable of inducing melanomas in animals. (25) For keratinocytes and melanocytes, the combination of slight initial damage, however, nearly complete repair results in only very slow malignant progression of skin cells. (9, 20) In the case of melanocytes, however, the number of cells at risk for cancer is significantly higher in the skin that receives and/a high dose of ultraviolet radiation.

Melanocyte Study Table of Results

Summary	Control-Non-Blocked Side	Sural Nerve Blocked Side
Clinical features	2 cm area of redness & swelling-lasting 72 hours	4 x 6 cm area of redness & swelling—lasting over 96 hours
Center of area of UV exposure Tissue Stains: (H&E, CD 1a, CD3, and S-100)	1. Slight edema 2. Slight increase in APC's 3. Slight increase in Langerhan's Cells 4. Slight increase in Melanin	1. Marked edema with disruption of tissue 2. Marked increase in APC's 3. Marked increase in Langerhan's Cells 4. Marked increase in Melanin
1cm dorsal to area of UV exposure Tissue Stains: (H&E, CD 1a, CD3 and S-100)	1. Slight increase in Langerhan's Cells 2. Normal appearance of APC's 3. Melanocytes appear normal	1. Moderate edema 2. Marked increase in Langerhan's Cells 3. Marked increase in APC's 4. Melanocytes and Melanin both increased

Stains: CD1a + = Langerhan's Cells; CD3 + = T Lymphocytes (APC's); S-100 + = Melanocytes and Langerhan's Cells

Melanocyte Study-Preliminary Conclusions

1. Melanocytes, derived from the neural crest, are a stable and long-lived population and are inextricably tied to the nervous system in the adult. (42–44)
2. This neuronal-melanocyte connection provides the basis for an exteroceptive sensory nervous system for the measurement of ultraviolet (and possibly other types) radiation from the environment.
3. The melanocyte, when exposed to ultraviolet radiation, is capable of orchestrating and mobilizing other neural crest derivative cells in the epidermis (Langerhan's Cells). (45)
4. The specific area exposed to ultraviolet radiation is marked-possibly at the post capillary venule region of the epidermis, utilizing free nerve endings and specific receptor endings. (13, 14)
5. Two types of sensory afferent stimuli are initiated, following which melanocyte stimulating hormone is then produced and released to activate those melanocytes that have been identified and receptors have been activated-that is the local area of exposure. These have been identified as A-delta and C fibers. (13–15)
    A. Location specific, monosynaptic and fast conducting impulses travel to the dorsal and ventral lateral thalamic nuclei and thence to the appropriate parietal cortex. (28)
    B. Type specific, polysynaptic and slower conducting impulses travel to multiple areas in the nervous system often ending in the centrum medianum and posterior thalamic nucleus and thence to the hypothalamus. There may even be differentiation as to the specific wave length frequency or energy levels. (45)
6. When the nervous system connection is interrupted, for example by nerve blockade, the normal distribution, orchestration and extent of a response is disordered (edema and cell migration).
7. Langerhan's cells are then transformed into antigen presenting cells (APC's) and recruited for the immune response to provide for a reaction to this form of epidermal insult. (45, 46) These cells thus present the intermediary cell between nerve cell (melanocyte) and immune cell (APC). They migrate from the skin to the lymph nodes and thymus gland and possess surface receptors that are common to macrophages (Fc and complement C3). (47, 48)
8. The Synapse in the immune system: The term immunological synapse was coined to describe the interface between T cells and B cells, which was analogous to neuronal synapses and neurotransmitter secretion. At the core of this synapse in the immune system is a junction that is formed at the surface between the antigen presenting cell (APC) and the responder T lymphocyte. (42, 43) At the periphery of the synapse TCR-mediated tyrosine kinase signaling occurs in naïve T cells and is largely abated before mature immunological synapse are formed. (49) The central zone of this structure contains T cell receptors, but the large adhesion molecules, such as integrin LFA-1, needed for the initial APC recognition, are excluded. Other important peptides include T cell receptors (TCR's), CD28 co stimulatory receptors and other smaller molecules. (50, 51) Actual engagement of the TCR with the peptide-MHC on the surface of the APC results in a peptide-MHC signaling within the APC. Secondary signaling only occurs with the interaction of the co-stimulatory receptor

CD28 with its ligands as this is transacted in the central region of the immunological synapse. This process is either enhanced or inhibited by effecter molecules such as cytokine IL-4 and the inhibitory peptide CTLA-4 that may be delivered to the central area by exocytosis. This process thereby limits the effect on bystander cells. This immunological synapse may be required for internalization of TCR's, which may be the way that TCR signaling is down regulated. (52)

9. There appears to be further evidence that the melanocyte functions as a neuro-endocrine organ with the discovery of MSH.
10. Thus the relationship between the nervous, immune and endocrine system appear to be inextricably interwoven into a single system for the protection of the individual from the ultraviolet radiation.

Summary

This preliminary study suggests that a reexamination of the role of melanocytes in the skin must be undertaken, particularly in their role in melanin production. Melanocytes have been shown to actually act as an exteroceptive sensor and orchestrate the mobilization of the nervous and immune systems in monitoring ultraviolet radiation. These phenomena could provide an explanation for the progressive discoloration of the legs of patients with peripheral neuropathy and exposure to sunlight. Further histochemical and immunological studies are contemplated, and are in progress using this individual self control model, in health and disease states utilizing other frequencies of energy and following different times of exposure and post exposure.

References

1. Haegel, H., Larue, L., Ohsugi, M., Fedorov, L., Herrenknecht, K. and Kemler, R. (1995) Lack of beta-catenin affects mouse embryonic development at gastrulation stage. *Development, 121:* 3529–3537.
2. Butz, S., and Larue, L. (1995) Expression of catenins during mouse embryonic development and in adult tissues. *Cell Adhes. Comm., 3:* 337–352.
3. Purves, D., Augustine, G., Fitzpatrick, D., Katz, L.C., LaMantia, A-S., McNamara, J.O., and Williams, S.M., eds. (2001) *NeuroScience*. Sinauer Associates, Inc., Sunderland, MA.
4. Larsen, W. (1993) Migration of Nerve Cells, In: *Human Embryology*. Churchill Livingston, New York, pp. 74–84.
5. Delmas, V., Pla, P., Feracci, H., Thiery, J. P., Kemler, R. and Larue, L. (1999) Expression of the cytoplasmic domain of E-cadherin induces precocious mammary epithelial alveolar formation but alters cell polarity and cell-matrix integrity. *Dev. Biol. 216:* 491–506.
6. Ohsugi, M., Larue, L., Schwarz, H., and Kemler, R. (1997) Cell-junctional and cytoskeletal organization in mouse blastocysts lacking E-cadherin. *Dev. Biol. 185:* 261–271.
7. Purves, D., Augustine, G, Fitzpatrick, D., Katz, L.C., LaMantia, A-S., McNamara, J.O., and Williams, S.M., eds. (2001) Cell migration. In: *NeuroScience*. Sinauer Associates, Sunderland, MA, pp. 489–491.
8. Larue, L., Ohsugi, M., Hirchenhain, J., and Kemler, R. (1994) E-Cadherin null mutant embryos fail to form a trophectoderm epithelium. *Proc. Natl. Acad. Sci. 91:* 8263–8267.
9. Yaar, M. and Gilchrest, B. (1991) Human melanocyte growth and differentiation. *J. Invest. Dermatol. 97:* 611–617.

10. Larue, L., Dougherty, N., Porter, S., and Mintz, B. (1992) Spontaneous malignant transformation of melanocytes explanted from Wf/Wf mice with a Kit kinase-domain mutation. *Proc. Natl. Acad. Sci. 89:* 7816–7820.
11. Reedy, M. (1998) Regulation of melanoblast migration and differentiation. *The Pigmentary System, Physiology and Pathophysiology.* Oxford University Press, New York, pp. 75–95.
12. Norris, D. (1998) Melanocyte interactions in the skin. *The Pigmentary System, Physiology and Pathophysiology*. Oxford University Press, New York, pp. 123–133.
13. Eccles, J, Ito, M. and Szentagothai, J. (1967) *The Cerebellum as a Neuronal Machine*. Springer Verlag, New York.
14. Crosby, E., Humphrey, T., and Lauer, E. (1962) *Correlative Anatomy of the Nervous System*. Macmillan Company, New York.
15. Johansson, O., Wang, L, Hilliges, M and Liang, Y. (1999) Intraepidermal nerves in human skin: PGP 9.5 Immunohistochemistry with special reference to the nerve density in skin from different body regions. *J. Peripher. Nerv. Syst. 4 (1):* 43–52.
16. Peters, A., Palay, S. and Webster, H. (1970) *The Fine Structure of the Nervous System*. Harper and Row, New York.
17. Hara, M., Toyada, M., Yaar, M., Bhawan, J., Avila, E., Penner, I., and Gilchrest, B. (1996) Innervation of Melanocytes in Human Skin. *J. Exp. Med. 184 (4):* 1385–1395.
18. Boissy, R., Hearing, V., King, R., and Ortonne, J. (1998) eds. *The Pigmentary System: Physiology and Pathophysiology*. Oxford University Press, New York, pp. 75–95.
19. Norris, D., Morelli, J., and Fuejata, M. (1998) Melanocyte interactions in the Skin. In: *The Pigmentary System: Physiology and Pathophysiology*. Norlund, J., Boissy, R., Hearing, V., King, R., and Ortonne, J, eds. Oxford University Press, New York, pp. 123–133.
20. Yaar, M and Gilchrest, B. (1991) Human Melanocyte Growth and Differentiation: as Decade of New Data. *J. Invest Dermatol. 97:* 611–670.
21. Pathak, M. (1991) Ultraviolet radiation and the development of non-melanoma and melanoma skin cancer. *Skin Pharm. 1; 4:* 85–94.
22. Gilcrest, B., Park, H-Y., Eller, M, and Yaar, M. (1998) The Physiology of the Tanning Response. In: Norland, S., Boissy, R., Hearing, V., King, R., and Ortonne, J., eds. *The Pigmentary System: Physiology and Pathophysiology*. Oxford University Press, New York, pp. 359–372.
23. Young, A. R. (1987) The Sunburn Cell. *Photodermatology 4:* 127–134.
24. Bayerl, C., Taake, S., Moll, I, and Jung, E. (1995) Characterization of Sunburn Cells after Exposure to Ultraviolet Light. *Photodermatol Photomed. 11:* 199–254.
25. Atillasoy, E., Seykora, L., Soballe, P., Elenitsas, R., Nesbit, M., Elder, D.E., Montane, K.T., Sauter, E., and Herlyn, M. (1998) UVB induces atypical melanocyte lesions and melanomas in human skin. *Am. J. Pathol. 152:* 1179–1186.
26. Klein-Parker, H., Warshawski, L and Tron, V. (1994) Melanocytes in Human Skin express bcl-2 protein. *J. Cutan Pathol. 21:* 297–301.
27. Danno, K. and Horio, T. (1987) Sunburn Cells: Factors involved in its formation. *Photochem Photobiol. 45:* 683–690.
28. Montgomery, R., Conway, T., Spector, A. and Chapell, D. (1996) *Biochemistry*. Mosby, New York, N. Y.
29. Champe, P. and Harvey, R. (1996) *Biochemistry, 2nd Edition.* L. B. Lippincott, Philadelphia, Pa.
30. Janeway, C and Travers, P. (1996) *ImmunoBiology*. Garland Publishing, Inc., New York, N. Y.
31. Male, D., Cooke, A., Owen, M., Trowsdale, J. and Chamion, B. (1996) *Advanced Immunology.* Mosby, New York, N. Y.
32. Jouneau, A., Yu, Y.Q., Pasdar, P., and Larue, L. (2000) Plasticity of cadherin-catenin expression in the melanocyte lineage. *Pigment Cell Res. 13 (4):* 260–272
33. Singer, A. and Clark, R. (1999) Cutaneous Wound Healing. *NEJM 341, 10:* 738–746.
34. Kimball, J. (2001) Melanocyte Stimulating Hormone. *Kimball's Biology*, 21, August 2001.

35. Scully, K and Rosenfeld, M. (2002) Pituitary Development: Regulatory Codes in Mammalian Organogenesis. *Science 295:* 2231–2235.
36. Lugar, T., Scholzon, T. and Grabbe, S. (1997) The role of alpha-melanocyte stimulating hormone in cutaneous biology. *J. Invest. Dermatol. Symp. Proc.* Aug. 2, (1): 87–93.
37. Chekraborty, A., Funasaka, Y, Slominski, A., Bolognia, J., Sodi, S., Inchih, M. and Pawalek, J. (1999) UV Light and MSH receptors. *Ann. NY Acad. Sci.* Oct. 20; *885:* 100–116.
38. Schuler, G., Dohlin, G. and Fritsch, P. (1981) Differences of cell surface distribution and redistribution patterns between mammalian keratinocytes and melanocytes. *J. Invest. Dermatol.* Oct. 7 (4): 347–353.
39. Pathak, M. (1991) Ultraviolet radiation and the development of non-melanoma and melanoma skin cancer: clinical and experimental evidence. *Skin Pharmacol. 4:* suppl 1: 85–94.
40. Liang, Y. and Johansson, O. (1998) Light and electron microscopic demonstration of the p75 nerve growth factor receptor in normal human cutaneous nerve fibers: new vistas. *J. Invest. Dermatol. 111* (1): 114–118.
41. Pathak, M. (1995) Functions of Melanin and Protection by Melanin. In: *Melanin: Its role in human photoprotection*. Zeise, L., Chedekel, M., Fitzpatrick, T., eds. Valdenmar Publishing, Overland Park, KS, pp. 125–134.
42. Lee, K-H, Holdorf, A.D., Dustin, M. (2002) T Cell Receptor Signaling Precedes Immunological Synapse Formation. *Science 295:* 1539–1542.
43. Hoseol, J., Murphy, G., Egen, C., Lerner, E., Grabbe, S., Asahina, A., and Granstein, R.D. (1993) Regulation of Langerhans cell function by nerves contained calcitonin gene related peptide. *Nature 363:* 159–162.
44. Beauvais-Jouneau, A., Pla, P., Bernex, F. Dufour, S., Salamero, J., Fässler, R., Panthier JJ, Thiery, J.P. and Larue, L. (1999) A novel model to study the dorso-lateral migration of melanoblasts. *Mech. Dev. 89:* 3–14.
45. Gilchrest, B. et. Al. (1999) The pathogenesis of melanoma induced by ultraviolet radiation. *NEJM 340,* 17: 1341–1348.
46. Larue, L., Antos, C., Butz, S., Huber, O., Delmas, V., Dominis, M., and Kemler, R. (1996) A role for cadherins in tissue formation. *Development 122:* 3185–3194.
47. Larue, L., Dougherty, N., Bradl, M., and Mintz, B. (1993) Melanocyte culture lines from Tyr-SV40E transgenic mice: models for the molecular genetic evolution of malignant melanoma. *Oncogene 8:* 523–531.
48. Larue, L., Dougherty, N., and Mintz, B. (1992) Genetic predisposition of transgenic mouse melanocytes to melanoma results in malignant melanoma after exposure to a low ultraviolet B intensity non-tumorogenic for normal melanocytes. *Proc. Natl. Acad. Sci. USA 89:* 9534–9538.
49. van der Merwe, P. and Davis, S. (2002) The Immunological Synapse-a Multitasking System. *Science 295:* 1479–1480.
50. Kochevar, I., PAthak, M. and Larrish, M. (1993) Photophysics, Photochemistry and Photobiology. In: *Dermatology in General Practice, 4th Edition. Vol 1*. Fitzpatrick, T., Eissn, A., Wolff, K., Freedberg, F., Austen, K., eds. McGraw Hill, New York, pp. 1627–1638.
51. Liang, Y. and Marcusson, J. (1999) Light and Electron Microscopic Immunohistochemical Observation of P72 Nerve Growth Factor Receptor-Immunoreactive Dermal Nerves. *Arch. Dermatol. Res. 291* (1): 14–21.
52. Liang, Y. (1999) Immunocytochemical studies of cutaneous nerves in human and Prurigo Nodularis skin. Doctural Thesis, Karlinska Institute.

Received February 10, 2003;
accepted August 19, 2003.

Physiol. Chem. Phys. & Med. NMR (2003) *35*: 43–53

Insulin Secretion in Monosodium Glutamate (MSG) Obese Rats Submitted to Aerobic Exercise Training

Claudio Teodoro de Souza, Wilton Marlindo Santana Nunes, Claudio Alexandre Gobatto, Maria Alice Rostom de Mello*

Departamento de Educação Física, Instituto de Biociências, Universidade Estadual Paulista (UNESP), 13506-900 Rio Claro, SP, Brazil
**Corresponding author*

Abstract: The present study was designed to evaluate the effects of aerobic exercise training on glucose tolerance and insulin secretion of obese male Wistar rats (monosodium glutamate [MSG] administration, 4mg/g-body weight, each other day, from birth to the 14th day). Fourteen weeks after the drug administration, the rats were separated into two groups: MSG-S (sedentary) and MSG-T (T = swimming, 1 h/day, 5 days/week, with an overload of 5% body weight for 10 weeks). Rats of the same age and strain injected with saline were used as control (C) and subdivided into two groups: C-S and C-T. Insulin and glucose responses during an oral glucose tolerance test (GTT) were evaluated by the estimation of the total areas under serum insulin (AI) and glucose (AG) curves. Glucose-induced insulin secretion by isolated pancreatic islets was also evaluated. MSG-S rats showed higher AI than C-rats while MSG-T rats presented lower AI than MSG-S rats. No differences in AG were observed among the 4 groups. Pancreatic islets from MSG-rats showed higher insulin secretion in response to low (2.8) and moderate (8.3 mM) concentrations of glucose than those from their control counterparts and no differences were observed between MSG-S and MSG-T rats. These results provide evidences that the hyperinsulinemia at low or moderate glucose concentrations observed in MSG-obese rats is, at least in part, a consequence of direct hypersecretion of the B cells and that chronic aerobic exercise is able to partially counteract the hyperinsulinemic state of these animals without disrupting glucose homeostasis.

THE MONOSODIUM glutamate (MSG) treated rat has been used as a model for the study of the possible relationship between obesity and hyperinulinemia (Marmo *et al.* 1994). Although it has been reported that the obese MSG-rat is hyperinsulinemic (Hirata *et al.*, 1997), the cause has not been established yet. Similar observations have been made using other animal models such as the obese Zucker rats (Curry & Stern, 1985) and the

obese male SHFF/*Mcc-fa* rat (Gao *et al.*, 1994). Investigators reporting insulin release by isolated islets from Zucker obese rats have provided evidence which suggest that the hyperinsulinemia is due, at least in part, to direct hypersecretion of the B cells in response to glucose (Milburn *et al.* 1995). The hyperinsulinemia in MSG-obese rats is observed even after an overnight fasting (Hirata *et al.*, 1997). Fasting hyperinsulinemia implies increased sensivity to low levels of glucose and this was documented in genetic models of obesity, including *ob/ob* mice (Tavassa *et al.*, 1992), Zucker rats (Chan *et al.*, 1996), and SHR./N-cp or LA/n-cp rats (Timmers *et al.*, 1992). A curious observation in the MSG-obese animals is that the hyperinsulinemia is accompanied by a relative normoglycemia (Hirata *et al.*, 1997). This observation is generally explained as being due to development of insulin insensivity by insulin dependent muscle tissue (Machado *et al.*, 1993). It has been suggested that this insulin insensivity leads to a compensatory pancreatic hypersecretion, to maintain normoglycemia in face of insulin resistance (Carpinelli *et al.*, 1996). Physical exercise, in turn, can be used effectively to improve insulin sensitivity and glucose tolerance (Hendriksen, 2002). Exercise was shown to improve insulin stimulation of skeletal muscle glucose uptake in both normal (James et al., 1985) and hyperinsulinemic rats such as the obese Zucker rat (Ivy *et al.*, 1989; Torgan *et al.*, 1993, Hendriksen, 2002) and the obese male SHHF/*Mcc-fa* rat (Gao *et al.*, 1994). On the other hand, little is known about the effects of exercise on insulin secretion by hyperinsulinemic animal models of obesity. The present study was designed to evaluate the effects of aerobic exercise training on glucose tolerance and insulin secretion in MSG-obese rats.

Methods

Animals and groups

Virgin Wistar female rats (90–100 days old) were obtained from the State University of São Paulo (UNESP) animal facilities. Mating was performed by housing males with females overnight and pregnancy was confirmed by examination of vaginal smears for the presence of sperm. Newborn, male pups were injected subcutaneously with MSG (4mg/g-body weight) every other day, from birth to the 14th day of life (Hirata *et al.*, 1997). At weaning, the pups were transferred to collective cages (4 animals per cage) and maintained in a temperature controlled room (22±1° C), with lights on from 7:00 to 19:00 h. Fourteen weeks after drug administration, the rats were separated into two groups: MSG-S (sedentary) and MSG-T (exercise training for 10 weeks). Rats of the same age and strain, housed similarly, injected with saline, were used as control (C), and assigned to two groups: C-S and C-T. All rats had free access to water and food (commercial rodent chow) and were weighed and measured (nose-to-anus length) weekly.

Exercise training

Rats in T groups were trained to swim 1 hour per day, 5 days a week, supporting an overload (weights in the form of fish sinkers, added to the chest) of 5% body weight, in collective tanks, filled with water maintained at 30±2° C, 8 rats per tank (Gobatto *et al.*, 2001).

Fitness test

At the last week of the experiment, all rats were submitted to an 1-hour swimming session, supporting an overload of 5% body weight. Blood samples were collected each 10 min from a cut in tail tip for lactate determination (Engel & Jones, 1978).

Oral glucose tolerance test (GTT)

An oral glucose tolerance test was performed on the rats at the end of experimental period. After an overnight fasting, glucose (200g/1) was administered into stomach through a gastric catheter, at a final dose of 2g/kg-body weight. Blood samples were obtained from cut tip tail at 0, 30, 60 and 120 min for serum glucose (Nogueira *et al.*, 1990) and insulin (kit Coat-A-Count, USA) determinations. The insulin and glucose responses during the glucose tolerance test were evaluated by estimation of the total area under the glucose curve (AG) and the total area under the insulin curve (AI), using the trapezoidal method (Mathews *et al.*, 1990).

Tissue sampling

At the end of the experimental period, all rats were sacrificed in the fed state by decapitation. The exercise-trained rats were kept at rest in the 48 hours that preceded the sacrifice. Trunk blood was collected, allowed to clot and serum stored at −30°C to measure insulin by RIA (kit Coat-A-Count, USA) and glucose by the glucose oxydase-peroxydase method (Nogueira *et al.*, 1990). The pancreas was excised for insulin content determination (Malaisse *et al.*, 1967) and islet isolation for glucose-induced insulin secretion evaluation. The carcass was eviscerated, weighed and dried to constant weight in an oven at 100° C. Then it was homogenized in a blender with benzene and extracted with several more changes of benzene. The powder was dried in the oven and weighed. Fat content was determined by difference in weight before and after benzene treatment.

Glucose-induced insulin secretion

To measure insulin secretion, groups of five islets isolated by digestion of the pancreas with collagenase, were incubated for 30 min at 37 °C in Krebs-bicarbonate medium of the following composition (in mmol/L): NaCl 115, KCl 5, $CaCl_2$ 2.56, Mg Cl_2 1, $NaHCO_3$ 24 and glucose 5.6, supplemented with BSA (3 g/L) and equilibrated with a mixture of 95% O_2 – 5% CO_2, pH 7.4. The solution was then replaced by fresh buffer containing low (2.8), moderate (8.3) or supraphysiological (16.7 mmol/L) concentrations of glucose, and the islets were incubated for a further 1 h (Prada *et al.*, 2001). The insulin content of the medium at the end of the incubation period was measured by RIA.

Statistical analysis

The results were expressed as means ± SD for the number of rats (n) indicated. When working with islets, n refers to the number of experiments performed. Each experiment was performed with islets from three rats per group. The data were analyzed by one way analysis of variance (ANOVA) followed by Bonferroni's where appropriate. P values < 0.05 were considered to indicate significance.

Results

During the experiment, MSG-rats gained less weight than C-rats and trained rats gained less weight than their sedentary counterparts (Table I). MSG-rats also were shorter and had significantly higher fat content in the carcass than C-rats at the end of the experimental period (Table I). Exercise training significantly reduced fat in the carcass in both C and MSG rats (Table I).

During the fitness test, trained rats showed lower blood lactate levels than their corresponding sedentary ones and MSG-rats always showed lower values than control rats (Figure 1).

There were no significant differences among groups in the serum glucose levels in the fed state while serum insulin was elevated in MSG-rats in relation to C-rats (Table II). Pancreas insulin content was higher in MSG than in corresponding control-rats. The highest value was observed in MSG-S rats (Table II).

No diffierences were observed among the 4 groups in the area under the serum glucose curve during the glucose tolerance test (GTT) (Figure 2A), while MSG-S rats showed

TABLE I. Body weight gain (g) from the 14th to the 24th week (end of the experimental period) after MSG or saline administration and body length (cm) and carcass fat content (g/100g) at the end of the experimental period.

	C-S	C-T	MSG-S	MSG-T
Body weight gain	95.2 ± 3.0	70.1 ± 9.4[a]	73.7 ± 3.9[a]	53.8 ± 7.5[abc]
Body length	25.3 ± 1.2	26.0 ± 0.8	21.8 ± 1.0[ab]	21.2 ± 1.5[ac]
Carcass fat	11.5 ± 1.3	9.5 ± 1.9[a]	28.5 ± 3.3[a]	24.6 ± 1.7[abc]

Results are mean ± SD from n = 17 (S-C); 18 (E-C); 19 (S-MSG) or 27 (E-MSG) rats, except for carcass fat, where n = 5 for all groups. C-S: sedentary control rats, C-T: exercise-trained rats, MSG-S: sedentary monosodium glutamate treated rats, MSG-T: exercise-trained monosodium glutamate treated rats.
Significant differences (ANOVA, $p < 0.05$): a ≠ C-S; b # C-T and c ≠ MSG-S.

TABLE II. Serum glucose (mmol/L), serum insulin (nmol/L) and pancreas insulin (nmol/g) in the fed state at the end of the experiment

	C-S	C-T	MSG-S	MSG-T
Serum glucose	7.10 ± 0.97	6.54 ± 0.65	7.9 ± 0.86	6.8 ± 0.70
Serum insulin	0.17 ± 0.02	0.16 ± 0.05	0.22 ± 0.04[a]	0.24 ± 0.01[ab]
Pancreas insulin	289.8 ± 86.1	230.07 ± 25.0	544.8 ± 312.6[a]	313.8 ± 33.5[abc]

Results are mean ± SD from n = 17 (S-C); 18 (E-C); 19 (S-MSG) or 27 (E-MSG) rats, except for carcass fat, where n = 5 for all groups. C-S: sedentary control rats, C-T: exercise-trained rats, MSG-S: sedentary monosodium glutamate treated rats, MSG-T: exercise-trained monosodium glutamate treated rats.
Significant differences (ANOVA, $p < 0.05$): a ≠ C-S; b # C-T and c ≠ MSG-S.

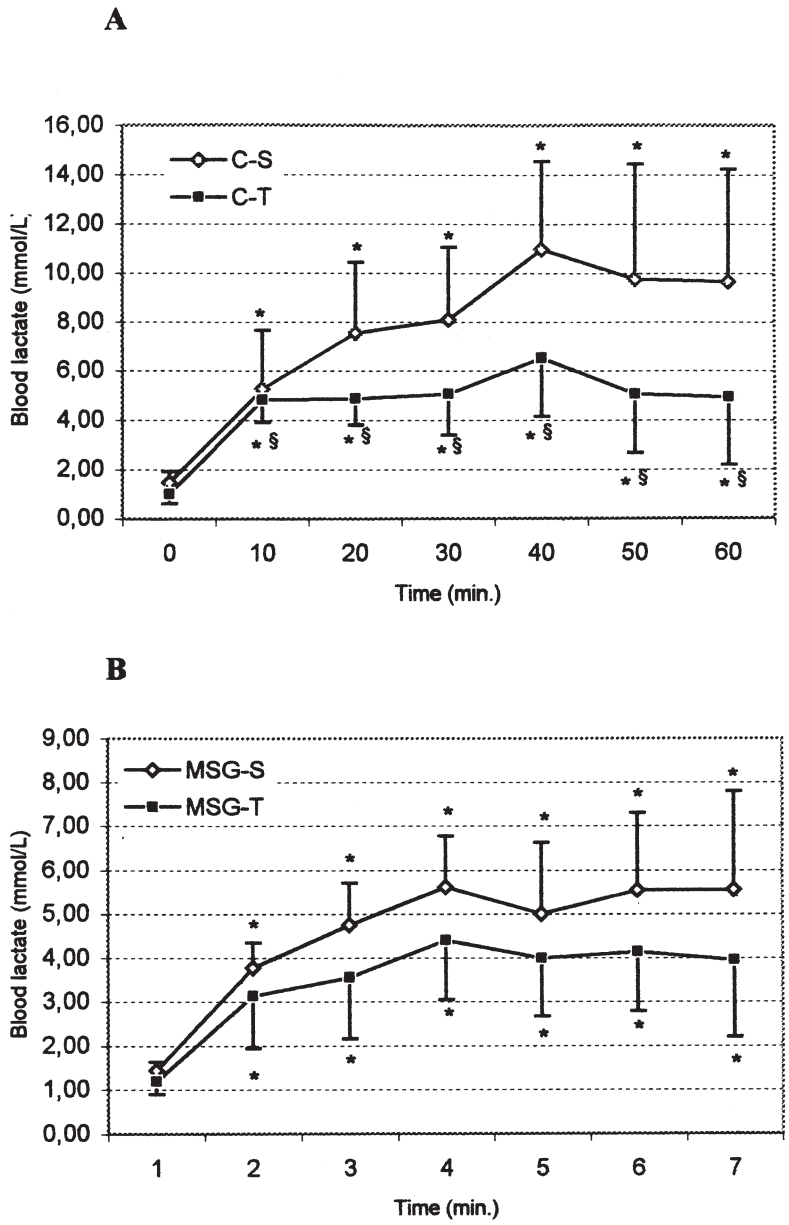

FIGURE 1. Blood lactate during the fitness test performed at the last week of experiment. Results are mean ± SD from n = 8 rats in each group. [A] C-S: sedentary control rats, C-T: exercise-trained rats and [B] MSG-S: sedentary monosodium glutamate treated rats, MSG-T: exercise-trained monosodium glutamate treated rats.
*Significantly different (ANOVA, $p<0.05$) from time 0.
§Significantly different (ANOVA, $p<0.05$) from C-S.

higher area under serum insulin curve than C-S rats during the test. MSG-T rats showed higher area under serum insulin curve during the GTT when compared to control rats but lower when compared to MSG-S rats (Figure 2B).

Pancreatic islets isolated from MSG-rats showed higher insulin secretion in response to low (2.8 mM) and moderate (8.3 mM) concentrations of glucose than those isolated from their control counterparts and no differences were observed between MSG-S and MSG-T rats (Figure 3).

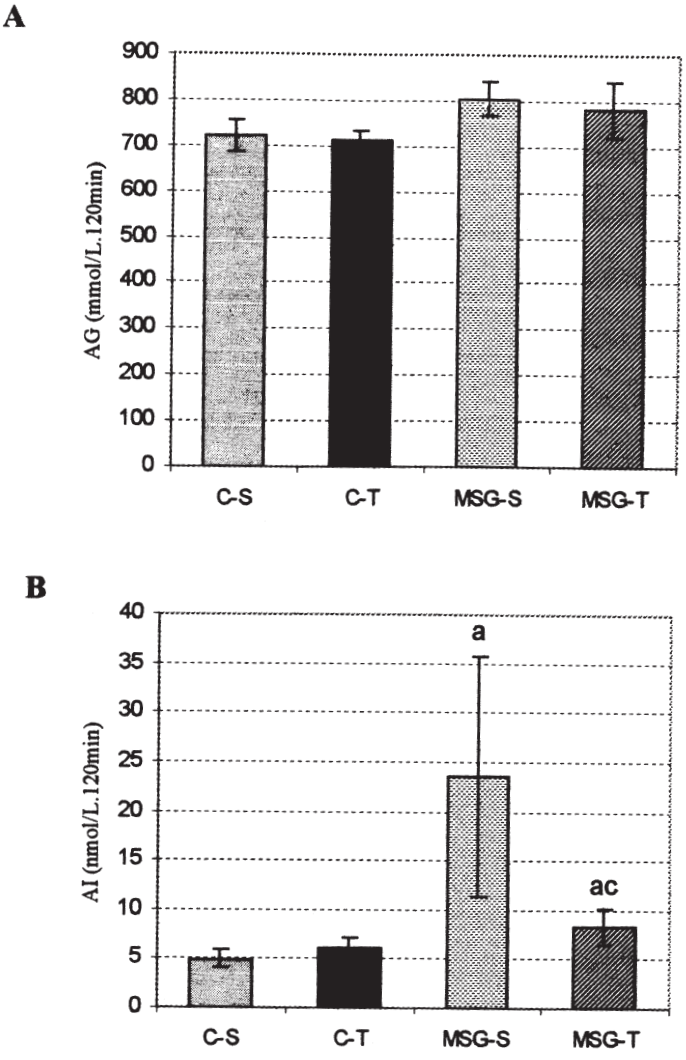

FIGURE 2. Areas under [A]: serum glucose (ΔG in mmol/l. 120 min) and [B]: serum insulin (ΔI in nmol/L. 120 min.) curves during the glucose tolerance test performed the last week of experiment in animals from all groups. Results are mean ± SD from n = 8 rats in each group. C-S: sedentary control rats, C-T: exercise-trained rats, MSG-S: sedentary monosodium glutamate treated rats, MSG-T: exercise-trained monosodium glutamate treated rats.
Significant differences (ANOVA, $p<0.05$): a ≠ C-S and c ≠ MSG-S.

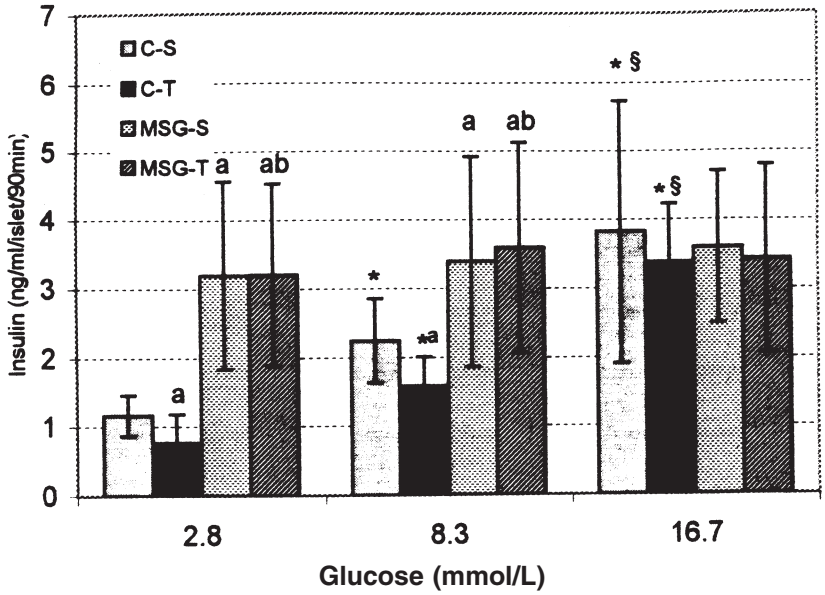

FIGURE 3. Glucose-stimulated insulin secretion by isolated pancreatic islets. Results are mean ± SD from n = 15 experiments in all conditions. C-S: sedentary control rats, C-T: exercise-trained rats, MSG-S: sedentary monosodium glutamate treated rats, MSG-T: exercise-trained monosodium glutamate treated rats.
Significant differences (ANOVA, $p<0.05$): a ≠ C-S and c ≠ MSG-S.
* ≠ 2.8 and § ≠ 8.3 for the same group of rats.

Discussion

In accordance with previous reports (Balbo *et al.*, 2000; Ochi *et al.*, 1988; Nikoletseas, 1977), MSG-treated rats are smaller and lighter than their control counterparts but have higher body fat content, as indicated by carcass fat, than their corresponding controls. This indicates the efficiency of the MSG treatment in inducing obesity in the conditions of the present study.

To evaluate the metabolic adaptation response to the aerobic exercise-training program, at the end of the last week of the experiment, we measured blood lactate in rats from all groups during a swimming session. Since aerobic physical training has been reported to reduce blood lactate accumulation in response to exercise in both human beings (Donovan & Pagliassoti, 1990) and rats (Gobatto *et al.*, 2001), our results showing that control and MSG exercised rats exhibited lower blood lactate levels along the test than their sedentary counterparts, indicate the efficiency of the exercise-training protocol used. Exercise training was also effective in reducing carcass fat content in both control and MSG rats. This beneficial effect of exercise was previously observed in other rat models of obesity such as the genetically obese Zucker rats (Jen *et al.*, 1992).

After an oral glucose load, serum insulin levels reached higher values in MSG-S obese rats than in C-S, in the presence of similar serum glucose concentrations. In consequence,

MSG-S rats showed higher area under the serum insulin curve than C-S rats while no differences in the area under the serum glucose curve were observed between them. This suggests that MSG rats developed glucose intolerance and/or an insulin resistant state. These findings are in accordance with previous reports in the literature (Hirata *et al.*, 1997).

Serum insulin in both fed state and after an overnight fasting (data not shown) were higher in MSG groups than in control groups and probably this hyperinsulinemic state helped the MSG rats in maintaining normal glycemic levels. Pancreas insulin content was also higher in MSG than in control rats.

Fasting hyperinsulinemia is a characteristic feature of insulin resistant states, including obesity and non-insulin dependent diabetes mellitus (Carpinelli *et al.*, 1996) and it is known that genetic obese Zucker rats secrete more insulin when tested *in vitro* under basal conditions (glucose concentration under 5 mmol/L) than do their lean counterparts (Zohu *et al.*, 1999). Our results provide evidence that the same occurs with MSG-obese rats, since pancreatic islets isolated from the MSG rats secreted more insulin in presence of low (2.8 mmol/L) or moderate (8.3 mmol/L) concentrations of glucose than control islets.

A number of possible mechanisms may be responsible for basal insulin hypersecretion in obese animals. These include elevated levels of serum free fatty acids, which have been demonstrated to increase basal insulin secretion *in vitro* (Melbourne *et al.*, 1995). An increase in the mass of insulin secreting B cells due to hypertrophy or hyperplasia could also explain an increase in basal insulin secretion. However, the increase in secretion is usually greater than the increase in B cell mass (Zohu *et al.*, 1999), indicating that intrinsic alterations in B cell sensitivity must play a role. Possible mechanisms that have been proposed to account for the increase in B cell glucose sensitivity include an increase in islet stores of glycogen (Malaisse *et al.*, 1992) and triglycerides (Lee *et al.*, 1994), alterations in islet uncoupling protein (UCP)-2 levels (Briaud *et al.* 2002) as well as an increase in the activity of the glucose phosphorylating enzyme glucokinase (Chan *et al.*, 1996). Further evaluations, such as protein content and cellularity of beta cells, fatty acids induced insulin secretion and UCP-2 protein expression, among others, are required to sort out the mechanisms underlying the basal hyperinsulinemia showed by this specific model of obesity.

Since exercise training has been shown to reduce sensitivity of the pancreatic B cells to the stimulant action of glucose in lean rats (Zawalich *et al.*, 1982), we tested here the effects of an aerobic exercise training protocol on insulin release by pancreatic islets isolated from our control and MSG-rats in response to low (2.8), moderate (8.3) and high (16.7 mM) concentrations of glucose.

Incubation of the isolated islets with 2.8 and 8.3 mM glucose resulted in lower insulin release by C-T than by C-S islets. In contrast, when the glucose concentration in the incubation medium was increased to 16.7 mM, insulin release was similar in C-T and in C-S rats. These results confirm the previous reports of Zawalich *et al*. (1982). The reduction in glucose-induced insulin secretion caused by exercise training was shown to be associated with a coordinate decrease in islet glucokinase and proinsulin mRNA and no change in islet glucose-transporter (GLUT-2) mRNA (Korianyi *et al.*, 1991). Pancreatic islets isolated from MSG-T secreted the same amount of insulin as MSG-S islets in all glucose concentrations tested, indicating that the aerobic exercise training protocol failed in counteracting the obesity induced insulin hypersecretion when evaluated *in vitro*. On the

other hand, exercise training was able to reduce *in vivo* glucose induced hyperinsulinemia, since MSG-T rats showed lower area under the serum insulin curve curve during the GTT than MSG-S rats while no differences in the area under the serum glucose curve were observed between them. Although hyperinsulinemia has been mainly assigned to pancreatic hypersecretion, some investigators report that a decline in hepatic insulin extraction could also be partially responsible, at least in patients with extreme upper-body fat distribution, for the high circulating insulin levels in obesity (Kautsky-Willer *et al.*, 1992). If reduced hepatic insulin extraction also plays a role in the genesis of the hyperinsulinemia in the MSG-obese rat, it may be that physical exercise exerts its main action at hepatic level and not at pancreatic islets level. This is an hypothesis that cannot be ruled out since there are evidences, provided by studies performed in men, that exercise training may increase hepatic insulin extraction (Dela *et al.*, 1992).

Taken together, the results of the present study provide evidences that the hyperinsulinemia at low or moderate glucose concentrations observed in MSG-obese rats is a consequence, at least in part, of direct hypersecretion of the B cells and that chronic aerobic exercise is able to partially counteract the hyperinsulinemic state of the animals without disrupting glucose homeostasis. Further studies are required to sort out the mechanisms involved in the effects of exercise training on the hyperinsulinemic state in this specific model of obesity.

The authors thank Clarice Y. Sibuya, José Roberto R. da Silva, Eduardo Custódio and Miriam G. de Chaves for technical assistance. Research supported by the Brazilian foundations: FAPESP, CNPq and FINEP/PRONEX.

References

Balbo, S.L., Mathias, P.C.D., Bonfleur, M.L., Alves, H.F., Siroti, F.J., Monteiro, O.G., Ribeiro, F.B., da Silva, A.C.M., Souza, F. (2000) Vagotomy reduces obesity in MSG-treated rats. *Res. Commun. Mol. Pathol. 108:* 291–296.

Briaud, I, Kelp, C.L., Johonson, L.M., Tram, P.O.T., Poitout, V. (2002) Differential effects of hyperlipidemia on insulin secretion in islets of langerhans form hyperglycemic versus normoglycemic rats. *Diabetes 51:* 662–668.

Carpinelli, A.R., Machado, U.F., Curi, R. (1996) Modulation of insulin secretion by feeding behavior and physical activity: possible benificial effects on obese and aged rats. *Neuroscience and Biobehavioral Reviews 20:* 183–188.

Chan, C.B., Lowe, J.M., Debertin, W.J. (1996) Modulation by glucose of insulin secretion and glucose phosphorylating activity in cultured pancreatic islets from obese (*fa/fa*) Zucker rats. *Int. J. Obesity 20:* 175–184.

Curry, D. and Stern, S. (1985) Dynamics of insulin hypersecretion by obese Zucker rats. *Metabolism. Clinical and experimental 34:* 791–976.

Dela, F., Mikines, K.J., Vonlinstow, M., Galbo, H.J. (1992) Does training spare insulin-secretion and diminish glucose levels in real life? *Diabetes Care 15:* 1712–1715.

Donovan, C.M., Pagliassotti, M.J. (1990) Enhanced efficiency of lactate removal after endurance training. *J. Appl. Physiol. 68:* 1053–1058.

Engel, P.C., Jones, J.B. (1978) Causes and elimination of erratic blanks in enzymatic metabolic assays involving the use of NAD in alkaline hydrazine buffers: improved conditions for the assay of L-glutamate, L-lactate, and other metabolites. *Anal. Biochem. 88:* 475–485.

Gao, J., Sherman, W.M., McCune, A.S., Osei, K. (1994) Effects of acute running exercise on whole body insulin action in obese male SHHF/*Mac-fa* rats. *J. Appl. Physiol. 77:* 534–541.

Gobatto, C.A., Mello, M.A.R., Sibuya, C.Y., Azevedo, J.R.M., Santos, L.A., Kokubun, E. (2001) Maximal lactate steady state in rats submitted to swimming exercise. *Comp. Biochem. Physiol.*[Part A] *130:* 21–27.

Hendriksen, E.J. (2002) Exercise effects of muscle insulin signaling and action — Invited review — Effects of acute exercise and exercise training on insulin resistance. *J. Appl. Physiol. 93:* 788–796.

Hirata, A.E., Andrade, I.S., Vaskevicius, P., Dolnikoff, M.S. (1997) Monosodium glutamate (MSG)-obese rats develop glucose intolerance and insulin resistance to peripheral glucose uptake. *Braz. J. Med. Biol. Res. 30:* 671–674.

Ivy, J.L., Brozinick, J.T., Torgan, C.E., Kastello, G.M. (1989) Skeletal muscle glucose transport in obese Zucker rats after exercise training. *J. Appl. Physiol. 66:* 2635–2641.

James, D.E., Kraegen, E.W., Chisholm, D.J. (1985) Effects of exercise training on in vivo insulin action in individual tissues of the rat. *J. Clin. Invest. 70:* 657–666.

Jen, K.L.C., Almario, R., Hagan, J., Zhong, S., Archer, p., Lin, P.K.H. (1992) *Int. J. Obesity 16:* 519–527.

Kautsky-Willer, A., Pacini, G., Ludvic, B., Scherthaner, G., Prager, R. (1992) B-cell hypersecretion and not reduced hepatic insulin extraction is the main cause of hyperinsulinemia in obese nondiabetic subjects. *Metabolism 41:* 1304–1312.

Koranyi, L.I., Boury, R.E., Slentz, C.A., Holloszy, J.O., Permutt, A. (1991) Coordinate reduction of rat pancreatic islet glucokinase and proinsulin mRNA by exercise training. *Diabetes 40:* 401–404.

Lee, Y., Hirose, H., Ohneda, M., Johnson, J.H., McGarsy, J.D., Unger, R.H. (1994) Beta-cell lipotoxicity in the pathogenesis of noninsulin dependent diabetes mellitus of obese rats: Impairment in adipocytes-beta-cell relationship. *Proc. Natl. Acad. Sci. USA 91:* 10878–10882.

Machado, U.F., Shimizu, Y., Sato, M. (1993) Decreased glucose transporter (GLUT-4) content in insulin-sensitive tissues of obese aurotioglucose and monosodium glutamate treated mice. *Horm. Metab. Res. 25:* 462–465.

Malaisse, W.J., Malaisse-Lagae, F., Wright, P. (1967) Effect of fasting upon insulin secretion in rats. *Am. J. Physiol. 213:* 843–848.

Malaisse, W.J., Marynissen, G., Sener, A. (1992) Possible role of glycogen accumulation in B-cell glucotoxicity. *Metabolism 41:* 814–819.

Marmo, M.R., Nunes, M.T., Volpato, C.B., Kettelhut, I.C., Hell, N.S., Lima, F.B., Dolnikoff, M. (1994) Reduced growth hormone mRNA levels in 28-d-old MSG rat impair protein and lipid metabolism. *European J. Physiol. 427:* R29.

Mathews, J.N.S., Altman, D.G., Campbell, M.J., Roystron, P. (1990) Analysis of serial measurements in medical research. *Br. Med. J. 27:* 230–235.

Milburn, J.L. Jr., Hirose, H., Lee, Y.H., Nagasawa, Y., Ogawi, A., Ohneda, M., BeltrandelRio, H., Newgard, C.B., Jonhson, J.H., Unger, R.H. (1995) Pancreatic B cells in obesity. Evidence for induction of functional, morphologic and metabolic abnormalities by increased long chain fatty acids. *J. Biol. Chem. 270:* 1295–1299.

Nikoletseas, M.M. (1977) Obesity in exercising, hypophagic rats treated with monosodium glutamate. *Physiology and Behavior 19:* 767–773.

Nogueira, D.M., Strufaldi, B., Hirata, M.H., Abdala, D.S.P., Hirata, R.D.C. (1990) *Métodos de Bioquímica Clínica.* São Paulo. Pascat Editorial.

Ochi, M., Fukuhara K, Sawada T, Hattori T, Kusunoki, T. (1988) Development of the epididymal adipose tissue in monosodium glutamate-induced obese mice. J. Nutr. Sci.Vitaminol. 34: 317–326.

Prada, F.J.A., Luciano, E., Carneiro, E.M., Boschero, A.C., Mello, M.A.R. (2001) Protein deficiency attenuates the effects of alloxan on insulin secretion and glucose homeostasis in rats. *Physiol. Chem. Phys. & Med. NMR. 33:* 73–82.

Tavassa, T.M., Okuda, T., Romsos, D.R. (1992) Insulin secretion from ob.ob mouse pancreatic islets: effects of neurotransmitters. *Am. J. Physiol. 71:* 34–39.

Timmers, K.I., Voyles, N.R., Recant, L. (1992) Gennetically obese rats with (SHR/N-*cp*) or without diabetes (LA/N-*cp*) share abnormal islet responses to glucose. *Metab. Clin. Exp. 41:* 1125–1133.

Torgan, C.E., Brozinick, Jr. J.T., Banks, E.A., Cortez, M.Y., Wilcox, R.E., Ivy, J.L. (1993) Exercise training and clenbuterol reduce insulin resistance of obese Zucker rats. *Am. J. Physiol. 264:* E373–E379.

Zawalich, W., Maturo, S., Felig, P. (1982) Influence of physical training on insulin release and glucose utilization by islet cells and liver glucokinase activity in the rat. *Am. J. Physiol. 243:* E464–E469.

Zohu, Y-P, Cockburn, B.N., Pugh, W., Polonsky, K.S. (1999) Basal insulin hypersecretion in insulin-resistant Zucker diabetic and Zucker fatty rats; role of enhanced fat metabolism. *Metabolism 48:* 857–886.

Received December 30, 2002;
accepted May 15, 2003.

Physiol. Chem. Phys. & Med. NMR (2003) *35*: 55–72

MRS Study of the Interaction of Dihydropyridines with Lipid Molecules in Phosphatidylcholine Vesicles

F. Boffi[1], S. Grande[2], S. Marzi[1], M. Dell'Ariccia[1], A. Rosi[2], V. Viti[2,3] and A. Congiu Castellano[1]

[1]Dipartimento di Fisica, Istituto Nazionale di Fisica per la Materia, Università "La Sapienza", 00185 Roma, Italy [2]Laboratorio di Fisica e INFN Gruppo Collegato Sanità, Istituto Superiore di Sanità, Roma, Italy. [3]To whom correspondance should be addressed

Abstract: Dihydropyridines (DHPs), synthetic molecules used as antihypertensive agents, bind to plasma membrane receptors following diffusion through the hydrophobic phase. In this study, MRS technique has been used to clarify the interactions of the dihydropyridines Nifedipine and Lacidipine within the lipid bilayer. 1D and 2D ^{1}H MRS at high field have been employed to examine the behavior of unilamellar dimyristoyl-phosphatidylcholine liposomes when the two drugs have been inserted in the bilayer. In particular, the study represents an innovative application of 2D ^{1}H NOESY technique to clarify different mechanisms of interactions of small molecules inside model membranes. On the other hand, ^{31}P measurements have been performed in multilamellar dimyristoylphosphatidylcholine liposomes to detect alterations of lipid polymorphic phases. The experiments show that the two dihydropyridines interact with the lipids by different modalities. Lacidipine undergoes a very strong interaction with lipids, possibly inducing a phase segregation of lipid molecules into the bilayer, while self-association seems to be the prevalent interaction of Nifedipine inside the bilayer.

1,4-DIHYDROPYRIDINES (DHPs) are synthetic molecules used as antihypertensive agents for the treatment of angina and other vascular diseases. They are hydrophobic molecules acting on voltage dependent calcium channels (1–2). The mechanism of inhibition of the opening of their target molecules has not been completely clarified. It has been suggested that these highly lipophilic drugs bind to plasma membrane receptors *via*

Abbreviations: DHP-1,4-dihydropyridines; DMPC-L_{α}-dimyristoylphosphatidylcholine; EDXD-energy dispersion X-ray diffraction; LAC-Lacidipine; MLV-multilayer vesicles; MRS-magnetic resonance spectroscopy; NIF-Nifedipine; SUV-small unilamellar vesicles,

the membrane bilayer following diffusion through the hydrophobic phase (3–4). As a consequence, also nonspecific interactions of the drugs with the lipids play an important role in subsequent recognition and binding of drugs to specific receptor sites.

Our attention has been devoted to the study of two DHP's in membranes, namely Lacidipine (LAC) and Nifedipine (NIF). Different techniques had been used to investigate their interactions. By electrophysiological measurements, it was demonstrated that LAC persistently inhibited the voltage dependent calcium channel (5). There was evidence of a partition coefficient of this latter molecule in the hydrocarbon phase much larger than that of NIF (6); this effect suggested that an excess of LAC stays in equilibrium with the membrane bilayer for times much longer than those of the recording of patch-clamp experiments. From the structural point of view, it was suggested by EDXD experiments (7) that LAC induces an energetically favorable phase separation into the membrane bilayer (excess of LAC increases the new phase population), while NIF randomly distributes inside the hydrophobic region.

In the present paper, we have applied Magnetic Resonance Spectroscopy (MRS) to probe the interactions of these drugs with lipid molecules. This technique has, in fact, been proven a very powerful tool for detecting structural modifications due to changes of molecular environment consequent to different kind of interactions (8–9). The main interactions of the drugs have been monitored by using ^{1}H MRS on small unilamellar vesicles (SUV's) loaded with NIF and LAC. 1D ^{1}H MRS experiments have been performed at high field to exploit the high resolution available under these conditions. Furthermore, the examination of the cross peaks present in 2D ^{1}H NOESY spectra allowed us to get more insight into the mechanisms of these interactions. Different interaction modalities of NIF and LAC inside lipid vesicles have been evidenced. In addition some ^{31}P measurements have been performed in multilayer dimyristoyl-phosphatidylcholine vesicles (MLV's) to detect alterations of lipid polymorphic phases.

Materials and Methods

L_α-dimyristoylphosphatidylcholine (DMPC) 99% crystalline was purchased from Sigma-Aldrich (St. Louis, MO) and used as the only lipid component of model membranes. This lipid presents a chain melting transition at about 23 °C (10); all experiments have been carried out in L_α phase. Nifedipine was purchased from Sigma-Aldrich (St. Louis, MO) while Lacidipine is produced by Glaxo. Molecular structure of the two drugs are shown in Figure 3.

Solutions of drugs in chloroform have been prepared by using deuterated chloroform purchased from CIL (Andover, MA).

To prepare the drug-loaded vesicles, 100 mg of DMPC were dissolved in chloroform. After solvent evaporation the DMPC powder was suspended in 5 ml of D_2O. SUV's were prepared by sonicating the suspension for 25 min. Figure 1 shows the distribution of the gyration radius of DMPC SUV's, obtained by light scattering measurements inverting the intensity autocorrelation function with the Contin algorithm. From the distribution, it is possible to determine the average particle radius R = 106 ± 21 nm. The doped samples were obtained by adding the DHP's to the chloroform solution in the required molar ratios.

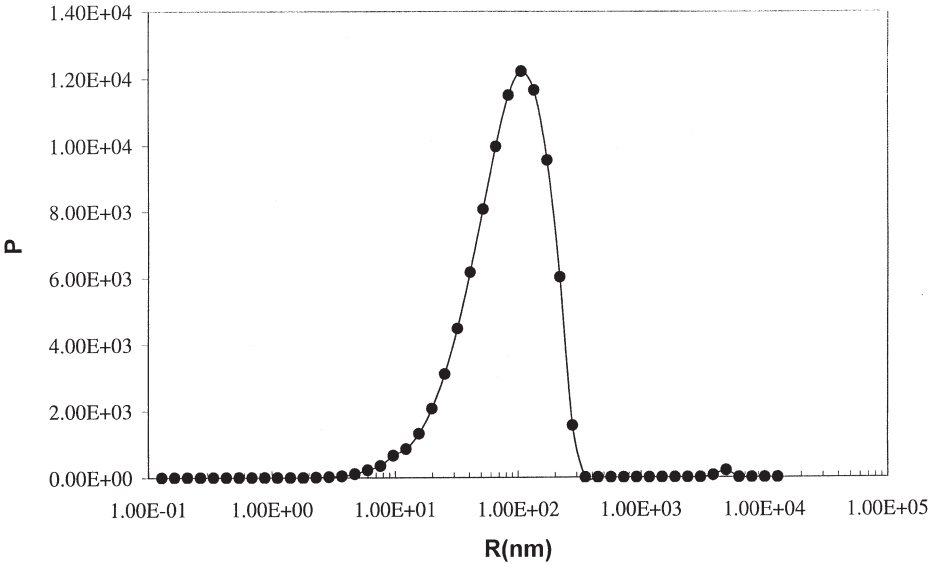

FIGURE 1. Distribution P of the gyration radium R of DMPC SUV's, obtained by light scattering measurements.

^{31}P spectra were run at 161.98 MHz on a Bruker Avance spectrometer equipped with a magnet of 9.40 T. On the other hand, ^{1}H MR experiments were performed under very high resolution conditions with a Bruker Avance spectrometer operating at 600.13 MHz, equipped with a magnet of 14.10 T. For ^{1}H MRS measurements, a 60° rf pulse and an interpulse delay of 3s were used. Residual HDO signal was gated irradiated. Chemical shifts were referred to external sodium 2,2-dimethyl-2-silapentane-5-sulfonate (DSS). Temperature was maintained at 27°C. 2D ^{1}H NOESY spectra were acquired with the pulse Bruker sequence NOESYGSTP, using different mixing times to keep spin diffusion effects as low as possible. The experiments were performed in the phase sensitive mode (TPPI), typically using 1K of memory for 512 increments. For ^{31}P MR measurements, spectra were obtained with a sequence of the WALTZ type (11) for proton decoupling. Accumulation of free induction decays was obtained up to 10000 scans. Recycle time was 1 s. ^{31}P chemical shifts are referred to 85% H_3PO_4 as external standard. A line-broadening of 15 Hz was applied to the free induction decays before performing the Fourier transformation.

To measure peak intensity ratios, resonance deconvolution of 1D spectra was performed by the Bruker software "1D WINNMR" (Bruker, AG, Darmstadt, Germany). The region of interest for quantification was that of $(\text{-}CH_3)_3$ of the choline peak (3.25 and 3.22 ppm), of $-OCH_3$ and $\varnothing\text{-}CH_3$ signals of the NIF at 3.33–3.46 ppm and at 2.59 ppm, respectively and of the aromatic signals of NIF and LAC. All peaks positions were fixed, while peaks intensities and line widths were fitted. Quantitative analysis of peaks was performed by measuring the fitted peak intensities.

Results

DMPC MLV's showed a ^{31}P spectrum typical of the bilayer configuration, characterized by a chemical shift anisotropy Δ_{csa} of 43.5 ppm (Figure 2), according to current literature (12). The structure was not completely maintained when liposomes were prepared in the presence of LAC. In this case, a phospholipid isotropic peak, beside the main signal from bilayer, appear around 0 ppm (Table I). A similar peak appeared also in DMPC-NIF MLV's, but at higher NIF concentration. Furthermore, the chemical shift anisotropy Δ_{csa} changes in DMPC-LAC MLV's (Table I).

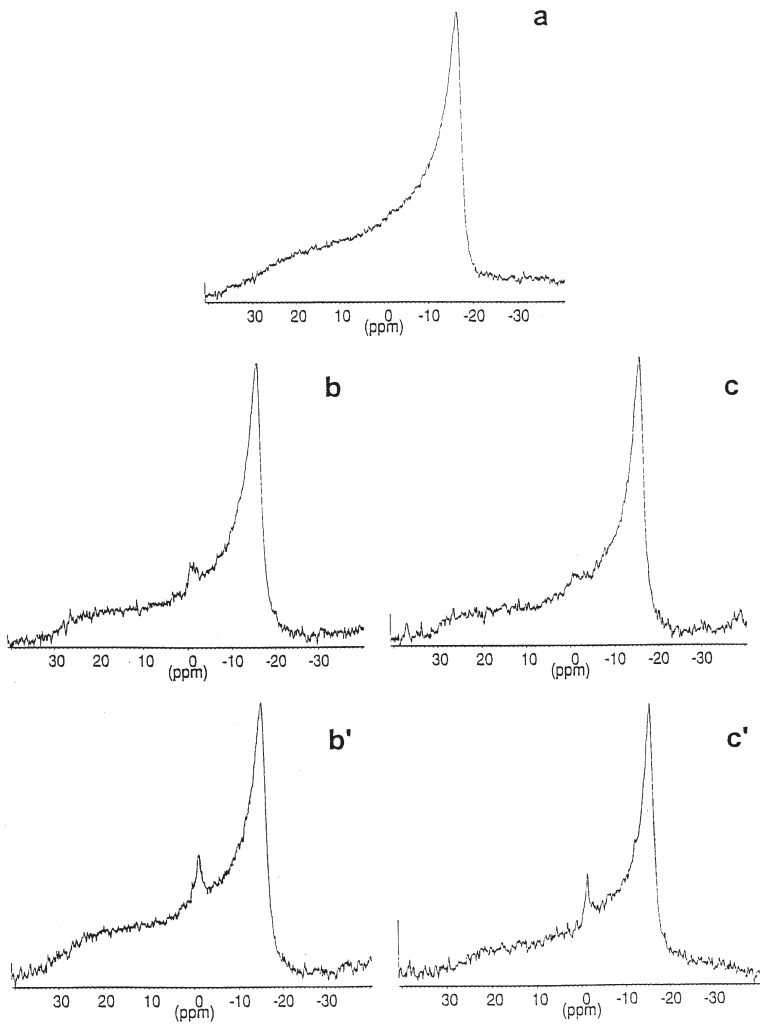

FIGURE 2. ^{31}P MR spectra of MLV's: a) DMPC MLV's; b,b') DMPC-LAC MLV's for drug to lipid molar ratio 1:2 and 1:1: c,c' DMPC-NIF MLV's for drug to lipid molar ratio 1:2 and 1:1.

TABLE I. Parameters of the ^{31}P MR spectra of DMPC MLV's containing NIF or LAC. $\Delta\nu_{csa}$ is the chemical shift anisotropy of the bilayer phase and δ_{is} is the chemical shift of the isotropic peak.

	$\Delta\nu_{csa}$(PPM)	δ (ppm)
DMPC	43.5 ± 0.5	—
DMPC-NMF	44.0 ± 0.5	0.9 ± 0.1
DMPC-LAC	39.0 ± 0.5	1.3 ± 0.1

NIF and LAC spectra in $CDCl_3$ are shown in Figures 3a and b. Assignments, performed on the basis of intensity of lines, chemical shift and J-coupling values, are reported in Tables II and III. Small signals from photo degradation products of the drugs were always present in the spectra, although at different extent in different preparations (signals due to these impurities are indicated with a star in Figure 3a, b).

We have then performed MRS experiments on DMPC SUV's loaded with the two drugs at different drug-to-lipid molar ratios. Figures 4a and b show the ^1H NMR spectra of DMPC when NIF and LAC were inserted in the SUV's at drug-to-lipid molar ratio 1:2. Spectra typical of SUV's could be observed in both cases and they did not change significantly when drug-to-lipid molar ratios ranged from 1:20 to 1:1. This latter observation indicates that disruption of model membrane did not take place even at the highest drug-to-lipid molar ratios and that the phenomena described in the following were irrespective of the drug concentration in this range. In the following we present the spectra relative to the ratio 1:2 because drug signals were well evident at this high drug concentration.

Assignments of lipid signals performed according to current literature (13–14) are reported in Tables II and III. Although the general appearance of these spectra was that of lipid SUV's, some specific features could be observed. In fact, both $(-CH_2)_n$ and terminal $-CH_3$ (tCH_3) signals from the acyl chains were split into two components when LAC was present in the bilayer (Figure 4b). This feature was present at a drug to lipid molar ratio as low as 1:20 (not shown). Furthermore, the choline peak from the external layer was shifted to lower field with respect to that of pure DMPC vesicles. To better show these effects, Figures 5b and b' report on details of the acyl chain and of the polar head group spectral regions of LAC-DMPC vesicles, while Table IV reports on relative chemical shifts (together with those of pure DMPC for a comparison). NIF produced a smaller effect, only slightly shifting the signal from the external head group and splitting the lipid chain signals (Figures 5 a and a' and Table IV).

Further evidence on the interactions of the two drugs with DMPC molecules was provided by the examination of the drug signals in the bilayer. In fact, low intensity signals in the aromatic spectral region of LAC- and in the aromatic and aliphatic spectral region of NIF-loaded vesicles are detectable (Figures 4 and 6). Comparison of the spectrum of NIF in $CDCl_3$ (Figure 3a), with that of the NIF containing vesicles (Figure 4a) shows that the two intense signals from the lateral $-OCH_3$ and $\varnothing$-CH_3 groups of the NIF, resonating in $CDCl_3$ at 3.59 and at 2.34 ppm respectively (Table II), are visible, although shifted, in the spectrum of the NIF in vesicles (Figure 4a). In particular, the two signals at 3.33 and 3.46 ppm are attributable to the $\varnothing$-$C\underline{H}_3$ group of NIF, now upfield shifted with respect to the same signal from NIF in $CDCl_3$ (Figure 4a and Table II). Only one signal at 2.59 ppm is present for the $-OCH_3$ group.

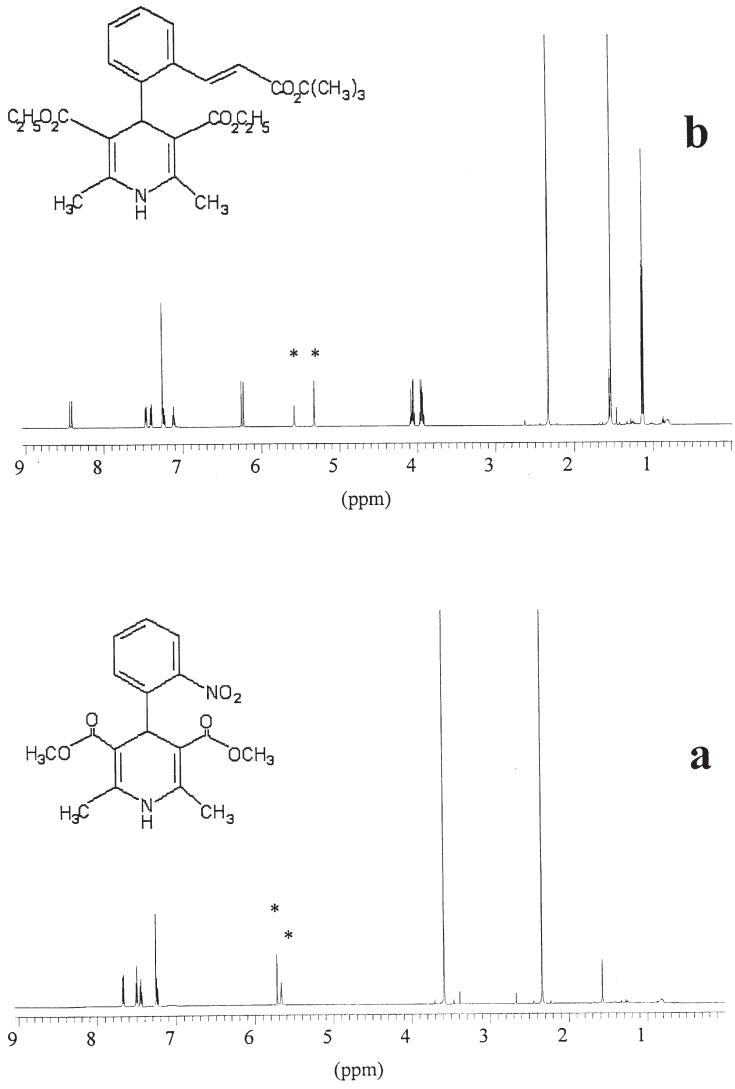

FIGURE 3. Molecular structures of Nifedipine (NIF) and Lacidipine (LAC). ^{1}H NMR spectra of a) NIF and b) LAC in $CDCl_3$ solution. Signal from residual $CDCl_3$ is at 7.26 ppm. The stars indicated signals from impurities due to photodegradation effects on the two drugs.

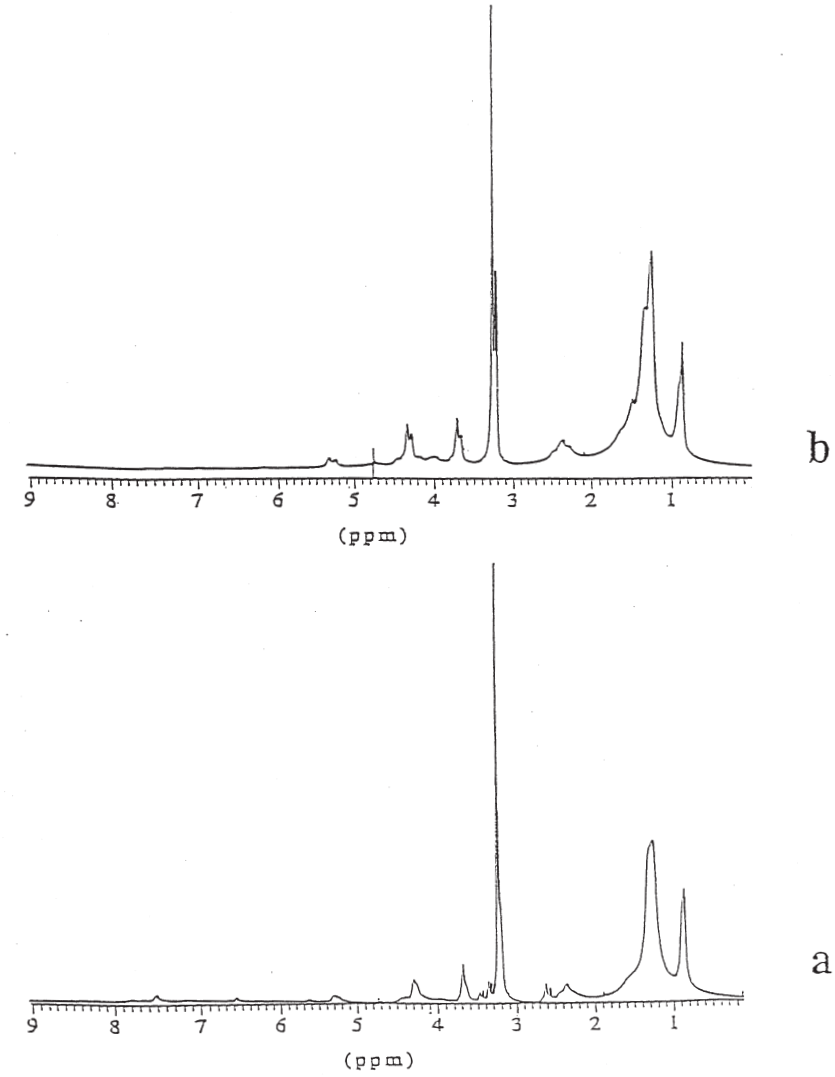

FIGURE 4. ^{1}H NMR spectra of NIF and LAC embedded in SUV's at a drug-to-lipid molar ratio of 1:2: a) DMPC-NIF SUV's; b) DMPC-LAC SUV's.

TABLE II. ^1H chemical shifts δ of NIF in $CDCl_3$ and of DMPC-NIF SUV's.

NIF in $CDCl_3$		DMPC-NIF SUV's			
NIF signals		DMPC signals		NIF signals	
	δ(ppm)		δ(ppm)		δ(ppm)
		CH_2-CH_2-$C\underline{H}_3$	0.86		
		CH_2-$C\underline{H}_2$-CH_3	1.26–1.31		
		OC-CH_2-$C\underline{H}_2$-CH_2	1.57		
		OC-$C\underline{H}_2$-CH_2-CH_2	2.32		
H_3C-∅	2.34			H_3C-∅	2.59
		$N(C\underline{H}_3)_3$	3.21–3.25		
H_3C-O-	3.59			H_3C-O-	3.33–3.46
		N-CH_2-$C\underline{H}_2$-OP	3.66		
		N-$C\underline{H}_2$-CH_2-OP	4.29		
		CH_2-CH_2-$C\underline{H}$=CH	5.26–5.30		
					6.58
aromatic protons	7.25			aromatic protons	7.21
aromatic protons	7.45			aromatic protons	7.52
aromatic protons	7.50			aromatic protons	7.68
aromatic protons	7.67			aromatic protons	7.82

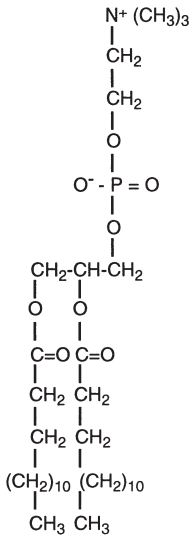

DMPC

TABLE III. ^{1}H chemical shifts δ of LAC in $CDCl_3$ and of DMPC-LAC SUV's.

LAC in $CDCl_3$		DMPC-LAC SUV's			
LAC signals		DMPC signals		LAC signals	
	δ(ppm)		δ(ppm)		
		CH_2-CH_2-$C\underline{H}_3$	0.87–0.91		
CH_2-$C\underline{H}_3$	1.14				
		CH_2-$C\underline{H}_2$-CH_3	1.26–1.35		
O-$C(C\underline{H}_3)_3$	1.54				
		OC-CH_2-$C\underline{H}_2$-CH_2	1.63		
		OC-$C\underline{H}_2$-CH_2-CH_2	2.33		
H_3C-∅	2.33				
		$N(C\underline{H}_3)_3$	3.22–3.27		
		N-CH_2-$C\underline{H}_2$-OP	3.68		
		N-$C\underline{H}_2$-CH_2-OP	4.28		
		CH_2-CH_2-$C\underline{H}$=CH	5.26–5.34		
$C\underline{H}_2$-CH_3	4.00				
CH=$C\underline{H}$-$CO_2C(C\underline{H}_3)_3$	6.25				
aromatic protons	7.12			aromatic protons	7.03
aromatic protons	7.24			aromatic protons	7.28
aromatic protons	7.40			aromatic protons	7.39
aromatic protons	7.47			aromatic protons	7.55
∅-$C\underline{H}$=CH	8.42				

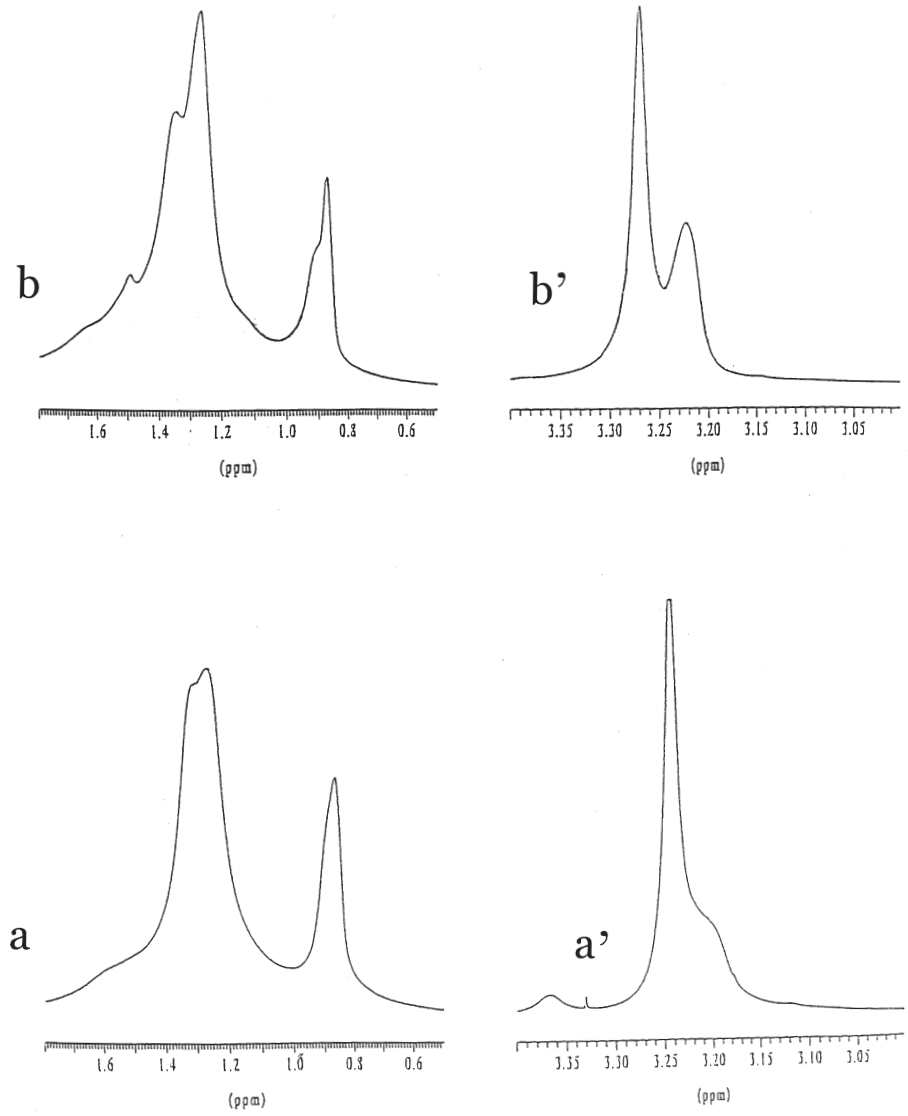

FIGURE 5. [1]H NMR spectra of lipid chain regions and polar head group of: a) DMPC-NIF SUV's lipid chain region; a') DMPC-NIF SUV's polar head group region, b) DMPC-LAC SUV's lipid chain region. b') DMPC-LAC SUV's polar head group region. The drug-to-lipid molar ratio was 1:2.

TABLE IV. Chemical shifts of lipid signals in the ^{1}H NMR spectra of DMPC SUV's containing and not containing drugs. δ_{out} is the chemical shift of the external polar head group, δ_{in} is the chemical shift of the internal polar head group, δ_{chain} is the chemical shift of the -CH_2 in the acyl chain, δ_t is the chemical shift of the terminal -CH_3.

	δ_{out}(ppm)	δ_{in}(ppm)	δ_{chain}(ppm)	δ_t(ppm)
DMPC	3.25 ± 0.01	3.22 ± 0.01	1.26 ± 0.01	0.88 ± 0.01
DMPC+NIF	3.25 ± 0.01	3.21 ± 0.01	1.26 ± 0.01 1.31 ± 0.01	0.86 ± 0.01 0.88 ± 0.01
DMPC+LAC	3.27 ± 0.01	3.22 ± 0.01	1.26 ± 0.01 1.35 ± 0.01	0.87 ± 0.01 0.91 ± 0.01

Intensities of the aromatic and aliphatic drug signals in the vesicles increased as a function of drug concentration, but they were inconsistent with the drug to lipid molar ratios in the sense that lower drug intensities were found with respect to the expected ones on the basis of the molar ratio drug to lipid and of the partition coefficients. Partition coefficients reported in the literature (6) are so high that the intensity of drug signals reflects mainly the molar concentration of the drug. As a consequence, one should expect a signal intensity ratio for the $-OCH_3$ and $\varnothing$-CH_3 signals of the NIF to the $-N(CH_3)_3$ choline peak of approximately 1 to 6 and for the aromatic signals due to a single hydrogen atom of NIF or LAC of approximately 1 to 18 in the spectra reported in Figure 4. These numbers are far away from the observed intensitity ratio, obtained by deconvolving signals as indicated in the Materials and Methods section, that resulted lower than 1 to 30 even for the most intense $-OCH_3$ and $\varnothing$-CH_3 signals.

In Figure 6a the aromatic region of NIF in $CDCl_3$ is seen. Intense signals are visible in this spectral region also for NIF-DMPC vesicles (Figure 6a'). In particular, the spectrum reported in this latter figure shows the interesting feature that narrow and broad signals are present at the same time. We have ruled out the possibility that the narrow signals derive from NIF decomposition because, as shown in Figure 3a, this produces a spectrum with a pattern different from that of intact NIF. On the contrary, the narrow signals present in NIF-DMPC vesicles have the same pattern as that of intact NIF, although resonances are shifted to different positions. We report in Table II chemical shifts of the four narrow multiplets and of the broad peaks. The narrow multiplets are present as three doublets and one triplet of the same intensity. This is the pattern present also in chloroform solution, although the signals are characterized by different chemical shifts. The integral ratio of the two species is strongly in favor of the broader components, but we do not report its value because it is affected by a very large error due to the very large differences in linewidths and intensities of the two species. Chemical shifts values reported in Table II indicate that the change in susceptibility passing from chloroform to vesicles is not the reason for the observed differences. In fact, the extent of the changes is not the same and mainly not in the same direction, for all signals. On the other hand, it is impossible to attribute the broad signals to the protons in the different positions of the aromatic ring because the information on the multiplet structure is lost. The peak at 7.52 ppm is approximately three times more intense than the peak at 6.58 ppm, while reliable signal intensities cannot be obtained for the broad less intense lines. Notably the broad signal at

6.58 ppm and the narrow at 6.68 ppm of NIF-DMPC vesicles (Figure 6a') are strongly shifted to higher field with respect to the main envelope of the aromatic signals of NIF in chloroform (Figure 6a).

As far as LAC containing vesicles are concerned, the spectrum does not show any intense signals from LAC lateral groups (Figure 4b). Particularly the very intense signal from $OC(CH_3)_3$, at 1.54 ppm in $CDCl_3$ (Figure 3b), is not visible in LAC-DMPC vesicles. Differently from the NIF-loaded vesicles, only very broad and low intensity signals from the aromatic ring are detectable in LAC-DMPC vesicles and only at the highest drug to lipid ratios (Figure 6b'). To get comparable line intensities of the aromatic signals, the vertical scale of LAC-DMPC spectrum (Figure 6b') has been multiplied for a factor of three with respect to the scale of the NIF-DMPC spectrum (Figure 6a'). In LAC-DMPC vesicles, the aromatic signals are slightly upfield shifted with respect to those in chloroform (compare Figures 6b and b').

To clarify the reason for the shifts of the NIF signals when this drug was embedded into the bilayer, we have performed 2D ^{1}H NOESY experiments. In sopramolecular lipid systems, significant spin diffusion may be present even at relatively short mixing times (15–16). To discriminate among spurious and real cross peaks, a series of measurements was performed with different mixing times (15, 30, 50, 200 ms). According to current literature (15), a criterion for the choice of a good mixing time for these kinds of samples is the absence of correlation between the tCH_3 of the fatty acid chain at 0.86 ppm and the methylene protons of the glyceride moiety near 4.5 ppm. This spurious cross peak was not found with a mixing time of 50 ms.

Figure 7a shows the 2D ^{1}H NOESY experiment of pure DMPC vesicles: only a cross peak between tCH_3 and bulk $(CH_2)_n$ is observable that can be due to dipolar interactions between chains of close molecules. The 2D ^{1}H NOESY spectra of NIF containing vesicles is shown in Figure 7b while two expanded regions are reported in Figures 7b' and b". Intense correlations due to both NIF-NIF (cross peaks 1, 2 and 3) and DMPC-NIF (cross peak 4) interactions are present in this sample. Table V reports on the relative chemical shifts. Analogously, Figure 7c shows the 2D ^{1}H NOESY full spectrum of the LAC containing vesicles, and Figure 7c' a detail of the same spectrum. Multiple LAC-LAC NOEs are present in the aromatic region, including the main correlation at 7.47–6.25 ppm, chemical shifts similar to those of LAC signals in chloroform (see Table IV). Only one cross peak attributable to the DMPC-LAC interaction is barely visible at 2.31–7.53 ppm (Figure 7c').

Discussion

Interactions of dihydropyridines with lipid molecules can be envisaged on the basis of previous evidences (4,7). In the present work, MRS has been used with the aim of obtaining direct information on these interactions when the dihydropyridines LAC and NIF were inserted in the bilayer. We have exploited the high resolution obtainable when examining the ^{1}H MRS high field spectra of SUV's containing the drugs. Although the quality of the spectra is generally poor due to the high dynamic range, some preliminary indications on drug-lipid interactions can be drawn from the present experiments.

The presence of both LAC and NIF in MLV's produces a small isotropic peak around 0 ppm in the ^{31}P MR spectra (Figure 2). A smaller concentration of LAC than of NIF

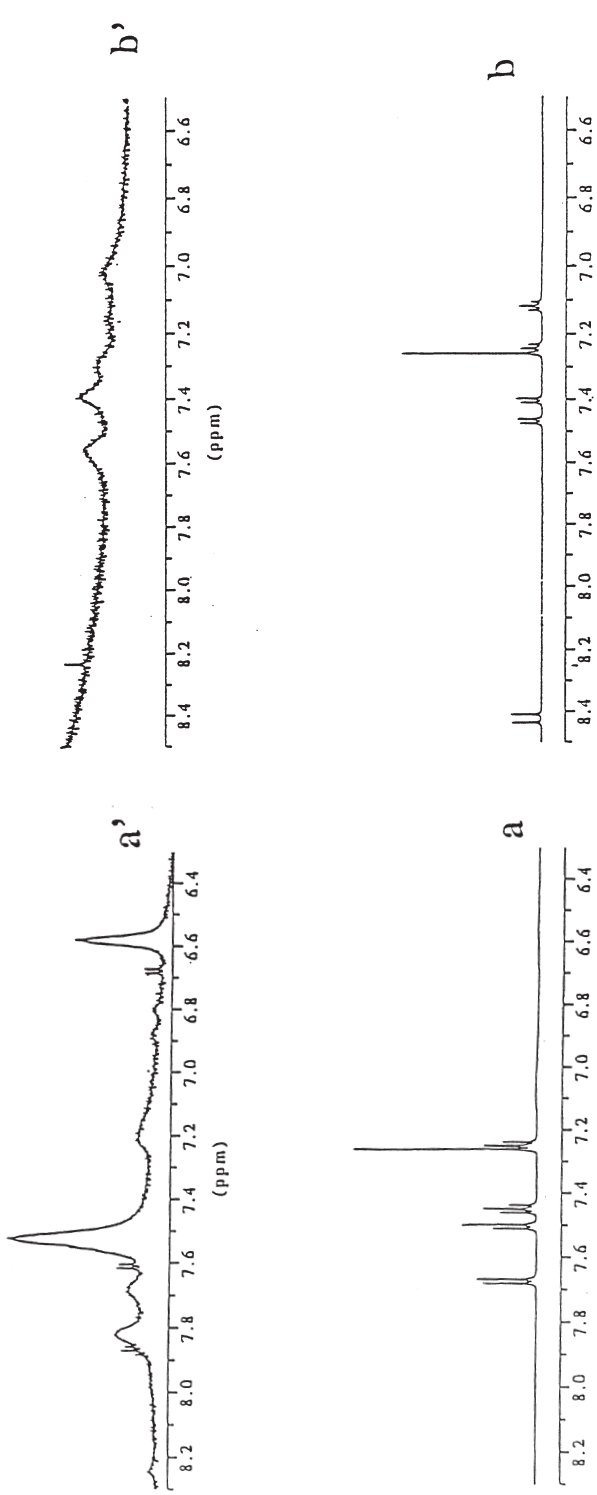

FIGURE 6. ^{1}H NMR spectra of aromatic region from a) NIF in $CDCl_3$; a') DMPC-NIF SUV's; b) LAC in $CDCl_3$; b') DMPC-LAC SUV's. The drug-to-lipid molar ratio was 1:2. The vertical scale of spectra of LAC-loaded vesicles had been multiplied for a factor of three with respect to the scale of the spectra relative to NIF-loaded vesicles.

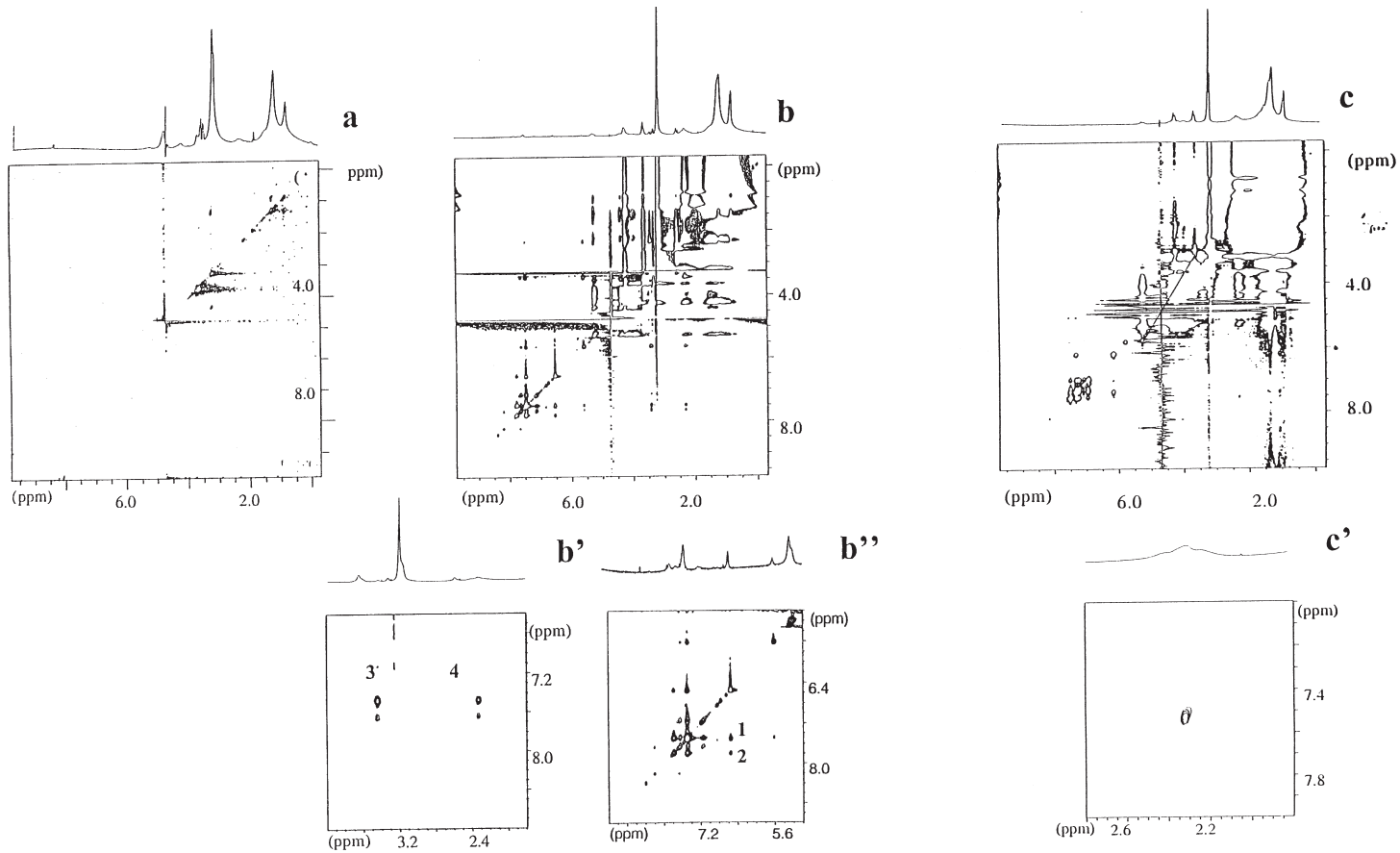

FIGURE 7. 2D ^{1}H NOESY spectra (mixing time 50 ms) of: a. DMPC SUV's; b. DMPC-NIF SUV's (b'. and b". two expanded regions); c DMPC-LAC SUV's (c'. an expanded region). The drug-to-lipid molar ratio was 1:2.

makes possible its detection. This kind of peak can arise from a population of vesicles with small diameters, from regions of high curvature of the bilayer structure or from the presence of small inverted micelles in the bilayer (17). This latter hypothesis would be strengthened by the observation that chemical shifts of the isotropic peak are different for the two drugs (Table I), thus indicating that the isotropic peak could derive from an interaction of lipid molecules with the drugs and not simply to segregation of lipid molecules inside the bilayer.

The decrease in chemical shift anisotropy $\Delta\nu_{CSA}$ in the presence of LAC in MLV's could be due to an increase in local curvature of the bilayer or to some specific interaction between drug and phosphate group. We are in favor of the second hypothesis because a perturbation of LAC on the lipid head group is present also in SUV's, as indicated by the shift to lower field of the choline peak from the external layer (Figure 5 and Table III).

The lipid acyl chain signals were separated into two peaks when both the two drugs were inserted in the vesicles (Figures 4 and 5), but this effect was particularly evident when LAC was present in the bilayer, pointing to a stronger interaction for LAC with DMPC than for NIF with DMPC. Analogously, an appreciable upfield shift of the signal from the outer leaflet of DMPC is visible only for LAC containing vesicles (Table IV and Figure 5b). This effect is also attributable to DMPC-LAC interactions because the trimethyl ammonium group of phospholipids is generally affected by the ring current of the aromatic rings when aromatic lipophylic drugs interact with the lipid molecules, resulting into an upfield shift of the corresponding protons (18–21). However, the shift is small, indicating a preferential dispersion of the LAC into the hydrophobic portion of the bilayer.

The examination of the aromatic region of NIF loaded vesicles suggests that there are distinct environments for NIF in the bilayer. The spectrum reported in Figure 6a' suggests the presence of at least two environments characterized by a restricted mobility. On the basis of line intensities, a first one is represented by the signals at 6.58 ppm and 7.52 ppm while the second one is represented at least by the signals at 7.82 and by other less intense signals. The peaks at 6.58 ppm, so strongly shifted with respect to all the aromatic signals of NIF in chloroform solution, is indicative of stacking interaction among NIF molecules. The stacking of NIF molecules consequent to self-association can produce, in fact, shielding effect above and below the plane of the aromatic rings (22). This hypothesis could be confirmed by the presence of the intense cross peaks 1 in the 2D NOE spectrum (Figure 7b" and Table V). The 2D NOE spectrum reported in Figure 7b", indicating a correlation of both peaks at 7.52 and 7.82 with the peak at 6.58, suggests that this latter signal derives from NIF molecules in both first and second environments.

TABLE V. Chemical shifts δ of relevant cross peaks in 2D ^{1}H NOESY spectra of DMPC-NIF SUV's.

		. δ (ppm)
1	NIF-NIF	6.58–7.52
2	NIF-NIF	6.58–7.82
3	NIF-NIF	3.46–7.52
4	DMPC-NIF	2.31–7.52

Stacking interactions produce an influence also on lateral groups of the NIF aromatic ring because intense correlations are observed at 7.52–3.46 ppm (peak 3 in Figure 7b'), that is at the frequencies corresponding to the most intense aromatic signal and to one of the signals attributed to H_3C-O-. This latter signal was upfield shifted with respect to the same signal of NIF in $CDCl_3$ (3.46 with respect to 3.59 ppm, see Table I). These two evidences point out that the stacking interaction influences also the pyridinic ring. The other signal at 3.33 ppm, that was upfield shifted in vesicles with respect to chloroform, did not show any cross peak with aromatic signals. On the other hand, the presence of the cross peak at 2.31–7.52 ppm (peak 4 in Figure 7b'), visible even when employing a short contact time, indicates that NIF is interacting also with lipid molecules, in particular through a direct interaction between the NIF and the -CH_2 group close to -CO in the lipid molecule. This result points out to the insertion of the drug into the bilayer at the level of the upper part of the lipid chain.

A third environment for NIF is related to the four narrow lines at 6.68, 7.55, 7.61 and 7.87 ppm (Figure 6a'). We have ruled out the possibility that the narrow signals derive from NIF decomposition because, as shown in Figure 3a, this produces a spectrum with a pattern different from that of intact NIF. On the contrary, the narrow signals present in NIF-DMPC vesicles have the same pattern of intact NIF, although resonances are shifted to different positions. In this environment, NIF molecules are characterized by a very high mobility, similar to that of chloroform solution, although chemical shifts are completely different. NIF-NIF interactions should prevail in this phase because the signal at 6.68 is shifted to higher fields with respect to all aromatic signals in chloroform, pointing out also in this case to a stacking interaction among NIF molecules. Unfortunately the absence of cross peaks in the 2D NOE spectra, most probably due to the very low intensity of the narrow signals, did not allow us to confirm this hypothesis.

The integral ratio of the broad and narrow species is strongly in favor of the broader components, but we do not report its value because it is affected by a very large error due to the very large differences in linewidths and intensities of the involved species.

Drug signals in spectra from LAC-loaded vesicles did not present features similar to those of NIF-loaded vesicles. In fact, only minor changes of chemical shifts of the aromatic signals appeared when LAC was inserted in the bilayer (Figure 6b') that could be attributed to local changes of magnetic susceptibility in different drug environment. The correlations in the aromatic region of the spectra from LAC-DMPC vesicles, including the main correlation at 7.47–6.25, most probably derive from intramolecular interactions and not LAC-LAC stacking interactions because LAC signals in spectra of LAC-DMPC vesicles are not shifted to higher field, contrary to NIF signals in spectra of NIF-DMPC. The barely detectable, not symmetry related, cross peak 7.53–2.31 (Figure 7c and c') is suggestive, although not definitely proof of, an interaction between LAC and DMPC in a definite position along the lipid chain. The high spectral dynamic range did not allow us to run spectra of good quality for these samples.

These results would indicate that the broad lines in the LAC-DMPC and NIF-DMPC spectra arise from LAC and NIF partitioned into SUV. The narrow resonances observed for NIF would indicate that some NIF is non-partitioned into SUV, consistently with the partition coefficient of NIF lower than that of LAC (6). As far as intensities of drug signals in vesicles are concerned, they increase by increasing drug concentration, but they are inconsistent with the corresponding molar ratios drug to lipid, being much lower than

expected (see Figures 4 and 6 and considerations reported in "Results" section). Furthermore, signals from LAC and NIF in the relative spectra of drug-DMPC vesicles are of similar intensities (Figure 6) although LAC has a much higher membrane partition coefficient than NIF (6), indicating that signal intensity is missing particularly for LAC. A possible explanation for these observations could be that drug molecules are partially immobilized inside the bilayer and that drug signals visible in the spectra derive from the most mobile drug molecules in equilibrium with a phase of drug molecules very strongly interacting with lipids. LAC interaction with the hydrocarbon core domain would favor accommodation in the bilayer of more LAC than NIF molecules in a phase strongly immobilized and therefore not visible in the spectra, in agreement with partition coefficient data (6). Further experiments are necessary to clarify this hypothesis.

The experiments here reported point to a different mechanism of interaction for the two drugs inside membranes. The strong interaction of LAC with the lipid molecules could be the reason for the previously observed long persistence of the drug in the membrane bilayer (5) and would explain the high partition coefficient of this drug. The evident separation of signals from (CH2)n and from -tCH3 suggests the presence of two lipid phases, one of which is very rich in LAC molecules, confirming and clarifying the Energy Dispersive X-ray Diffraction (EDXD) data (7). The presence of a second lipid phase rich in drug is suggested also for NIF containing vesicles, but the smaller separation of the -(CH2)n signal indicates that in this case, the amount of the drug interacting with the lipid molecules would be smaller. In fact, from the 2D NOESY experiments, we can infer that NIF is present in two states, one dominated by NIF-lipid interactions and a second one, very probably in an aqueous compartment, where NIF-NIF interactions prevail.

In conclusion, this study has shown that MRS can be an useful tool to investigate interaction of dihydropyridines with lipid molecules. Further experiments could contribute to clarifying the role of these drugs in perturbing the lipid bilayer. Results shown here are in agreement with EDXD experiments. Moreover MRS clarifies the different behavior of the two DHPs giving new opportunities for future work aimed at getting more insight into Nifedipine stacking. The combined approach with X-Ray diffraction and MRS has been shown useful in this kind of study and particularly 2D ^{1}H NOESY experiments can provide a powerful tool for investigating intermolecular association in this type of complex systems.

We thank Glaxo-Wellcome for providing Lacidipine and Prof. F. Gambale for suggesting this work and for stimulating discussion. Thanks are also due to Dr. D. Capitani and Prof. R, Caminiti for helpful discussions.

References

1. Bean, B.P., Sturek, M., Puga, A., Hermsmeyer, K. (1987) Nitrendipine block of calcium channels in cardiac and vascular muscle. *J. Cardio. Pharm. 9:* 517–524.
2. Chester, D.W., Herbette, L.G., Mason, R.P., Joslyn, A.F., Triggle, D.J., Koppel, D.E. (1987) *Biophys. J. 52:* 1021–1030.
3. Rhodes, D.G., Schoch, P., Mohler, H., Haefely, W. (1986) Benzodiazepine receptors resolved. *Experientia 42:* 121–126.
4. Mason, R.P., Moring, J., Herbette, L.G. (1990) A molecular model involving the membrane bilayer in the binding of lipid soluble drugs to their receptors in heart and brain. *Nucl. Med. Biol. 17:* 13–33.

5. Gambale, F., Dellacasagrande, F. (1994) New DPH Lacidipine persostently inhibits L-type calcium currents in GM3 cells. *J. Cardio. Pharm. 24:* 114-119.
6. Herbette, L.G., Gaviraghi, G., Dring, R.J., Briggs, L.J., Mason, R.P. (1993) Interactions of lacipidine and other calcium channel drugs with biological membranes: a structural model for receptor/drug binding utilizing the membrane bilayer. (1993) *J. Hypertens. 11:* S16–19.
7. Boffi, F., Caminiti, R., Sadun, C., Capuani, S., Giovannelli, A., Congiu, Castellano A. (1998) A structural and kinetic study by energy dispersion X-ray diffraction; interaction between 1,4-dihydropyridines and biological membranes. *Chem. Phys. Lett. 28:* 473–478.
8. Warschaski, D.E., Traikia, M., Devaux, P.F., Bodhenausen, G. (1998) Solid-state NMR for the study of membrane systems: the use of anisotropic interactions. *Biochimie 80:* 437–450.
9. Maurer, N., Wong, K.F., Hope, M.J., Cullis, P.R. (1998) Anomalous solubility behavior of the antibiotic ciprofloxacin encapsulated in liposomes: a 1H NMR study. *Biochim. Biphys. Acta 1374:* 9–20.
10. Janiak, M., Small, D., Shipley, G. (1979) Temperature and compositional dependence of the structure of hydrated dimyristoyl lecithin. *J. Biol. Chem. 254:* 6068–6072.
11. Shaka, A.J., Keller, J., Freeman, R. (1983) Evaluation of a new broad-band decoupling sequence: Waltz 16. *J. Magn. Reson. 53:* 313–315.
12. Seelig, J. (1978) 31P NMR and the head group structure of phospholipids in membranes. *Biochim. Biophys. Acta 515:* 105–140.
13. Sze, D.Y., Jardetzky, O. (1990) Determination of metabolite and nucleotide concentrations in proliferating lymphocytes by ^{1}H-NMR of acid extracts. *Biochim. Biophys. Acta 1054:* 198–206.
14. Lean, C.L., Mackinnnon, W.B., Delikatny, E.J., Whitehead, R.H., Mountford, C.E. (1992) Cell-surface fucosylation and magnetic resonance spectroscopy characterization of human malignant colorectal cells. *Biochemistry 31:* 11095–11105.
15. Bonaccio, S., Capitani, D., Segre, A.L.,Walde, P., Luisi, P.L. (1997) Liposomes from phosphatidyl nucleosides: an NMR investigations. Langmuir *The ACS J. of Surfaces and Colloids. 13:* 1952–1956.
16. Olejniczak, E.T., Gampe, R.T. Jr., Fesik, S.W. (1986) Accounting for spin diffusion in the analysis of 2D NOE data. *J. Magn. Reson. 67:* 28–41.5
17. Yeagle, P.L. (1990) Phosphorus NMR of membranes. *Biol. Magn. Reson. 9:* 1–54.
18. Colley, C.M., Metcalfe, J.C. (1972) The localization of small molecules in lipid bilayers. *FBS letters 24:* 341–346.
19. Jendrasiak, G.L., Estep, T.N. (1977) The interaction of 1-anilo-8-naphtalene-sulfonate with lipids: a nmr study. *Chem. Phys. Lipids 18:* 181–198.
20. Jones, G.P., Marker, A., Paleg, L.G. (1984) Complex formation between indole-23-acetic acid and phospholipid membrane components in aqueous media. Parameters of the systems. *Biochemistry 23:* 1514–1520.
21. Erikson, G.L.E.(1987) Interaction of charged amphiphilic drugs with phospahtidylcholine vesicles studied by NMR. *Biophys. Chem. 26:* 9–18.
22. Pople, J.A., Schneider, W.C., Bernstein, H.J. (1959) High resolution NMR, McGraw Hill, New York, pp. 180–183, 424–428.

Received January 22, 2002;
accepted December 15, 2002.

Physiol. Chem. Phys. & Med. NMR (2003) *35*: 73–90

The Thermo-Photoelectric (TPE) Properties of the Hornet Cuticle: Correlation with the Morphological Structure

Vitaly Pertsis,[*] Anna Sverdlov and Jacob S. Ishay[†]

Department of Physiology and Pharmacology, Sackler School of Medicine, Tel-Aviv University, Ramat- Aviv 69978, Israel.
**Part of the Ph.D. thesis of V. P.*
†Author correspondence

Abstract: The present study investigated thermoelectric phenomena in the cuticle of the Oriental hornet *Vespa orientalis* (Hymenoptera, Vespinae). This was done in dependence on the pigment extant at various cuticular region, that is, the brown cuticle in which the primary pigment is melanin and embedded within the cuticle, and the yellow stripes in which the yellow pigment is comprised of purines and pteridines that are located in special pockets between the upper part of the cuticle and the basement membrane. The yellow pigment could be separated from the cuticle proper, but the brown pigment was not thus separable. We found that all cuticular regions of the gaster evinced a thermoelectric response, in that with rise in temperature there was a rise in the thermoelectric current, and *vice versa*. Additionally, the intact hornet displayed a negative photoelectric response in each of its yellow segments, so that upon illumination with UV light, the maximal current dropped by about 40–50%. Measurements taken on individual stripes in the gaster segments revealed that the photoelectric response is elicited only in the yellow stripes. In all the latter the photoelectric response persists but the maximal current level is lower than in the intact whole hornet. If the yellow pigment is detached mechanically or by bacterial incubation, the photoelectric property of the cuticle is abrogated. Likewise the photoelectric property is abrogated upon immersion of the cuticle in alcohol, even though the yellow pigment is still retained. The specific heat of the yellow stripes in the cuticle is about twice as high as that of the same stripes that had been depleted of their yellow pigment, amounting to 1.8–1.9 J/g.K vs. 0.8 J/g.K.

OVER THE years, we have been engaged in measuring the electric properties of hornet cuticle (e.g., Croitoru *et al.*, 1978). Many studies have shown that the hornet's cuticle is comprised, especially in the gaster region, of segments endowed with a yellow pigment (gastral segments 3+4) and other segments displaying brown pigment only (segments 1+2,

5+6*).* In all the gastral segments, one can detect and measure a thermoelectric property by attaching electrodes to them — a procedure previously described (Sverdlov *et al.,* 2000). Using this procedure we found that when the ambient temperature (incubator) was increased (at a relative humidity in excess of 90%), the current gradually increased as we proceeded from 20°C to 30°C. This temperature range was selected both for its great utility and because it contained the optimal temperature in a hornet's nest, which is usually 29°C (Ishay and Rutner, 1971; Spradbery, 1973). At the latter temperature, the resistivity is the lowest and the current is the highest, and we presume that this is true also within the natural nest. To date, all studies on this subject have shown that the reported results are obtained under condition of darkness. Lately, however, we have found that under UV light, the current rises less with rise in temperature (usually by only 50–60%) than it does in the dark, thus pointing to a possible additional effect — the photoelectric phenomenon in hornet cuticle beside the thermoelectric. Intrigued by this finding, we set out to ascertain what was responsible for this phenomenon, and whether it was one of the pigments in the cuticle (brown or yellow). Additionally, we deemed it worthwhile to clarify whether the specific heat of the yellow stripe changes when the stripe is stripped of its pigment. The present paper attempts to provide answers to these questions.

Materials and Methods

The present study investigated the thermophotoelectric (TPE) properties of the Oriental hornet *Vespa orientalis.* To this end, adult hornets were obtained from natural nest in the field. The hornets were subjected to ether anesthesia and transported to the laboratory as previously described (Ishay, 1975). The extracted hornets were kept at −20°C until use. The electric measurements, which included attaching electrodes to the measured body part of the hornet, and the sequence and protocol of the measurements are as previously described (Sverdlov *et. al.,* 2000). Our study explored the correlation of the electric current with temperature; that is, the thermoelectric properties of the hornet cuticle, and also the correlation of the current level with the extent of illumination. To this end, we changed the temperature in the test incubator in fixed cycles within a temperature range of 20–30°C, and the specimens were measured in cycles performed both in the dark as well as in light within the visible range (400–800 nm) or UV light (at 254 and 366 nm), in brief light within the UVA and UVC ranges, using a Desaga lamp (Heidelberg, Germany) emitting a strength of 44 Lux. A series of measurements were taken, with at least six replications in series. The following series were performed: 1) on entire hornet specimens, with the electrodes attached below (i.e., behind) the yellow stripes of the gaster (segments 3+4); 2) ditto, but with the electrodes affixed below the brown stripes of the gaster; 3) on a yellow gastral segment (segment 3) separated from the rest of body but the cuticle left intact with its yellow pigment; 4) on yellow gastral segments whose yellow pigment was scraped off mechanically, leaving only the transparent cuticle or alternatively on yellow segments that were left to incubate for a month in tap water — a procedure leading to development of a bacterial flora which attacks the yellow pigment and the surrounding tissue, ultimately leaving a clear cuticle just as in the mechanical removal procedure or on yellow stripes of the gaster, previously incubated for 30 min. in a solution of 75% ethyl alcohol; 5) on brown gastral segments detached from the body, with the electrodes attached below the brown segment (No. 2); and 6) on the hornet wing, which is essentially

an almost transparent cuticle, and this for the purpose of comparison with the above-mentioned measurements at the rate of changes in the incubator.

In all the above measurements the electrodes were affixed onto the inner side of the cuticle. Specific heat measurements on the yellow or brown stripes were performed by the same precise adiabatic calorimeter device of the Tel Aviv University as has been used in a previous study (Ishay *et al.,* 2002).

Results

In Figure 1 we present six examples of measuring results on yellow stripes (gastral segment 3) obtained from the dorsal (tergum) side, with the electrodes attached longitudinally, on the underside of the cuticle. In each of the presented pictures, the initial two or three measurements were made in the dark (D), the next two were made in light (L) and UV (in the UVA and UVC ranges) at a general intensity of 700 Lux, and immediately after another 2–3 measurements in the dark. When assessing the influence of wavelength on the photoelectric phenomenon, we found that whenever the visible light was turned off, the UV light alone still exerted an effect (much as it did in combination with visible light), which leads us to conclude the influence of light is contributed solely by the UV light (of 44 Lux only). In general, what one sees in all throughout the six pictures presented in Figure 1 is that measurements made in the dark yield a higher current between 20–140 nA, whereas upon exposure to light the values are invariably lower, ranging between 5–80 nA. Actually the current produced under illumination is about 60% of that obtained in the dark. In general, the heating curve is faster than the cooling curve (especially evident in Figure 1E), but the reverse also occurs occasionally (e. g. Figure 1F). In all the measurements, both in dark and in light, we noticed also a thermoelectric phenomenon, in that with rise in temperature there was a rise in the current, and *vice versa.* We also observed a negative photoelectric phenomenon wherein, upon exposure to light, the current was always lower (by about 40%) than that recorded in the dark (a thermoelectric current).

Figure 2 presents the results of 6 measurements taken as in Figure 1 except that here the electrodes were fastened below the brown stripe (gastral segment 2). The sequence of measurements here was the same as in Figure 1 (i.e. , 2 or 3 cycles of measurement in dark, 2 in light (UV) and again 2 in dark). Once more, as in Figure 1 the thermoelectric phenomenon is clearly evident except that: a) there is great disparity between the results here, with the current values ranging between 4–145 nA; b) most of the results display inverse polarity so that except in Figure 2A, in all the other pictures the current values are in the minus range; and c) light exerts no effect here, in that there is no evidence whatsoever to a photoelectric effect.

Figure 3 presents current values except that in this case the electrodes were fastened onto the inner side of the yellow stripe (gastral segment 3) after its separation from the hornet's body. The maximal values in the dark in all six specimens measured were in the range of 10–30 nA, while the maximal values obtained under illumination ranged from 6 nA to 20 nA, with the ratio between average values in the dark to average values in light being 0.64. In this regard, there was no significant difference in the results for single stripe versus entire body but the current values for single stripe were relatively very low compared to those for entire body, comprising 35% and 37% of the latter for recordings in the dark and light, respectively.

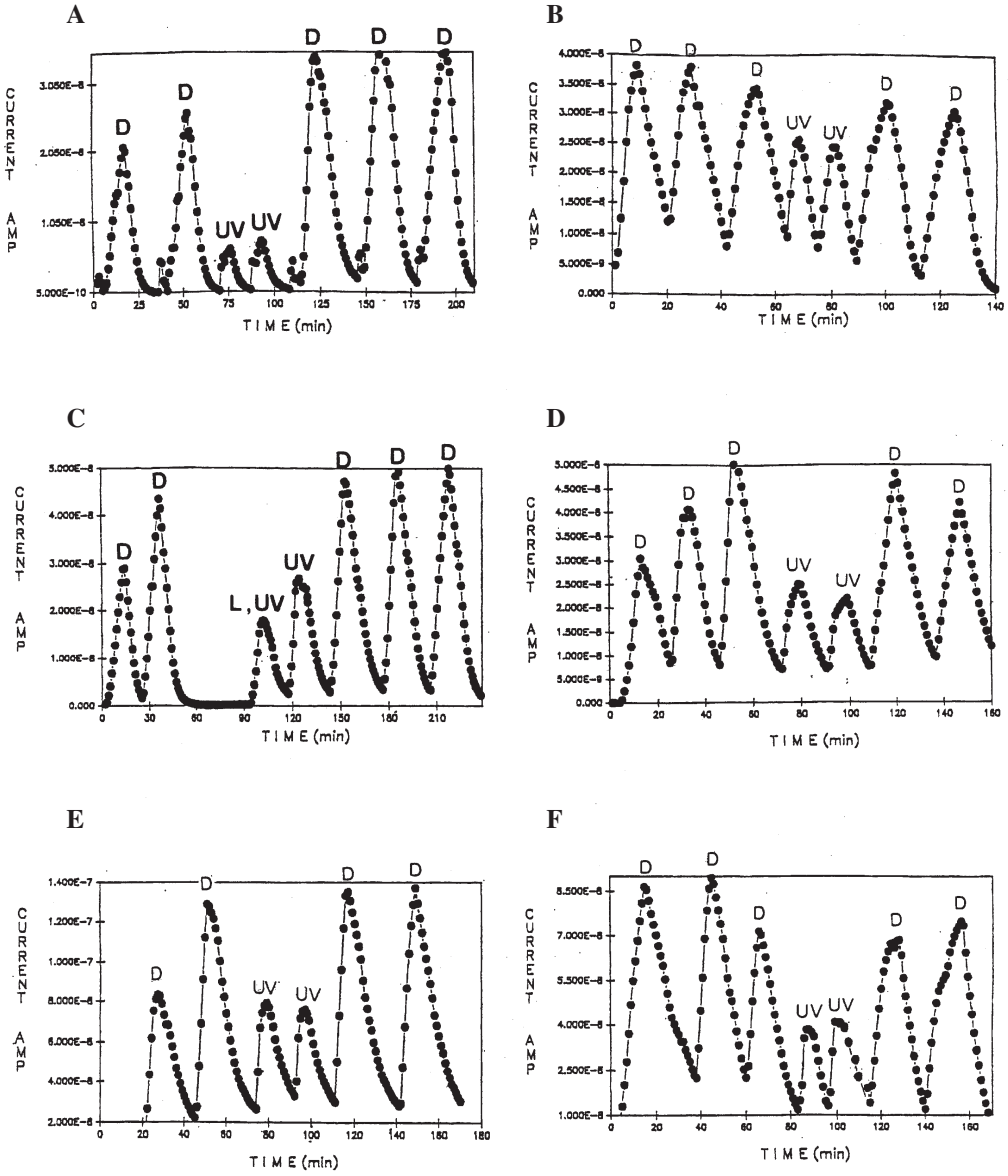

FIGURE 1. The thermoelectric effect as measured on yellow stripe of the complete hornet body. As can be seen, in every cycle of warming the current rises while at cooling the current decreases. Every measurement comprises firstly 2 or 3 cycles of warming and cooling in the dark, then 2 cycles of warming and cooling under UV light and after that 2 or 3 cycles of warming and cooling again in the dark. Generally, the measurements recorded in the dark show higher current level than those measured under UV irradiation. As can be seen, the current level in the dark attains between 45 nA and 140 nA, while under UV the current level attains between 5 nA and 80 nA (D = dark, L = light, UV = ultra violet light).

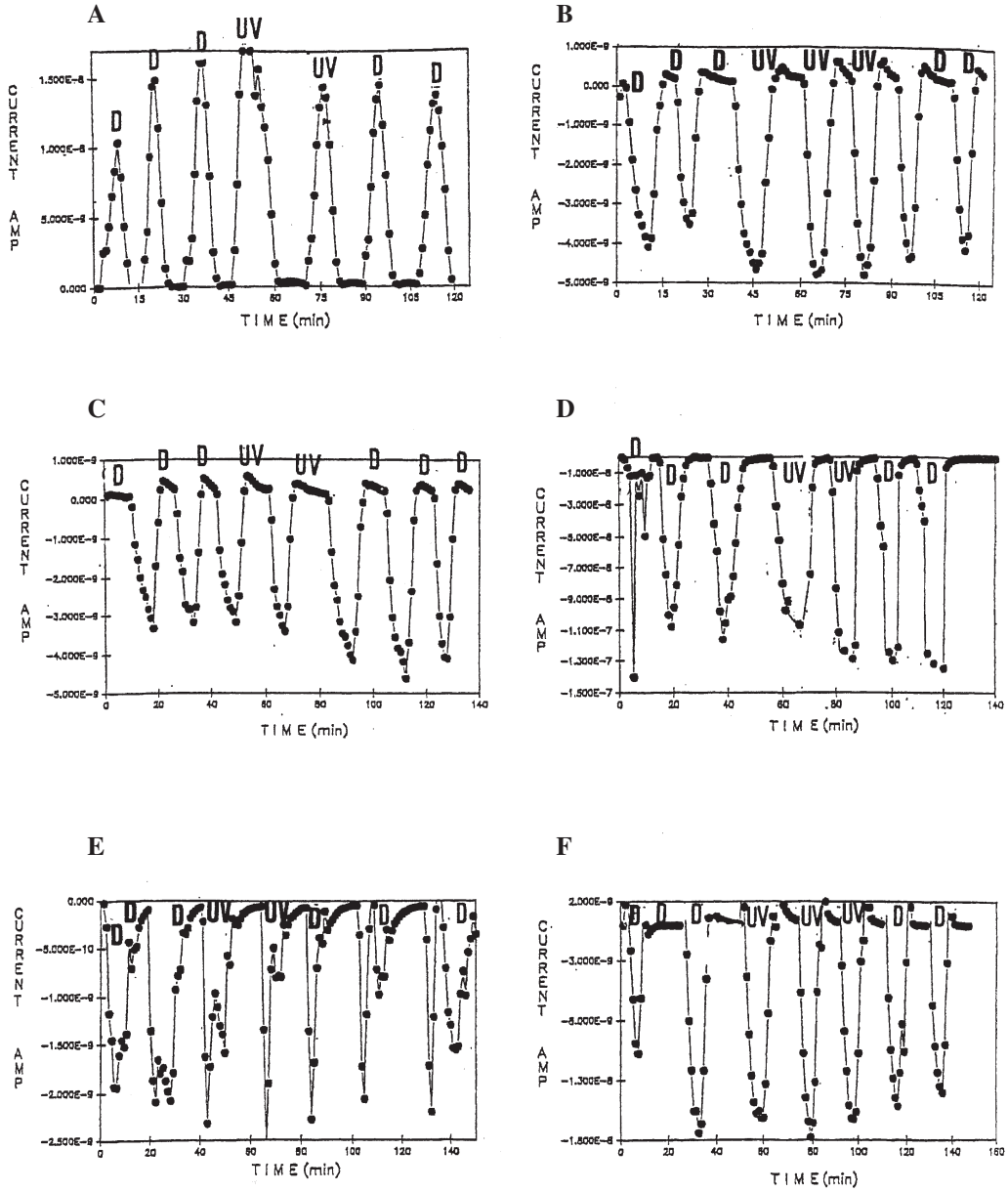

FIGURE 2. Thermoelectric measurements on a brown stripe of the hornet cuticle. Most of the values are lower than those measured on the yellow stripe of the entire body, and in 5 out of 6 measurements the values are negative, while their level is between 1.5 nA and — 130 nA. There is no effect of light, i.e., there is only thermoelectric and no photoelectric effect whatsoever. Warming and cooling cycles as in Figure 1.

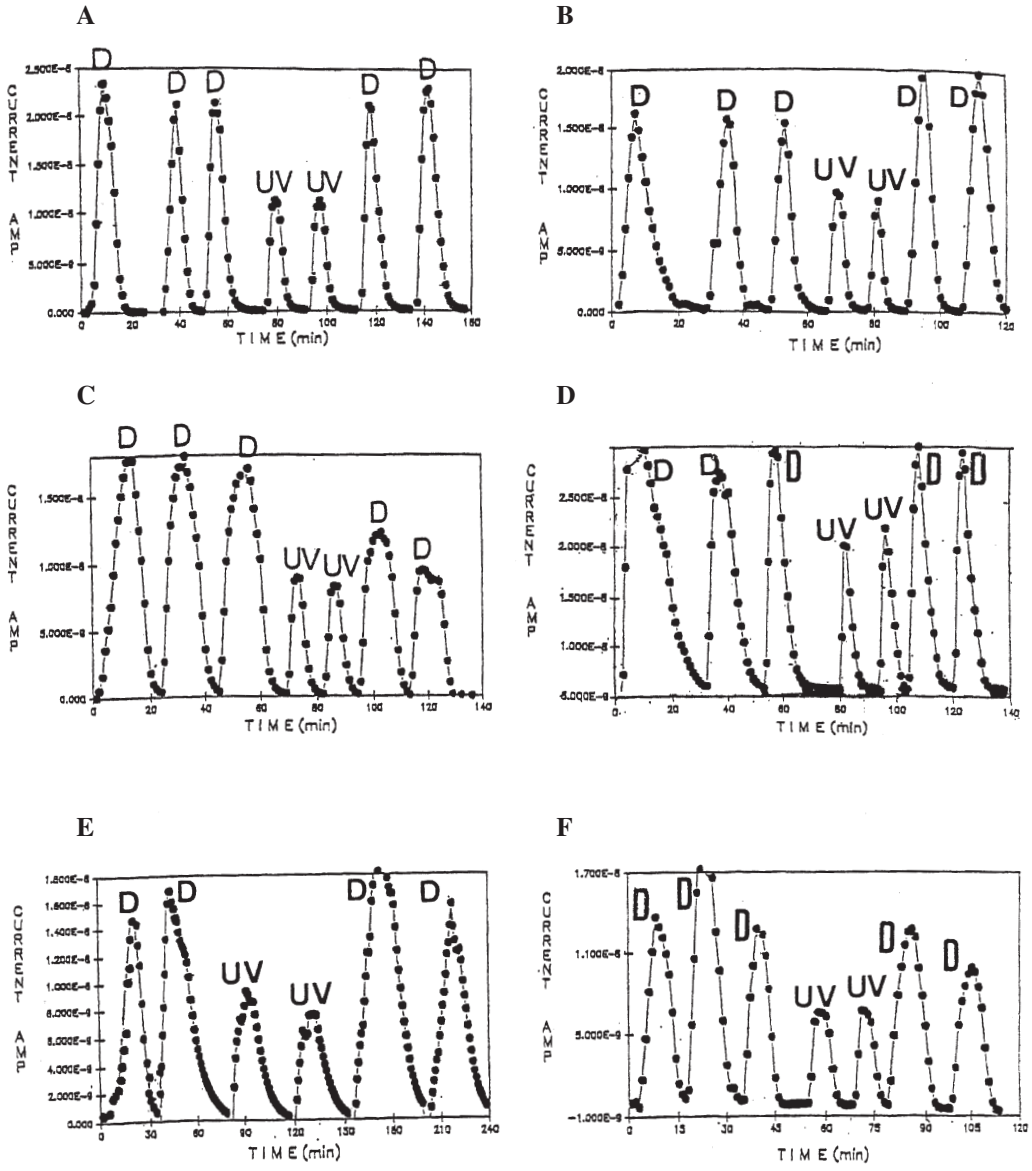

FIGURE 3. Thermoelectric and photoelectric measurement on yellow stripes separated from the body, but with the yellow pigment intact. As in Fig. 1, every measurement is composed of cycles of warming and cooling, first 2 or 3 in the dark, then 2 under UV irradiation, and the latter 2 or 3 again in the dark. As can be seen, the current level in the dark is higher, attaining around 20 nA while under UV irradiation the current attained is lower — between 6 and 20 nA, but in general the current values obtained in separated yellow stripes are lower than those obtained in yellow stripes of the entire body. There is definitely a thermoelectric as well as a (negative) photoelectric effect.

When the yellow pigment is separated mechanically (by scarping) from the cuticle, we get the results shown in Figure 4. Here, a thermoelectric effect is evident, albeit lower than in prior measurements taken on separated yellow stripes. The values are in fact about a third as high as in the pigment containing yellow stripes, and there is no photoelectric effect in evidence. In another series measurements taken in yellow stripes whose yellow pigment was depleted by prolonged incubation in tap water, the obtained results were quite similar. In a further experiment involving yellow stripes that were submerged for 30 min in a 75% ethyl alcohol solution, the measurements revealed the persistence of the thermoelectric but the complete loss of the photoelectric property. In this respect, the results of submersion in alcohol are similar to those shown in Figure 4. Having said that, we should emphasize that the yellow cuticular tissue remains seemingly intact in all organic solvents tested, so that extinction of the photoelectric effect is probably due to denaturation of the protein.

In Figure 5 we show the results of measurements taken from a preparation of brown stripes (second gastral segment) that had been separated from the hornet's body. One can see that the results here are actually on the same order of magnitude as in the measurements of brown stripes that has not been separated from the body; we observe a thermoelectric phenomenon but not the photoelectric one, just as in the case of the brown stripe in the intact body.

In order to assess both the accuracy of our measurements in the incubator as well as that of the response of cuticle practically devoid of pigment, we decided to perform some of our measurements on hornet wing, which is practically transparent and actually stems from a folding of the cuticle, and in parallel record the temperatures within the incubator. The results of six such measurements are shown in Figure 6, in which the A-F present the per minute responses to temperature changes by a preparation of a front wing of a hornet, with the temperature being recorded both automatically by the incubator mechanism as well as manually by an attendant.

Insofar as the wing was concerned, we noted that: 1) it responded to heating and cooling just as the cuticle did, that is, it displayed a thermoelectric response; 2) it did not respond to light, thus lacking a photoelectric response; and 3) its thermoelectric response was relatively low — resulting in a few nA in 2 of the six cases and several dozen nA in the other four cases. This result is very similar to that obtained with an isolated brown stripe (see Figure 6).

Perusal of the response in the incubator (unbroken line) reveals: a) that the heating attains higher values than does the maximal response, taking into account that the maximal response is usually around 27–28°C; b) that usually the maximal response stops, that is, reaches saturation before the peak of heating; c) that response of the cuticle in the wing is retarded, meaning that there is a time lag of a few minutes between the heating in the incubator and the onset of cooling; d) that usually the cuticular response occurs after the incubation's response, barring the measurements in the first cycles shown in Figure 6F; e) that the heating (and cooling) of the incubator are 'acute' processes whereas charging of the cuticle, which reaches maximum at 27–30°C, is a blunt process, and at times there is a difference between the heating line and the cooling line: heating was faster than cooling in all five cycles observed but in Figure 6F, there is no difference between the heating and the cooling; f) that the number of cycles measured in the wing within the time range of 130–180 minutes was only five, whereas in other parts of the gastral cuticle within the

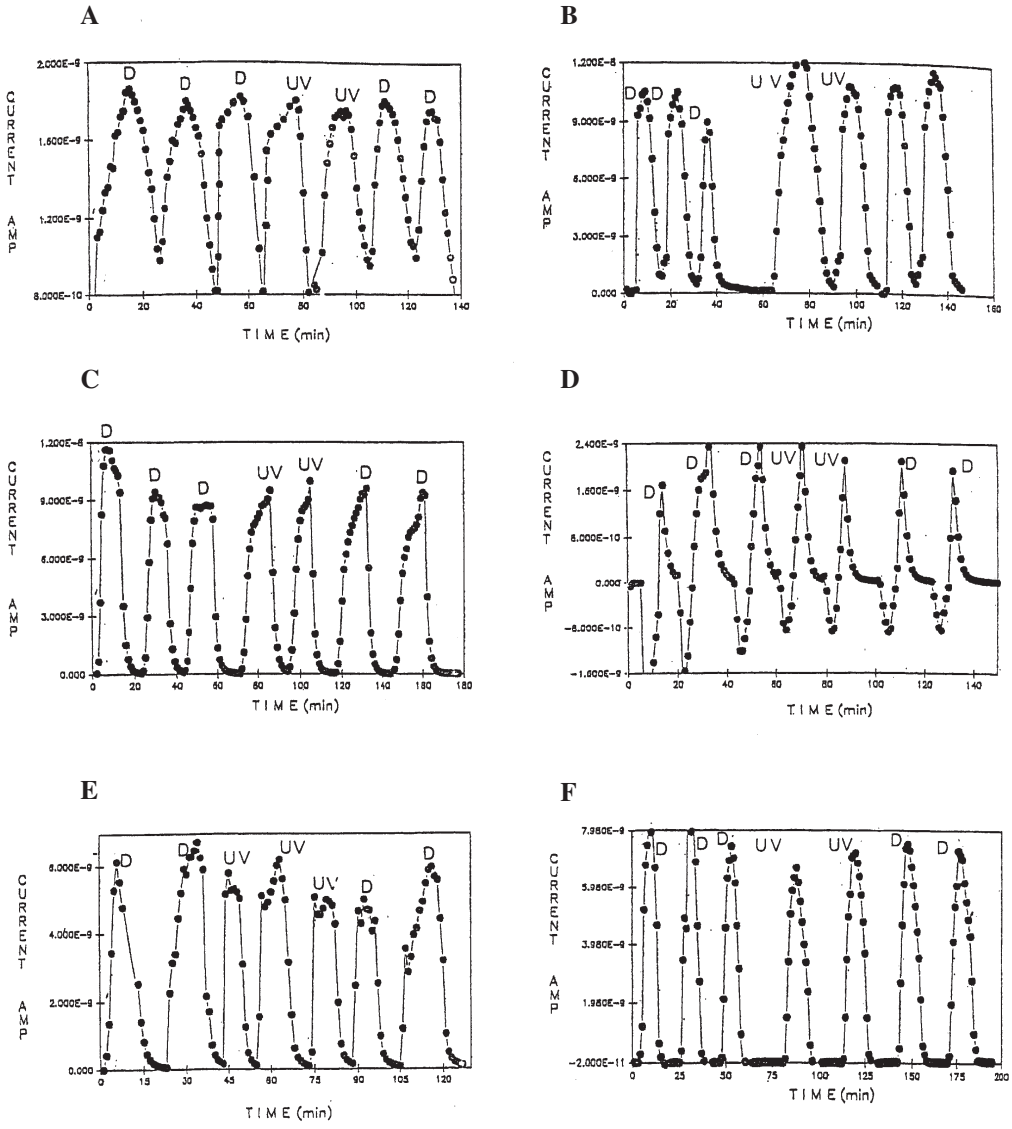

FIGURE 4. Thermoelectric and photoelectric measurements on separated yellow stripes when the yellow pigment was scrapped off. One can see that the cuticle still preserved a thermoelectric effect with the current increasing after each warming cycle and decreasing by cooling, and there is no photoelectric effect. The current levels are lower than before the treatment undergone by scrapping off the yellow pigment. Generally the same results were obtained after removing the yellow pigment by incubation the yellow stripes in tap water, or by incubation in ethyl alcohol. This latter procedure does not remove the yellow pigment, but denaturates it.

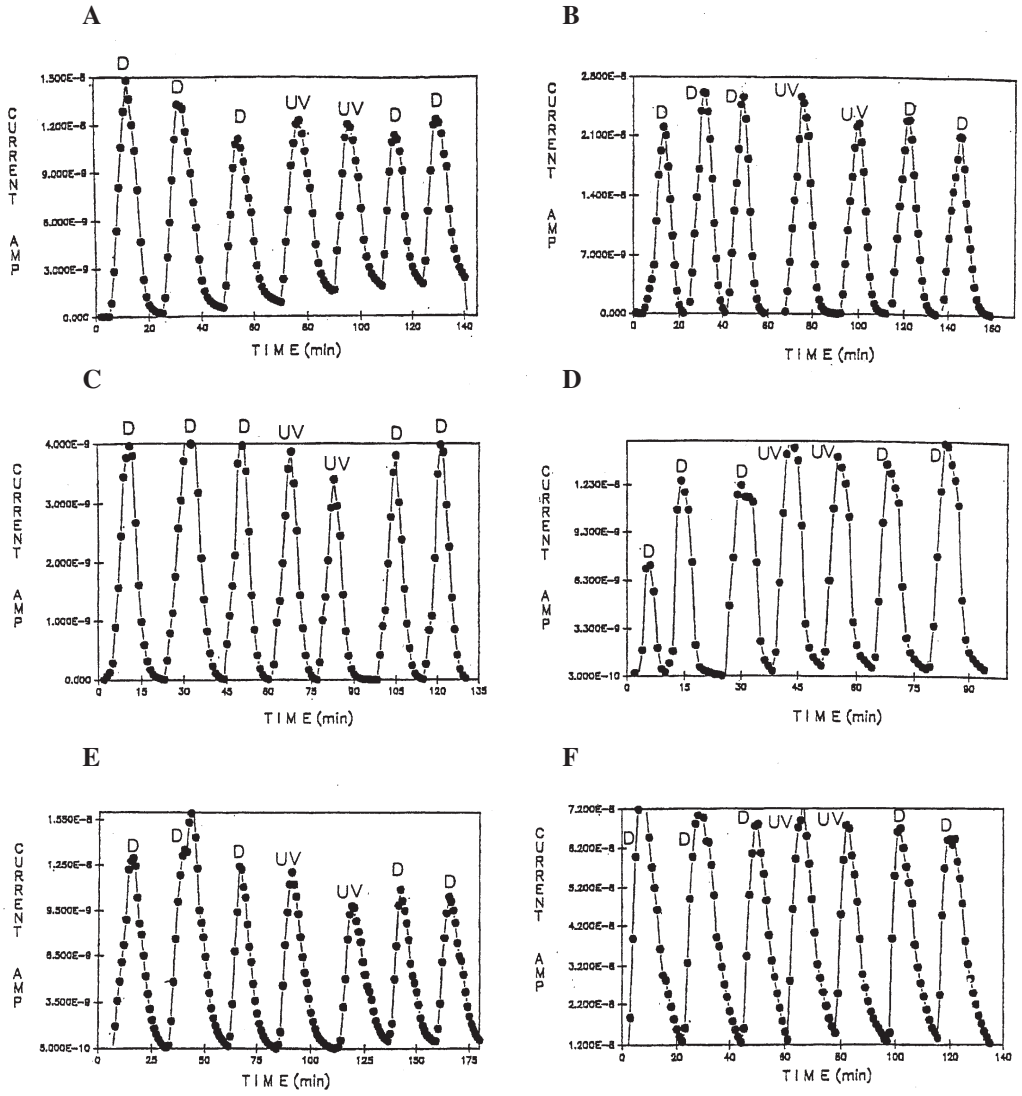

FIGURE 5. Thermoelectric measurements on brown stripes separated from the body. As can be seen, the stripes are still thermoelectric and when warmed produce between 4 and 72 nA.

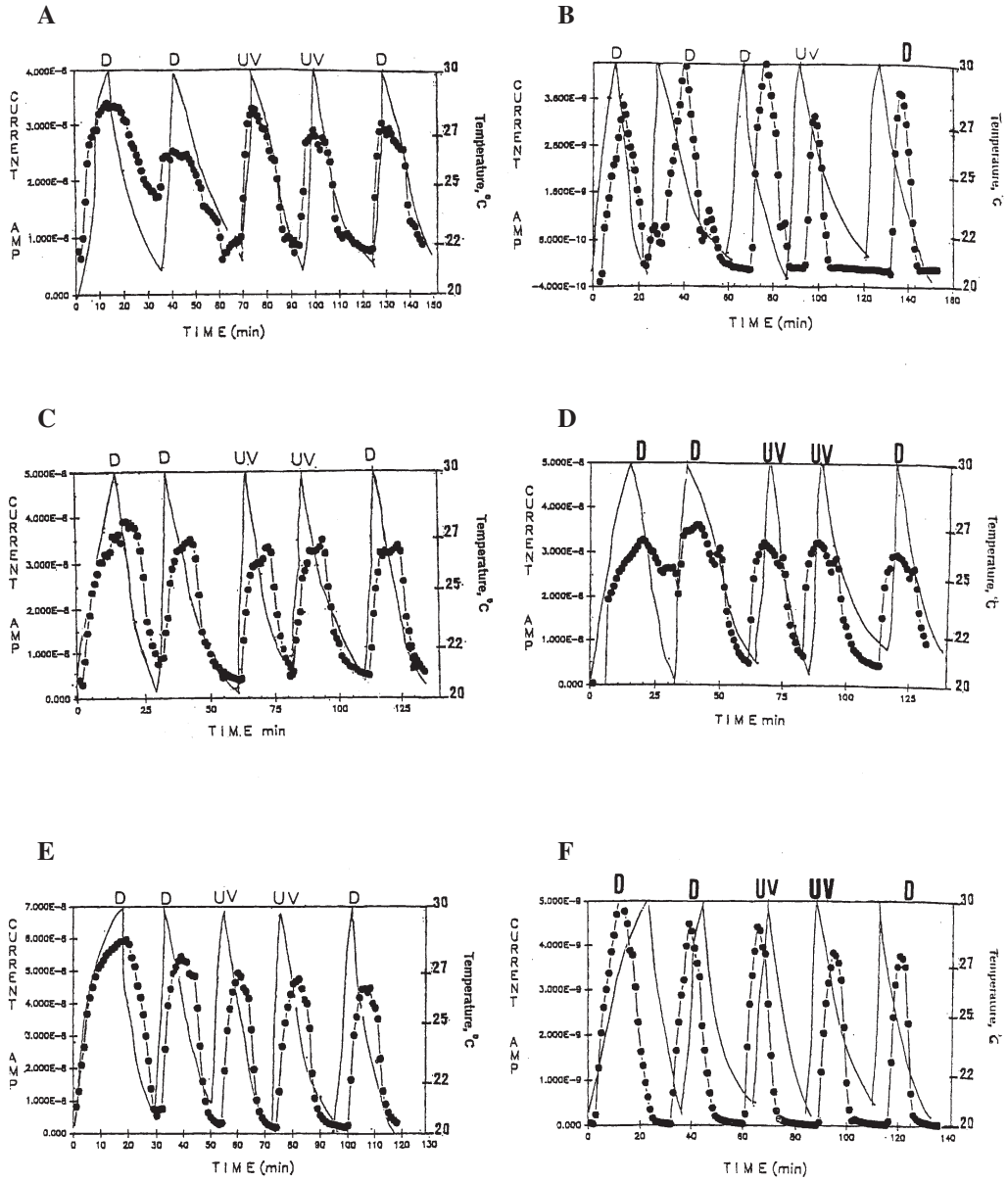

FIGURE 6. Synchronous recording of the thermoelectric current on the wings of a hornet and of the temperature of the incubator. As can be seen, the wing is also thermoelectric and when warmed between 20 and 30°C, there is a rise in current. The current of the wing attains between 4 to 40 nA. But, as can be seen, there is a lag between the maximal temperature and the maximal current. For further details consult text.

same time frame we recorded up to seven cycles, which means that in the wing each cycle of measurement is longer, lasting on the average, about 28 min, compared to the average 24 minutes per cycle in cuticle. In both brown and yellow cuticle the 'mixed' cycle (light-dark) lasted 22.2 min, while in same yellow cuticle (stripe), in the absence of a photoelectric effect, i.e., in the dark, the cycle was only 21 min.

Do other parameters in the yellow cuticle change upon removal of the yellow pigment? We got our answer by examining the specific heat of yellow stripes with pigment intact (Figure 7A) and ones with pigment removed by incubation in tap water, which coincides with that of the brown stripe (Figure 7B). As we can see from Figure 7A, cuticular stripes with yellow pigment intact yielded a specific heat of 1.60 J/g.K at 20°C, and the specific heat increases with rise in temperature to about 1.87 J/g.K at 30°C; thereafter the 'hump' drops gradually to values which at equivalent temperatures resemble those of brown cuticular stripe. In other words, the primary difference between cuticle with yellow pigment and one without yellow pigment is the 'hump' which considerably hikes up the specific heat at optimal nest temperature (29–30°C). When the yellow pigment is removed as by incubation in tap water, the value of the specific heat drops to values quite similar to those of the brown stripes (Figure 7B). So far as rate of heating was concerned, this exerted no significant difference.

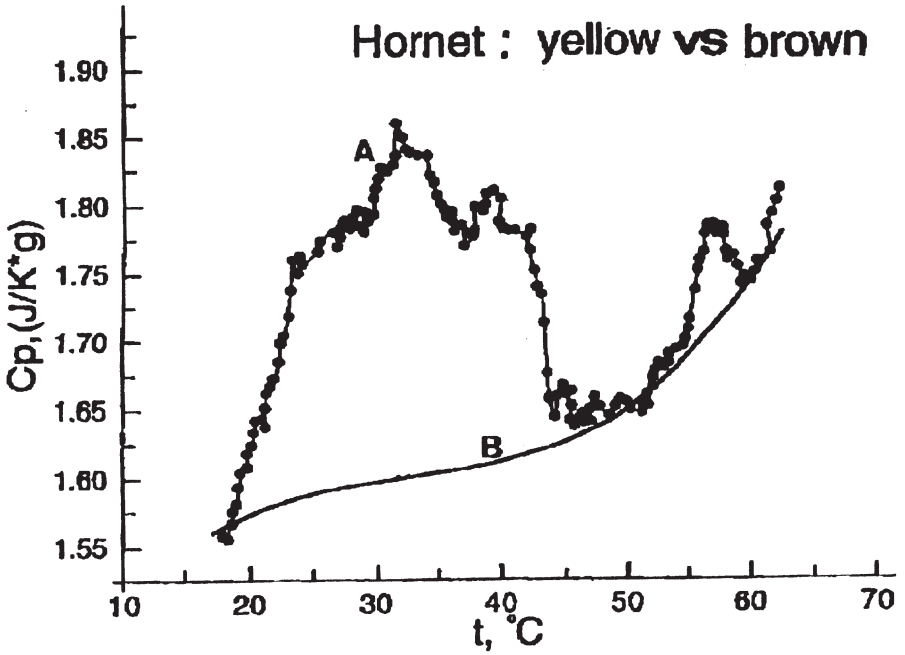

FIGURE 7. Measurement of specific heat: A) upper line — specific heat of the yellow stripe with pigment intact; lower solid line — specific heat of the brown stripe. As can be seen, there is a hump of specific heat in the yellow stripe between 20 and 45°C. In this area the maximal specific heat is 1.87 J/g.K while in the same area of the brown stripe (B) is only about 1.6 J/g.K. After scrapping off the yellow pigment the specific heat of the yellow stripes is close to that of the brown stripe.

Discussion

We start off by a reminder that in the present study, the electrodes were attached underneath the hornet cuticle in order to rule out the effect of light on the electrodes or on their connection. The purpose of our study was to elucidate the roles of the various pigments in the cuticle of the Oriental hornet, specifically in the observed photoelectric and thermoelectric phenomena. Our findings may be summarized as follows: 1) in all parts of the hornet cuticle, whether yellow, brown or the almost pigmentless wing cuticle, one can record a thermoelectric response both in cuticle of the intact hornet as well as that overlying disparate segments (Figures 1–6), but the values for the intact body are higher by as much as 20–140 nA than those recorded in individual segments detached from the body (amounting to a few nA or, at most, several dozen nA), which means a difference by 1–2 orders of magnitude; 2) a photoelectric response occurs only when measuring yellow stripes in the intact body (Figure 1), or yellow stripes with pigment that are separated from the body (Figure 3); there too, the values are higher (by about 3-fold) in intact cuticle than in separated stripes, and furthermore, when the yellow stripes are depleted of their yellow pigment, they cease responding to light (Figure 4); in this connection, it matters not if the pigment is scraped off mechanically or removed *via* bacterial incubation or submersion in organic solvent like ethyl alcohol (which denatures protein). Submersion in ethyl alcohol of the entire hornet body (Ishay, unpublished observations) or of the brown segments only, does not alter the thermoelectric effect nor does it produce any visible change in the pigment, the cuticle apparently remaining as yellow as before; 3) both in the brown stripes of the intact cuticle (Figure 2) as well as in the isolated brown segments (Figure 5) or the wing (Figure 6) light exerts no effect, that is, there is no photoelectric response; 4) the heat capacity in the yellow stripes is relatively high in cases where the yellow pigment is retained and the temperature is optimal for hornets. Thus, in separated yellow stripes we get Cp = 1.87 J/g.K, as opposed to only Cp = 1.58 J/g.K in brown stripe at same temperature. However, if you remove the tissue containing the yellow pigment, the capacitance value drops to 1.58 J/g.K. From the above it follows that in yellow stripes the photoelectric phenomenon is associated with a high specific heat value and that there are higher values of the electric current in yellow stripe than in brown stripe.

The combined findings of specific heat, current and a photoelectric effect suggest that hornet cuticular tissue is very active in these respects, much more than the surrounding tissues, and that such activity is performed primarily by the yellow tissue. The fact that the photoconductive activity is displayed only in wavelengths within the UV range suggests that there is no connection between such activity and photosynthetic activity which, as we know, takes place within light in the wavelengths of blue and red. Yet, we know that hornets can see also within the UV range (Schremmer, 1941; Beier and Henzel, 1972; Mazorkin-Porshniakov, 1960; Edwards, 1980). It is rather enigmatic that with their compound eyes hornets can see also within the blue and green wavelengths whereas their yellow cuticle is not responsive to these wavelengths. As is known, there are in hornet cuticle extraretinal peripheral photoreceptors (PP) (Menaker, 1977). The PP in the hornet cuticle have already been described (Ishay *et al.,* 2000). Moreover, in the past we have detected in Oriental hornet cuticle the following compounds: Xanthopterin, Isoxanthoterin, Biopterin, Violapterin, Hypoxanthine and Adenine — all of which absorb light in the UV range be-

tween 255–390 nm (Ikan and Ishay, 1967). These pigments are known also in other species of the order Hymenoptera (Leclerq, 1950). While measuring the photoelectric phenomenon in hornets, we noticed that the current level upon illumination, is on the decline, suggesting the presence in the yellow cuticle of a factor that under illumination absorbs the current, or at least a major part of it from the entire body, so that the current generated under light is smaller than that generated in the dark, all other conditions being equal.

In the dark, an electric current is formed as a result of the above-described thermoelectric effect under which heat converts into current (see Figure 1-6) (Gutmann *et al.,* 1983). Under illumination, we notice two processes occurring, namely: a) in the whole (intact) cuticle, heat converts to electric current, and b) in tissue with yellow pigment in it the current is partially absorbed and consequently the overall current level is lower than in the dark. In fact, under UV irradiation of greater intensity (Ishay, unpublished observations) it becomes possible to absorb all of the formed current, so that upon illumination, no current at all is formed (or can be measured). In brown cuticle, the photoelectric phenomenon does not occur and only the thermoelectric phenomenon does and therefore it is reasonable to assume that the pigments in yellow tissue absorb the current. The yellow pigment grains are very numerous. They form a 'sea' of dense particles around each individual peripheral photoreceptor (Ishay *et al.,* 2000). As is known, the natural solar energy reaching earth has the shortest wavelength of about 312 nm (Thorington, 1985), while the energy above 312 nm, in the UVB and UVC range, is absorbed by the ozone layer. We now know that the solar energy between 312 ≅410 nm is picked up by the yellow pigment particles in hornet cuticle and is stored in them. It stands to reason that in the living hornet this stored energy is subsequently converted to or utilized in vespan motor or metabolic activities, whereas in the dead organisms used in the present study it is stored to saturation without being utilized. We now know that live hornets are attracted to UV light (Spradberry, 1973; Ben-Bashat *et al.,* 1999) and in fact commercial hornet traps have been built which capitalize on this attraction to UV light. As for the absorption of UV light by the yellow pigment of hornet cuticle, this phenomenon has also been known for many years now. Already in 1961, Hoffman and Langer maintained that "the pterines function as a light filter in the near UV and blue regions".

We also know that in hornets the pigments are arranged within xantosomes shaped like an elongated cylinder which, upon maturation of the hornets, break up into much shorter cylinders of about 0.5 μm each (Ishay and Shimony, 1982). The cuticle above the yellow region is translucent and, in fact, above the duct of the PP there is only a layer of epicuticle (Ishay *et al*., 2000).

It has long been known that hornets are active only in the warm season and even then they are out in the open in foraging flights only during the daytime hours. The bulk of flight activities outside the nest is during the period of nest digging, and these flight activities take place mainly in the noon hours (Ishay and Kirshboim, 2000).

We assume that what transpires in hornet cuticle upon exposure to light is the following: the energy of light (photons) induces in it an electric field (D. C.) which, in turn, causes the dipoles of the active material (possibly in a protein) to polarize, i.e., to arrange in uniformly charged parallel plates (domains) which give rise to an identical electric field, wherein one plate has a (+) charge density and the other, a (–) charge density. In other words, under illumination due to the electric field induced by the high frequency

wavelengths of light, the pyroelectric material arranges in planes of homogenous negative charges which are separated (by the domain walls) by planes of opposite (positive) charges, with the end result that the material transforms into an *electrical capacitor* whose spatial dimensions are probably dependent, *inter alia,* on the duration of exposure to light, the intensity of the light, its wavelength, and so on (Ishay and Litinetsky, 1998).

This explains the voltage that is obtained under illumination (which thus far has been measured in cuticle — see Ishay *et al.,* 1992), and the fast changes in current (drop) and voltage (an increase) when the specimen kept in the dark is exposed to light (Ishay *et al.,* 1987)

The rationale of the protracted electric current measured in the dark is that in the absence of illumination and at the appropriate temperature, the dipoles in the material gradually revert (in dependence on the temperature) to a state of spontaneous polarization wherein it releases the excess energy accumulated during the illumination as D. C. current. In light, such a recombination is prevented due to the continuous supply of energy that "keeps" the dipoles from relaxation. Note that the process of exposing such ferroelectric material to light, which results in its electric charging (with photons), induces the photovoltaic process (Ishay *et al.,* 1992) which is, in principle, closely related to the photosynthetic process in green plants (Gutmann *et al.,* 1983).

In a usual active nest of social wasps (or hornets) the cuticle is polarized many times a day — everytime the insect leaves the nest to fly in sunlight — and the polarization acquired is gradually reversed once it returns to the dark nest. While in a state of relaxation, whether in the dark or under cooling (4°C), such materials possess positive charges alternating spontaneously with negative charges. This is probably the state with the lowest energy level (Kittel, 1986; Ferendeci, 1991).

Turning back now to the subject of the yellow matter in hornet cuticle, we remind that at the center of each aggregate of yellow pigment grains in the cuticular yellow stripes there is a PP. We presume that this PP is sensitive to the light that reaches it after passing though the epicuticle only. In other words, the light reaching the PP does not have to filter through all the cuticular layers, as does the light that ultimately reaches the yellow matter. The light-sensitive pigment in the PP is most likely rhodopsin — the visual purple comprised of conjugated proteins in which the photosensitive component of the molecule, the chromophore, is retinaldehyde (Gillott, 1995). In compound eyes the photosensitive cells are usually surrounded by primary and secondary pigment cells in which the pigments are mainly ommachromes, but in our case the pigments are usually purines and pteridines in very large amounts (Ishay *et al.,* 2000).

In the eyes of vertebrates, the visual pigments, located in photoreceptor cells of the retina, absorb photons and produce vision by exciting the photoreceptor cells and changing the potential across the plasme membrane (Honig, 1982). In contrast to the typical structure of a compound eye in an insect, wherein each ocular unit contains eight retinular cells (Goldsmith and Bernard, 1974) surrounded by pigment cell containing mainly ommachromes in the compound eye of the Oriental hornet, in the center of each unit of peripheral photoreceptors (PP) there are only 1–3 retinular cells (Goldstein *et al.,* 1996) surrounded on all sides except upwards (in line with the path of the penetrating light) by numerous granules of yellow pigment. The latter pigment fluoresces when excited by light at a wavelength of 353 nm and the speed of response is less than 25 ps (Ishay *et al.,* 1990). Interestingly, in bacteriorhodopsin, which is the key protein participating in the halo-

bacterial photosynthetic processes (Hamp, 2000), the initial photoinduced charge separation occurs in less than 5 ps (Simmeth and Rayfield, 1990). Honig (1982) has shown that in bacteriorhodopsin, the protein absorbs a photon and uses its energy to pump protons across the membrane, moving them about 40 Ängstroms, and that the resulting proton gradient is used to drive the metabolic processes in the cell.

In our case, we presume that in hornet cuticular yellow stripe the process of energy uptake transpires in the following manner. The mass of yellow pigment granules receives photons which pass through the cuticular layers and undergo polarization. The electric resistance now rises, causing drop in the current which, in turn, increases the voltage and produces a rise in the capacitance. As for the PP, light reaches them after passing through the thin layer of epicuticle, meaning that there is less filtration of and great sensitivity to the arriving photons which alter the PP membranes potential. Photons from everywhere commence flowing through the membrane into the PP cell activating metabolism of the cells. As to which cells are thus affected remains to the clarified but our guess is that it is the manner in which voltage is discharged in the yellow pigment granules which we arbitrarily assume to act as a miniature battery. If our assumption is correct, then these granules draw and attract all electric charges formed everywhere in the hornet's body, including also those in brown stripes.

In line with our conjecture, we should point out the PPs are ubiquitous in hornet cuticle (Reichel-Kvital *et al.,* 1999), yet: 1) in yellow stripes they are more numerous; 2) only in yellow stripes are they embedded amidst yellow pigment granules; 3) as in ocular cornea (whether compound eyes or ocelli), the cuticle in yellow stripes is clear and transparent; 4) from an ecological standpoint, the species of Vespinae prevalent in regions with a colder climate (be it due to northerly location or higher elevation, that is, latitude or altitude) possess more color spots or yellow stripes than do the 'warmer' species (Ishay, unpublished observation). In the latter regard, we contemplate that in the colder regions of the earth, greater importance is ascribed to uptake of energy from the sun and its conversion to metabolic energy.

Continuing this line of thought, we presume that under natural conditions, that is, upon exposure to direct sunlight, whose energetic intensity is vastly greater than that of the humble lamp we were using in our laboratory experiments (consider, for instance, that at noon, in Israel, during the summer months the intensity of insolation is about 150,000 Lux or more, of which 7% comprise UV waves). Not surprising, then, that a hornet exposed to such solar intensity during its noon flights outside the nest soon reaches saturation of its yellow stripes, forcing it to return to the dark nest after a brief flight in order to discharge its electric charge. This discharge probably transpires by the returning foraging hornet placing its feet upon the silk caps of the pupae or on the walls of the comb cells that serve as storage depots for energy. In this connection, we find the manner in which hornet cuticle responds to light and/or temperature somewhat surprising. We hasten to point out that by cuticle we actually mean three types of cuticle, to wit: brown cuticle in which the pigment is melanin, transparent cuticle which contains no pigment but overlies a layer containing the yellow pigment, and semi-transparent cuticle such as is encountered in the wings of the hornet. In all these types of cuticle the current rises in the dark upon increase of the temperature (between 20–30°C) and drops upon decrease of the temperature. Such behavior befits organic semiconductors that possess electric conductance under certain conditions.

Our observations on the manner in which hornets build their nest have informed us that they attach the nest only to a substrate that does not conduct heat. Thus they refrain from building on metals but do build on glass (Ishay *et al.,* 1986), and we suppose that the heat conductance of the vespan comb is very low. Consequently, we tend to view the materials from which vespan cuticle is made up — and this within the narrow temperature range of hornet activities (~ 20–30°C) — as endowed with a crystal-like electrical conductivity (σ) but a glass-like thermal conductivity (κ). This could explain why one gets a certain amount of electric current even in the dark, because the ambient thermal energy upon heating is utilized for the creation of electric energy — the thermoelectric phenomenon — and is not radiated outward as heat but rather the cuticle serves as sink for the ambient heat. In other words, instead of the heat leaking out of the cuticle, it is rather collected by it. If this be true, such a process could assist in thermoregulation of the hornets and their milieu by decreasing the ambient heat when it becomes too warm, and conversely, the stored electric energy could contribute to raising the temperature when the nest is too cold. The issue becomes important both within the nest as well as when the Oriental hornet flies outside in the burning noontime sun in its range of distribution which includes also sweltering deserts.

In the above regard, we already have the theory proposed by Slack (1997) who maintains that in some materials rattling motions of guest atoms produce low-frequency anharmonic phonon modes, which strongly scatter the heat carrying acoustic modes. This rattle scattering will reduce significantly the thermal conductivity without reducing the electrical conductivity. Such materials should contain two basic ingredients: 1) semiconducting crystals as hosts, and 2) encapsulated small guest atoms as rattlers.

Of known substances that theoretically fit in this group of materials, we have the clathrates (Mahan, 1997; Dong *et al.,* 2000). As for hornet cuticle, we have shown (Ishay and Kirshboim, 2000) that it is composed of very numerous sub-layers (about 100) which gradually taper as we proceed from the outside downward. In each such sub-layer, the primary component is chitin and the minor one is protein (Neville, 1975). We are still uncertain whether in hornet cuticle there is a compound identical or resembling a clathrate, but we do know, and have identified in cuticle such elements as Na, K and Ca, which are surrounded by large molecules of chitin which may serve as host.

References

Beier, W. and Menzel, R. (1972) Untersuchungen über den Farbensinn der deutschen Wespe *(Paravespula gemanica* F. Hymenoptera, Vespidae). Verhaltensphysiologicher Nachweis des Farbensehens. *Zool. Jb. AlIg. Physiol. Tiere 76*: 441–454.

Ben-Bashat, D., Navon, G., Litinetsky, L. and Ishay, J.S.(1999) Phosphorous metabolites in the Oriental hornet and honeybee: NMR examinations. *Physiol. Chem. Phys. & Med. NMR 31*: 65–75.

Dong, J., Sankey, O.F., Ramachandran, G.K. and McMillan, P.F. (2000) Chemical trends of the rattling phonon modes in alloyed germanium clathrates. *J. App. Phys. 87(11)*: 7726–7734.

Edwards, R. (1980) *Social Wasps.* Rentokil Limited, East Grinstead, G. B.

Ferendeci, A.M. (1991) *Solid State and Electron Devices*. McGraw-Hill Int. New York.

Gillott, C. (1995) *Entomology,* 2nd ed. Plenum Press, New York.

Goldsmith, T.H. and Bernard, G.D. (1974) The visual system of insects. In: *The Physiology of Insecta,* 2nd ed. Vol. II (M. Rockstein, ed.) Academic Press, New York.

Goldstein, O., Litinetsky, L. and Ishay, J.S. (1996) Extraretinal photoreception in hornets. *Physiol. Chem. Phys. & Med. NMR. 28:* 129–136.

Gutmann, F., Keyzer, H., Lyons, L.E. and Somoano, R.B. (1983) *Organic Semiconductors,* Part B. R. E. Krieger Publ. Co., Malabar, Florida.

Hamp, N.A.(2000) Bacteriorhodopsin: mutating a biomaterial into an optoelectronic material. *App. Microb. & Biotechn. 53(6):* 633–639.

Hoffmann, C. and Langer, H. (1961) Die spectrale Augenemphindlicheit der Mutante chalky von *Calliphora erythrocephala. Naturwissenschaften 48:* 605. Berlin.

Honig, B. (1982) Visual pigments: a new type of molecular switching device. In: *Molecular Electronic Devices,* (Carter, F. L. ed.), Naval Research Laboratory, Washington, D. C., Marcel Dekker, Inc. New York, pp. 137–139.

Ikan, R. and Ishay, J. (1967) Pteridines and purines of the queens of the Oriental hornet *Vespa orientalis. J. Insect Physiol. 13:* 159–162.

Ishay, J. (1975) Orientation by pupating larvae of *Vespa orientalis* (Hymenoptera, Vespinae). *Insectes Sociaux 22(1):* 67–74.

Ishay, J.S. and Kirshboim, S. (2000) Ultraviolet B light stimulates hornet activities: a review. *Semiconductor Science and Technology*, Inst. of Physics *15:* 704–723.

Ishay, J.S. and Litinetsky, L. (1998) Ferroelectric-like properties of hornet structures and constructions. *Physiol. Chem. Phys. & Med. NMR 30(2):* 185–201.

Ishay, J. and Ruttner, F. (1971) Die thermoregulation in Hornisennest. *Z. v. Physiol. 72:* 423–434.

Ishay, J.S. and Shimony, T.B. (1982) Temperature dependence electrical resistivity of the hornet cuticle. *J. Thermal Biol. 7:* 91–94.

Ishay, J. S., Rosenzweig, E., and Pechhacker, H. (1986) Comb building by workers *of Vespa crabro, V. orientalis* and *Paravespula germanica* (Hymenoptera: Vespinae): Interaction between worker groups of these species while engaged in various social tasks. *Monitor Zool. Italiano N.S. 20:* 31–51.

Ishay, J.S., Peled, N., Tischler, J.R. and Rosenzweig, E. (1987) Photoconductivity in the hornet cuticle: a theoretical approach. *Physiol. Chem. Phys. & Med. NMR 22:* 45–60.

Ishay, J.S., Chernobrov, H.L., Abes, A.H. (1990) Electric properties of the hornet cuticle: Voltage, Current, Resistance and Capacitance and their compliance to changes in temperature. *Physiol. Chem. Physics & Med. NMR 22:* 45–60.

Ishay, J.S., Benshalom-Shimony, T., Ben-Shalom, A. and Kristianpoller, N. (1992) Photovoltaic effects in the Oriental hornet. *J. Insect Physiol. 38(1):* 37–48.

Ishay, J.S., Rozenzweig, E., Litinetsky, L. and Kirshboim, S. (2000) The solar unit in hornet cuticle: nm to μm scale. *J. Elect. Micros. 49(4):* 559–568.

Ishay, J.S., Litinetsky, L., Pertsis, V., Linsky, D., Lusternik, V. and Voronel, A. (2002) Hornet silk: thermophysical poperties. *J. Thermal Biol. 27:* 7–15.

Kittel, C. (1986) *Introduction to Solid State Physics.* 6th ed. John Wiley & Sons, Inc., New York.

Leclercq, J. (1950) Occurrence of pterin pigments in Hymenoptera. *Nature (London) 165:* 367–368.

Mahan, G.D. (1997) Good thermoelectrics. In: *Solid State Physics* (H. Ehreinreich and F. Spaepen eds.) 51: 81–157. Academic Press, New York, p. 81.

Mazokhin-Porshniakov, G.A. (1960) Evidence of the existence of colour vision in wasps (Vespidae). *Zool. Zh. 39:* 553–557 (in Russian with English summary).

Nevill, A.C. (1975) *Biology of the Arthropod Cuticle.* Springer Verlad, Berlin.

Reichel-Kvital, E. Ishay, J.S., Kalicharan, D. and Jongebloed, W.L. (1999) The extraretinal photoreceptors in the Oriental hornet: Morphology and Morphometry. *Phys. Chem. Phys. & Med. NMR 31:* 55–64.

Schremmer, F. (1941) Versuche zum Nachweis der Rotblindheit von *V. rufa L. Z. vergl. Physiol. 28:* 457–466.

Simmeth, R. and Rayfield, G.W. (1990) Evidence that the photoelectric response of bacteriorhodopsin occurs in less than 5 picoseconds. *Biophys. S. 57(5):* 1099–1101.

Slak, G.A. (1997) Design concepts for improved thermoelectric materials. In: *Thermoelectric Materials — New Directions and Approaches* (T. M. Tritt, G. Mahan, H.B. Lyon and M.G. Kanatzides eds) Material Research Soc., Pittsburgh, P. A. *478:* 47.

Spradbery, J.P. (1973) *Wasps.* Sidgwick and Jackson, London.

Sverdlov, A., Litinetsky, L., Pertsis, V. and Ishay, J.S. (2000) Thermophotovoltaic (TPV) properties of hornet cuticle as dependent on relative humidity. *Physiol. Chem. Phys. & Med. NMR, 32:* 57–66.

Thorington, L. (1985) Spectral, irradiance and temporal aspect of natural and artificial light. *Ann. NY Acad. Science 453:* 28–54.

Received July 25, 2002;
accepted November 25, 2002.

Life

at the **Cell** and **Below-Cell** Level

The **Hidden History** of a
Fundamental
Revolution in **Biology**

Gilbert N. Ling

Pacific Press
New York

Quick Order Form

Fax orders:	631-390-0053. Send this form or Xerox copy.
Telephone orders:	877-390-7730 toll-free. Have your credit card ready.
Computer orders:	Email: pacificpressny@aol.com; Website: http://www.pacificpressnewyork.com
Postal orders:	Pacific Press, PO Box 1452-11, Melville, NY 11747

Please send me the following:

_____

_____

Name: _____

Address: _____

City:_____State: _____Zip _____ - _____

Telephone:_____

E-mail address: _____

Sales tax: Please add 8.5 % for products shipped to New York addresses. For a $19.95 book, the total is $21.65.

Priority shipping: US $4.00.

Payment: ❑ Cheque

❑ Credit card

Visa MasterCard AMEX Discover

Card number: _____

Name on card:_____Exp. date:_____ / _____

Signature: _____